Abstract

EYCEÖZ, TUGAY. Deterministic Modeling and Long Range Prediction of Fast Fading Channels with Applications to Mobile Radio Systems. (Under the direction of Prof. Alexandra Duel-Hallen)

In wireless communication systems, the direct signal and the reflected signals form an interference pattern resulting in a received signal given by the sum of these components. They are distinguished by their Doppler shifts at the mobile. Since the parameters associated with these components are slowly varying, the fading coefficients can be accurately predicted *far ahead*. We introduced a novel algorithm for long range prediction of fading channels. This algorithm finds the linear Minimum Mean Squared Error (MMSE) estimate of the future fading coefficients given a fixed number of previous observations. We show that the superior performance of this algorithm is due to its longer memory span achieved by using lower sampling rate given fixed model order relative to the conventional (data rate) methods of fading prediction. This long range prediction capability for fading channels would provide enabling technology for accurate power control, reliable transmitter and/or receiver diversity, more effective adaptive modulation and coding and improvements in many other components of wireless systems. In this thesis, we demonstrate that large improvements in the performance are possible for both flat and frequency-selective

rapidly varying fading channels when the proposed prediction method is used. We illustrate the performance enhancements both at the transmitter and the receiver with both theoretical and simulation results.

DETERMINISTIC MODELING AND LONG RANGE PREDICTION OF FAST FADING CHANNELS WITH APPLICATIONS TO MOBILE RADIO SYSTEMS

by

TUGAY EYCEÖZ

A dissertation submitted to the Graduate Faculty of
North Carolina State University
in partial fulfillment of the requirements for
the Degree of Doctor of Philosopy

DEPARTMENT OF ELECTRICAL ENGINEERING
Center for Advanced Computing and Communication,
North Carolina State University,
Raleigh, North Carolina

March 2001.

APPROVED BY:

Prof. A. Duel-Hallen (Chair)	Prof. J. K. Townsend
Prof. S. T. Alexander	Prof. H. Hallen

BIOGRAPHY

Tugay Eyceöz was born in Ankara, Turkey on May 28, 1971. In 1993 he received his Bachelors of Science degree in Electrical Engineering from Middle East Technical University, Ankara, Turkey. He went on to earn his Master of Science degree in Electrical Engineering from North Carolina State University in 1995. During this period, he worked as a Teaching and Research Assistant. Prior to starting his Ph.D. Degree in June 1996, he worked for Nortel Networks. During his Ph.D. studies he was employed by the Center for Advanced Computing and Communication of NCSU as a Research Assistant till June, 1999. Then, he rejoined the Wireless Systems Engineering Group of Nortel Networks as a Senior Member of the Scientific Staff with high responsibilities in the research and development of CDMA, GSM, TDMA, GPRS, and next generation wireless networks such as 1xRTT (CDMA2000) and UMTS. He is currently employed by Cisco Systems, Inc. in Dallas, Texas in the Mobile Wireless Group. His current research and professional interests are in the development and design of next generation IP based Wireless Networks.

ACKNOWLEDGMENTS

I would like to thank my advisor, Prof. A. Duel-Hallen, for her support and guidance during my academic career. I also would like to thank Professors J.K. Townsend, S.T. Alexander, and H. Hallen for serving on my advisory committee. I appreciate their thoughtfulness and encouragement during my academic career at NCSU.

I am very thankful to the Center for Advanced Computing and Communication at NCSU for providing me their full support during both my Masters and Ph.D. studies.

The most heartfelt gratitude goes to the three most special people in my life, my father, my mother and my wife. I would like to thank my parents and my wife for making my life a wonderful one. To my father and mother, for their endless support, love and pride in me. To my wife Zeina, I am deeply grateful for her continued love and devotion. I am thankful for her and her wonderful family for believing in me and giving me their full support. To my precious son Mustafa, who brings joy into my life every day. To my family and friends. This work is dedicated to them.

Contents

List of Tables

List of Figures

Chapter 1

Introduction and Motivation

The first practical use of mobile radio communication was demonstrated in 1897 by Marchese Guglielmo Marconi, who is credited with first successfully establishing radio transmission between a land-based station and a tugboat, over an 18 miles path. Since then, the development of efficient wireless communication systems have been a challenge for modern communication engineering toward the realization of universal personal telecommunications which will offer access to all kinds of information services at a reasonable cost at any place and time. Cellular and cordless telephony as well as wireless data for wide or local area services can be considered as a first step in this direction. Recent overviews of wireless personal communications are given in [1, 2]. Furthermore, an excellent in-depth treatment and overview of wireless communication systems can be found in books such as [3, 4, 5, 6, 7, 8].

A deep knowledge of the radio propagation phenomena or the radio channel characteristics is a prerequisite to achievement of the optimum system design. The performance of wireless communication systems is limited by the intermittent power losses, or "deep fades", associated with the fading channel [9, 10, 11, 12, 13]. The transmission path between the transmitter and the receiver can include reflections by terrain configuration and the man-made environment. Therefore, the fading sig-

nal results from interference between several scattered signals and perhaps the direct signal [3, 14, 15, 16]. Propagation studies in a variety of environments show that the multipath signal consists primarily of a small number of discrete sinusoidal components (often 10 or fewer). The superposition of these components changes rapidly as the vehicle moves, producing the familiar fast-fading signal envelope observed in practice. However, the amplitude, frequency and phase of each component change on a much slower time scale, e.g. on the order of 100 times the coherence time of the signal envelope. This variation is slow enough that the fading coefficient can be predicted far beyond the coherence time. In particular, these estimates can be used to *forecast signal fades before they occur.*

Consider a low-pass complex model of the received signal:

$$r(t) = c(t)s(t) + n(t), \tag{1.1}$$

where $c(t)$ is the flat fading coefficient (multiplicative), $s(t)$ is the transmitted signal, and $n(t)$ is additive white Gaussian noise (AWGN).

Let the transmitted signal be $s(t) = \sum_k b_k g(t-kT)$, where b_k is the data sequence, $g(t)$ is the transmitter pulse shape, and T is the symbol delay. At the output of the matched filter and sampler, the discrete-time system model is given by

$$y_k = c_k b_k + z_k, \tag{1.2}$$

where c_k is the fading signal $c(t)$ sampled at the symbol rate, and z_k is a complex discrete AWGN process with variance $N_0/2$. Usually, $c(t)$ and c_k are modeled as correlated complex Gaussian random processes with Rayleigh distributed amplitudes and uniform phases [5, 16]. The expressions for the autocorrelation function and the power spectral density of the flat fading signal are also widely used in practice [16, 17, 18].

Several adaptive channel estimation methods have been developed by using this statistical description to estimate rapidly varying fading coefficients (e.g. [19, 20, 21, 22, 23, 24, 25, 26, 27, 28, 29, 30, 31]). For example, the minimum mean square error (MMSE) estimate using the Kalman filter is usually found by constructing a Gauss-Markov model of the fading [31]. In this model, the mean square error is given by the variance of the excitation noise. This error grows as the Doppler shift increases and limits the performance of the detector. Furthermore, the bit error rate (BER) approaches the saturation level (error floor) as the signal-to-noise ratio (SNR) increases. More recently, estimating the fading signal by decomposing it along a deterministic basis was addressed in [32, 33, 34]. In addition, these algorithms do not address the most serious limiting factor in communication over fading channels. Although the estimation error causes performance degradation, it is not the most serious limiting factor in communication over fading channels. The greatest BER loss and the associated high power requirements result from "deep fades" in the fading signal. Therefore, it is desirable to predict deep fades, and, in general, fading variations and compensate for the expected power loss at the transmitter. Therefore, we address the *long range* prediction of the variations in c_k [14, 15, 35, 36, 37, 38, 39]. By prediction we imply estimating an entire future block of coefficients c_k based on the observation of the received signal during an earlier time interval. This task is not feasible with current Kalman filtering and other adaptive channel estimation techniques, which can predict only one coefficient at a time, and require observation of the received sample to produce this estimate. We describe the prediction algorithm which characterizes the channel as an autoregressive model (AR) with low sampling rate, and computes the MMSE estimate of the future fading coefficient sample based on a number of past observations. This algorithm can reliably predict future fading

coefficients far beyond the coherence time for a fading channel with an arbitrary number of scatterers.

The other traditional approach to coping with fading is to use diversity (e.g., antenna arrays, additional bandwidth, interleaving) to average signal power fluctuations over space, time, or frequency [3, 4, 5, 7]. However, diversity gains come at the cost of additional antenna elements, increased delay, or expanded bandwidth. Moreover, because the channel changes rapidly, the transmitter and receiver are not generally optimized for current channel conditions, and thus fail to exploit the full potential of the wireless channel. The shorter wavelengths proposed for future mobile radio will only serve to aggravate these problems. This research outlines a new approach to communication over fast-fading channels. The unifying idea is to predict future fading conditions using the physics of mobile radio propagation prior to transmission and to use these predictions as the basis for new communication techniques that adapt to current conditions. In particular, the timing of future "deep fades" would be revealed and the variations in the received signal power could be compensated. This long range prediction capability for fading channels would provide enabling technology for accurate power control, reliable transmitter and/or receiver diversity, more effective adaptive modulation and coding and improvements in many other components of wireless systems. The ultimate goal of this work is to more fully exploit the potential capacity of wireless communication channels, and in the process reduce the associated power and bandwidth requirements. Moreover, while this method is resulting in accurate prediction of future channel coefficients, it does not introduce significant complexity increase relative to present communication techniques for fading channels.

This thesis is organized as follows: The propagation models and fading in Wireless Communication Systems are explained in Chapter 2. The signaling effects on the

channel model is discussed with the emphasis on the both flat and frequency-selective fading channels. The deterministic fading channel model used in this research is also introduced in this Chapter. In Chapter 3, the techniques which are used to resolve the interference pattern and to predict fading coefficients are developed for the flat fading channels. The system model, both the analytical and the simulation results, and the performance measures are discussed in this chapter. Then, in Chapter 4, we extend our results for the frequency-selective case which introduces intersymbol interference (ISI) to the system. The estimation of the channel impulse response is investigated by using pilot signaling. Then, we demonstrated the feasibility of the long range prediction of the channel impulse response of the frequency selective fading channels by using these estimated channel impulse response coefficients. Two different approaches used for the long range prediction are also discussed in this section. Furthermore, in this Chapter, the theoretical matched filter bounds for the generalized frequency selective fading channel with arbitrary path strengths and delays are derived and used as a reference performance bound for the analysis. We also demonstrated that how the novel long range prediction technique enables enhanced adaptive equalization techniques to combat ISI both at the receiver and at the transmitter. The antenna diversity systems are inseparable with the proposed research for the optimum system performance. Therefore, we address antenna diversity both at the transmitter and at the receiver in Chapter 5. Both theoretical and the practical implementation issues are investigated. Application of the novel long range prediction to the Selective Transmitter Diversity technique for future generation wireless system is studied in this chapter. Finally, we complete the thesis by conclusions, impacts and future direction of our research in Chapter 6.

Chapter 2

Propagation Modeling and Fading

In this chapter, we will review characteristics of fading channel to understand the terminology used in this thesis.

2.1 Long-term Fading vs Short-term Fading

It is common to observe significant variations in the amplitude and the phase of the received signal, known as fading. Based on what we know about the cause of signal fading, the Cellular Mobile Radio (CMR) channel is characterized either in *long-term* or *short-term* statistics [3, 5, 6, 9, 11, 13].

Long-term propagation models focus on predicting the average received signal strength at a given distance from the transmitter. Predicting the mean signal strength for an arbitrary distance between the transmitter and the receiver is useful in estimating the coverage area of a transmitter. (For example, long-term fading describes signal strength variations which arise when the mobile is obscured by terrain configuration, such as hills and mountains.) This fading is rather slowly varying. Once behind the mountain, the channel will not change much until the mobile leaves the vicinity of the mountain. This typically takes several minutes.

On the other hand, short-term propagation models characterize the rapid fluctu-

ations of the received signal strength over very short travel distances (a few wavelengths) or a short time durations (on the order of seconds). As a mobile moves over very small distances, the instantaneous received signal strength fluctuates rapidly causing short-term fading. The reason for this is that the received signal is a sum of many contributions coming from different directions by local scatterers, such as houses, buildings and cars surrounding a mobile unit.

The envelopes of the long-term and the short-term fading channels are usually modeled by a log-normal distribution and a Rayleigh distribution (Rice distribution if there exists a direct path between the base station and the mobile unit), respectively. In this work, we only considered short-term fading. In the next section, we discuss the parameter used to define the characteristics of short-term fading.

2.2 Fading Parameters

If a pulse is transmitted over a time-varying multipath channel, the received signal might appear as a train of pulses. Hence, one characteristic of a multipath channel is the time spread introduced in the received signal. A second characteristic is the time variation of the multipath. Such time variations include changes in the values of individual pulses, in the relative delays among the pulses, and in number of pulses observed. Let's consider the transmitted signal $s(t)$ represented by

$$s(t) = Re[u(t)e^{j2\pi f_c t}], \tag{2.1}$$

where $u(t)$ is the equivalent lowpass signal transmitted over the channel and f_c is the carrier frequency. Assuming N propagation paths with different propagation delays, $\tau_n(t)$, and attenuation factors, $\alpha_n(t)$, $n = 1 \cdots N$, the received bandpass signal is

expressed in the form

$$x(t) = \sum_{n=1}^{N} \alpha_n(t) s(t - \tau_n(t)) \tag{2.2}$$

Substituting (2.1) into (2.2) yields the equivalent lowpass received signal [5]

$$r(t) = \sum_{n=1}^{N} \alpha_n(t) e^{-j2\pi f_c \tau_n(t)} u(t - \tau_n(t)). \tag{2.3}$$

Then the equivalent lowpass channel is described by the time-variant impulse response

$$c(\tau; t) = \sum_{n=1}^{N} \alpha_n(t) e^{-j2\pi f_c \tau_n(t)} \delta(t - \tau_n(t)) \tag{2.4}$$

where $c(\tau; t)$ represents the response of the channel at time t due to an impulse applied at time $t - \tau$.

When there are a large number of closely time-spaced propagation paths in the medium, the time-variant impulse response $c(\tau; t)$ can be modeled as a complex-valued gaussian random process in the t variable. Then, by the central limit theorem, the real and imaginary parts of c, c_I and c_Q, are independent, zero-mean Gaussian random processes [1] [5, 7, 9, 16]

$$c = c_I + j c_Q = \alpha e^{j\theta}. \tag{2.5}$$

The components c_I and c_Q are described by the bivariate Gaussian distribution with probability density function (pdf) of

$$p(c_I, c_Q) = \frac{1}{2\pi\sigma^2} e^{-\frac{c_I^2 + c_Q^2}{2\sigma^2}} \tag{2.6}$$

[1] the time dependence of channel impulse response is implicit.

where the mean power (or variance), σ^2, of the channel impulse response is

$$\sigma^2 = \frac{1}{2}E[|c|^2] \tag{2.7}$$

Moreover, it follows that the channel impulse response's envelope, α, phase, θ, and instantaneous power, $|c|^2 = \alpha^2$, have Rayleigh, uniform and exponential distributions, respectively

$$p(\alpha) = \frac{\alpha}{\sigma^2}e^{-\frac{\alpha^2}{2\sigma^2}}, \qquad 0 \leq \alpha < \infty \tag{2.8}$$

$$p(\theta) = \frac{1}{2\pi}, \qquad 0 \leq \theta \leq 2\pi \tag{2.9}$$

$$p(\alpha^2) = p(|c|^2) = \frac{1}{2\sigma^2}e^{-\frac{|c|^2}{2\sigma^2}}, \qquad 0 \leq |c|^2 < \infty \tag{2.10}$$

In order to define the characteristics of fading multipath channels some special correlation functions and power spectral density functions are used. The equivalent lowpass impulse response $c(\tau; t)$ is assumed to be complex-valued, zero mean, gaussian random process in the t variable, and wide-sense-stationary. Letting $t = 0$, the resulting autocorrelation function $\phi_c(\tau; 0) = \phi_c(\tau)$ is simply the average power output of the channel as a function of time delay τ. For this reason, $\phi_c(\tau)$ is called the *multipath intensity profile*. The range of values of τ over which $\phi_c(\tau)$ is essentially nonzero is called the *multipath spread*, T_m, of the channel. The shape and duration of the multipath intensity profile play an important role in determining the performance of the signaling and detection schemes to be investigated.

Time-varying multipath channels are also characterized completely in the frequency domain. By taking the Fourier Transform of $c(\tau)$ with respect to delay τ, we obtain the time-variant transfer function $C(f) = F[c(\tau)]$. Therefore, the correspond-

ing autocorrelation function is defined as

$$\phi_C(\Delta f) = F[\phi_c(\tau)]. \tag{2.11}$$

Furthermore, the $\phi_C(\Delta f; \Delta t)$ is called *spaced-frequency spaced-time correlation function* of the channel [5]. Since $\phi_C(\Delta f)$ is an autocorrelation function in the frequency variable, it provides us with a measure of the frequency coherence of the channel. Hence, the reciprocal of the multipath spread, T_m, is a measure of the *coherence bandwidth* of the channel:

$$(\Delta f)_c \approx \frac{1}{T_m} \tag{2.12}$$

The time variations of the channel are also very important because they affect the adaptive requirements and performance of any adaptive detection scheme. The *Doppler power spectrum* is defined as [5]

$$S_C(f_d) = F[\phi_C(\Delta t)]. \tag{2.13}$$

The function $S_C(f_d)$ gives the signal intensity as a function of Doppler frequency f_d. Note that, if the channel is time-invariant, i.e., $\phi_C(\Delta t) = 1$ and $S_C(f_d) = \delta(f_d)$, then the signal will not experience any spectral broadening or Doppler shift.

The range of values of f_d over which $S_C(f_d)$ is essentially nonzero is called the *Doppler spread*, B_d, of the channel. The reciprocal of B_d is a measure of the coherence time of the channel. That is,

$$(\Delta t)_c \approx \frac{1}{B_d} \tag{2.14}$$

where $(\Delta t)_c$ denotes the *coherence time*. A channel which changes slowly has a large coherence time and, equivalently, a narrow Doppler spread. This situation is highly desirable for adaptive receivers.

2.2.1 Doppler Shift

For mobile communications case where the mobile receiver travels through the standing wave propagation pattern of the channel, the fading nature of the received signal at the mobile can be quantified by Doppler frequency [3, 6, 9, 16]

$$f_d = f_c(\frac{v}{c})\cos\phi \tag{2.15}$$

where f_c is the carrier frequency, v is the speed of mobile, c is the speed of light, ϕ is the incident angle of signal reception. Note that, Doppler frequency is maximum when $\cos\phi$ is $+1$ or -1. Signals arriving from the direction of motion will experience a positive Doppler shift, while those arriving opposite from the direction of motion will experience a negative Doppler shift. Consequently, multipath components which arrive different directions contribute to Doppler spreading of the received signal, thus increasing the signal bandwidth.

2.2.2 Flat vs Frequency Selective Fading

Let $u(t)$ be the equivalent lowpass signal transmitted over the channel and let $U(f)$ denote its frequency content. The equivalent lowpass received signal, without noise is given by [5]

$$\begin{aligned} r(t) &= \int_{-\infty}^{\infty} c(\tau;t)u(t-\tau)d\tau \\ &= F^{-1}[C(f;t)U(f)] \end{aligned} \tag{2.16}$$

Suppose we are transmitting digital information at rate $1/T$, where T is the signaling interval. Clearly $U(f)$ is distorted by $C(f;t)$. When the coherence bandwidth, $(\Delta f)_c$ is small relative to the bandwidth of the transmitted signal, W, $U(f)$ suffers

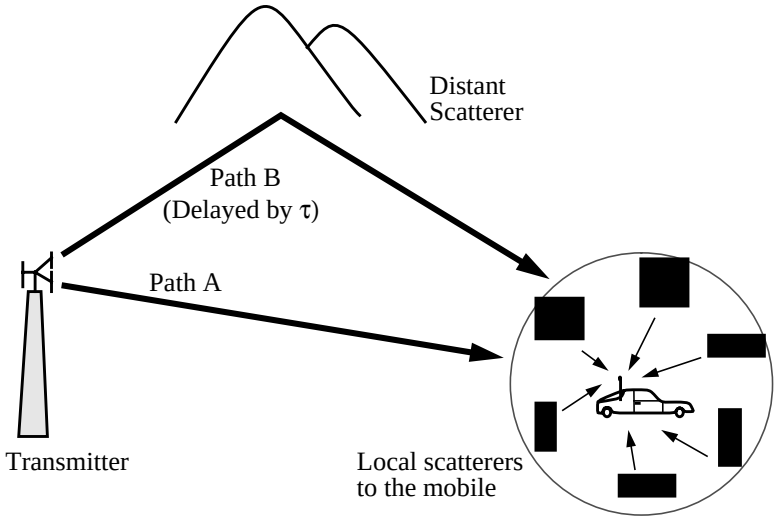

Figure 2.1: Typical multipath environment

frequency selective distortion and the channel is said to be *frequency selective*. When $(\Delta f)_c$ is large relative to the signal bandwidth, the channel is said to be *flat fading* or *frequency nonselective*.

In other words, the multipath spread, T_m, is relatively small compared to the signaling interval, T, the channel is considered flat fading. For example, in North American Cellular System standards the signaling interval, T is 40 μsec. Assuming the local scatterers around the mobile is in 1 mi radius, the corresponding multipath Spread is around 4 μsec which is one tenth of the signaling interval. Therefore, actual systems are mostly considered flat. However, there are sometimes very distance scatterers, such as a mountain or a hill. These act as another transmitter and the signal comes to the receiver with a delay, τ, comparable to symbol interval, T, as seen in Figure 2.1. Therefore, the delayed received signal causes intersymbol interference (ISI) and channel is considered frequency selective. On the other hand, we can use the frequency selectivity of the channel into our advantage by using a matched filter

(MF) utilizing the channel as a diversity channel as explained in Chapter 4. The MF should be followed by an equalizer to combat ISI.

2.2.3 Fast vs Slow Fading

$U(f)$ also suffers fading distortion because of the time variations in $C(f;t)$. Depending on how rapidly the transmitted signal as compared to the rate of change of the channel, a channel may be classified either as a *fast fading* or *slowly* fading channel. If the signaling interval, T, is greater than the coherence time, $(\Delta t)_c$, the channel is said to be *fast fading channel*. That is the channel impulse response changes rapidly within the symbol duration. This causes frequency dispersion (also called time-selective fading) due to Doppler spreading, which leads to a signal distortion. It should be noted when a channel is specified as a fast or slowly fading channel, it does not specify whether the channel is fat fading or frequency selective in nature. Fast fading only deals with the rate of change of the channel due to motion of the mobile unit.

Otherwise, when $(\Delta t)_c$ is large relative to the signaling interval, the channel is said to be a *slowly fading channel*. In this case the channel impulse response changes at a rate much slower rate than the transmitted signal. Therefore, the channel may be assumed to be static over one or several reciprocal bandwidth intervals. In the frequency domain this implies that the Doppler spread of the channel is much less than the bandwidth of the signal, W.

2.3 The Jakes Fading Channel Model

The Jakes fading model is a deterministic method for simulating time-correlated Rayleigh fading wireless communication channels. The model was originally formu-

lated by Jakes in 1974 [16] and is widely used today. The model has been slightly reformulated in order to ensure multiple uncorrelated waveforms [17]. One of the advantages of using Jake's method is that the autocorrelation and, hence, the power spectral density (psd) of the inphase and quadrature components of the received signal can be generated to reflect an isotropic scattering environment, with a simulator of reasonable complexity [4].

The Original Jakes Model

Doppler fading occurs in Cellular Mobile Radio (CMR) communications due to vehicular motion. Real and imaginary components of the channel impulse response (CIR) are independent, zero-mean, Gaussian random processes. This corresponds to a CIR whose envelope, phase, and instantaneous power have Rayleigh, uniform and exponential distributions, respectively [7, 9, 16]. Moreover the CMR channel is characterized at baseband by the autocorrelation function, $r(\Delta t)$, and the baseband power spectrum , $S(f_d)$, [16, 18]

$$r(\Delta t) \propto J_0(2\pi f_{dm}\Delta t) \tag{2.17}$$

$$S(f_d) \propto \begin{cases} [1-(\frac{f_d}{f_{dm}})^2]^{-\frac{1}{2}} & |f_d| \leq f_{dm} \\ 0 & |f_d| > f_{dm} \end{cases} \tag{2.18}$$

where $J_0()$ is the zeroth-order Bessel function of first kind, f_d is the Doppler frequency, f_{dm} is the maximum Doppler frequency, and Δt is the time difference.

The Jakes fading model uses a sum of weighted oscillators with discrete frequencies spanning the Doppler spectrum. First, the model assumes there are N equal strength rays arriving at a moving receiver with uniformly distributed arrival angles, α_n. This assumption places the arrival angles at

$$\alpha_n = \frac{2\pi n}{N}, \quad 1 \leq n \leq N \tag{2.19}$$

The ray n would then experience a Doppler shift of

$$\omega_n = 2\pi f_{dm} \cos(\alpha_n) = \omega_{dm} \cos(\alpha_n) \tag{2.20}$$

where the maximum Doppler shift ω_{dm} is given by

$$\omega_{dm} = \frac{2\pi f_c v}{c} \tag{2.21}$$

where f_c is the carrier frequency, v is the vehicle speed, and c is the speed of light. Note that using the definition for α_n given above, the magnitudes of the Doppler shifts possess quadrantal symmetry except at the angles 0 and π. Due to this quadrantal symmetry we see that we can model the fading waveform with $N_0 + 1$ complex oscillators where

$$N_0 = \frac{\frac{N}{2} - 1}{2} \tag{2.22}$$

The $(N_0 + 1)^{st}$ complex oscillator has the frequency ω_{dm} and is used for the purpose of frequency shifting from the carrier.

The in-phase and quadrature components are derived from the oscillators by summing the outputs of the available individual oscillators multiplied by proper gain factors. The in-phase and quadrature components appear as

$$X_i(t) = 2 \sum_{n=1}^{N_0} \cos \beta_n \cos \omega_n t + \sqrt{2} \cos \alpha \cos \omega_{dm} t \tag{2.23}$$

$$X_q(t) = 2 \sum_{n=1}^{N_0} \sin \beta_n \cos \omega_n t + \sqrt{2} \sin \alpha \cos \omega_{dm} t \tag{2.24}$$

Consequently, we get the final output waveform to be of the form

$$C(t) = K\left[\frac{1}{\sqrt{2}}[\cos\alpha + j\sin\alpha]\cos(\omega_{dm}t + \theta_0) + \sum_{n=1}^{N_0}[\cos\beta_n + j\sin\beta_n]\cos(\omega_n t + \theta_n)\right] \tag{2.25}$$

Jakes selects $\alpha = 0$ and chooses simple selections for β_n and $\theta_{n,j}$:

$$\beta_n = \frac{\pi n}{N_0 + 1} \tag{2.26}$$

$$\theta_{n,j} = \beta_n + \frac{2\pi(j-1)}{N_0 + 1}, \tag{2.27}$$

where $j = 1$ to N_0 is the waveform number index.

With this model, the use of large number of weighted oscillators leads to a more accurate Rayleigh fading model. It has been shown that Rayleigh fading can be accurately simulated with this method using just nine ($N_0 = 8$) discrete oscillators [16, 18]. However, the autocorrelation tends to deviate from the desired values at large lags. This can be improved upon by increasing the number of oscillators that are used in the simulator [4].

The Modified Jakes Model

The original Jakes channel model is a good approximation of the nature of Rayleigh fading channels. However, when the user attempts to generate multiple uncorrelated waveforms, correlations between some of the generated waves can be significant. Dent, Bottomley, and Croft proposed a remedy for this problem by a slight reformulation of the original model [17].

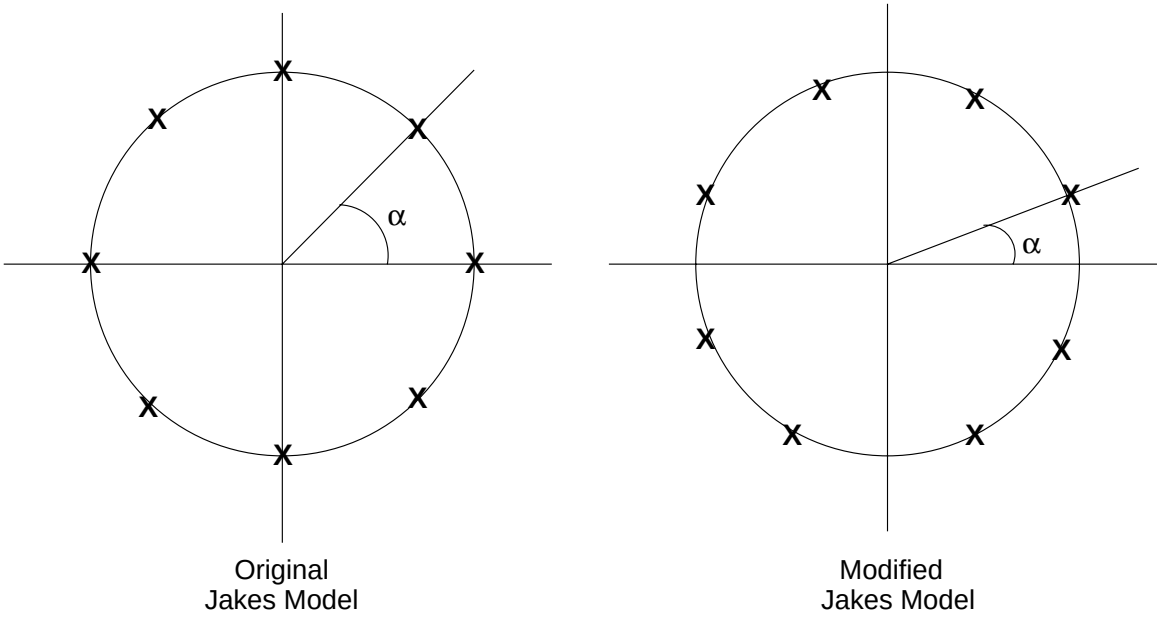

Figure 2.2: Arrival Angles at the Mobile Receiver

The modification of the model involves revisiting the original definition of the uniformly distributed arrival angles, α_n. Figure 2.2 shows the differences in the arrival angles between the original model and the reformulation. The original Jakes definition of α_n was given by equation (2.19). The Jakes α_n's possessed quadrantal symmetry except at the angles 0 and π. Dent, Bottomley, and Croft redefined α_n such that

$$\alpha_n = \frac{2\pi(n - 0.5)}{N} \quad 1 \leq n \leq N, \tag{2.28}$$

thus providing quadrantal symmetry for all of the Doppler shifts. Following a derivation similar to Jakes, they arrived at a model of the form

$$C(t) = \sqrt{\frac{2}{N_0}} \sum_{n=1}^{N_0} [\cos \beta_n + j \sin \beta_n] \cos(\omega_n t + \theta_n)] \tag{2.29}$$

This formulation of the model simplifies β_n further to

$$\beta_n = \frac{\pi n}{N_0} \tag{2.30}$$

These values for β_n cause the real and imaginary parts of $C(t)$ to be uncorrelated and of equal power. The definition of θ_n has also been changed. Previously, it was given by (2.27). In the reformulation θ_n is randomized in order to provide the different waveform realizations. Note that the normalization factor has been selected to be $\sqrt{\frac{2}{N_0}}$ in order to obtain $E[C(t)C^*(t)] = 1$.

The next problem of interest was to provide the capability of simulating multiple uncorrelated waveforms. This objective was achieved by multiplying the oscillator coefficients by an orthogonal vector set such that the inner product terms became zero. We now have a model that produces multiple uncorrelated waveforms with the jth waveform given by

$$T(t) = \sqrt{\frac{2}{N_0}} \sum_{n=1}^{N_0} A_j(n)[\cos\beta_n + j\sin\beta_n]\cos(\omega_n t + \theta_n)] \tag{2.31}$$

$A_j(n)$ represent the Walsh-Hadamard codewords that have ± 1 values. The Walsh-Hadamard transform was selected for this reformulation due to the relative ease of generating these codewords through a Fast Walsh Transform [40].

2.4 The Deterministic Fading Channel Model

The fading signal results from interference between several scattered signals. Our approach to prediction of future fading is based upon estimates of the important scatterers – their relative phases, direction and amplitudes. To understand the physical origin of how one can predict the fading signal, we must look at the process from two

different frames of reference [14, 15]. The first picture is from the point of view of the ground. We will assume all scatterers are stationary and the receiver moves. Then, all frequencies are the same (no Doppler shifts in this frame) and an interference pattern results. The receiver passes through this interference pattern. The positions of destructive interference are the deep fades. What we learn from this picture is the expected length scale between the deep fades – on the order of the wavelength, and therefore from the speed of the receiver the time between deep fades. We also can use this picture to estimate the types of scatterers which will produce sufficient intensity to create significant interference, and the spatial distribution of such interference. A different physical picture of the interference pattern derives from the frame of reference of the mobile rather than the ground. From the point of view of the mobile, the fading coefficient at the receiver is given by a sum of N Doppler shifted signals [16]

$$c(t) = \sum_{n=1}^{N} A_n e^{j(2\pi f_n t + \phi_n)} \tag{2.32}$$

where (for the n^{th} scatterer) A_n is the amplitude, f_n is the Doppler frequency, and ϕ_n is the phase. As described earlier, the Doppler frequency is given by

$$f_n = f_c \left(\frac{v}{c}\right) \cos \alpha_n \tag{2.33}$$

where f_c is the carrier frequency, v is the speed of mobile, c is the speed of light, and α_n is the incident angle relative to the mobile's direction. Due to multiple scatterers, the fading signal varies rapidly for large vehicle speeds and undergoes "deep fades" [3, 5]. In Figure 2.3, we can observe the time variations of the power of Rayleigh fading channel and the "deep fades" for max Doppler frequency of 100 Hz. The complex Gaussian distribution of the fading signal (the Rayleigh fading) is derived based on

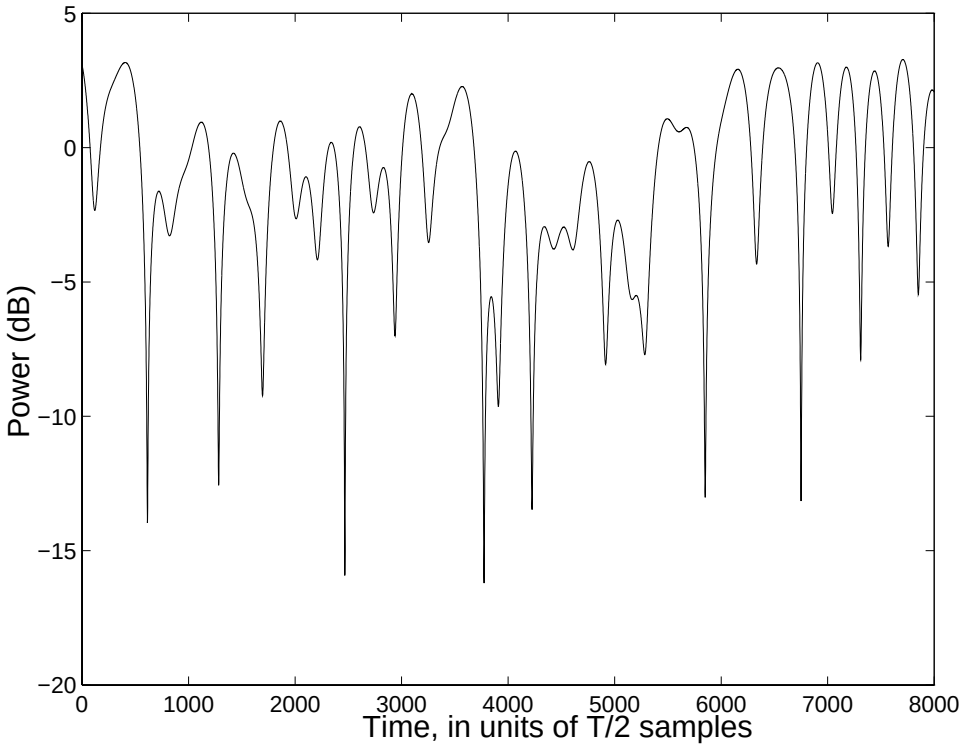

Figure 2.3: Time variations of the power of Rayleigh fading channel for max Doppler frequency of 100 Hz

the assumption that the scattered signals are distributed uniformly around the mobile, and that there is a continuum of scatterers [16]. Although the exact derivation of the Rayleigh fading distribution requires this assumption, it has been demonstrated that the Rayleigh fading signal can be closely approximated by a relatively small number number of scatterers. For example, as explained earlier in the popular deterministic Jakes model, as few as nine scatterers can be used to model Rayleigh fading characteristics [16]. Physical evidence suggest that the actual number of significant scattered signals is modest [15]. All significant scatterers must have an amplitude similar to that of the most powerful signal, otherwise their interference effects will

be negligible. Such signals will result from specular (mirror-like) scattering from the ground, water, buildings or perhaps vehicles [3, 41, 42]. Trees and vegetation tends to absorb the signal so they will not be important in this analysis [41, 42, 43]. Since the specular reflection occurs close to a specific geometry and scattering efficiencies are small enough [41, 44] that multiple scattering effects are greatly reduced, only a few scatterers are expected, as confirmed by observations [45]. Propagation studies also show that the number of significant scatterers is modest, usually not more than twenty [46, 47]. The use of model scatterers is justified by the application of superposition. If we have a complicated scatterer, we can represent it as the sum of simple ones. Therefore, we consider only simple scatterers in our examples. The assumption of small number of scatterers was also made in promising work on fading channel estimation presented in [27, 32, 33]. However, our prediction method is not limited by the number of scatterers and it can handle up to thousands of significant scatterers as explained in the next chapter. More on the physical modeling can be found in [48, 49, 50, 51, 52]

In this research, we demonstrate the feasibility of long range prediction of the rapidly varying fading signal, c_k (1.2). If the parameters such as amplitude, A_n, frequency, f_n, and phase, ϕ_n, in (2.32) for each of the scatterers were known and remained constant, the fading channel could be predicted indefinitely. In practice, they vary much slower than the actual rapidly varying fading coefficient $c(t)$ and are not known *a priori*. Since we consider short term fading, the propagation characteristics will not change significantly during any given block, and we can safely assume these parameters are approximately constant or change very slowly for the duration of the data block. These slow changes can easily be tracked adaptively both at the receiver and the transmitter [36]. In the next chapter, the novel long range prediction tech-

nique and its implementation enabled by lower sampling rate will be explained and the performance results will be discussed for both the transmitter and the receiver.

Chapter 3

Performance Results for Flat Fading Channel

3.1 Prediction of the Flat Fading Channel

Consider a low-pass complex model of the received signal:

$$y(t) = c(t)s(t) + n(t), \tag{3.1}$$

where $c(t)$ is the flat fading coefficient (multiplicative), $s(t)$ is the transmitted signal, and $n(t)$ is additive white Gaussian noise (AWGN).

Let the transmitted signal be $s(t) = \sum_k b_k g(t - kT)$, where b_k is the data sequence ($b_k \in \{+1, -1\}$), $g(t)$ is the transmitter pulse shape, and T is the symbol delay. At the output of the matched filter and sampler, the discrete-time system model is given by

$$y_k = c_k b_k + z_k, \tag{3.2}$$

where c_k is the fading signal $c(t)$ sampled at the symbol rate, $\mathrm{E}|c_k|^2 = 1$, and z_k is a complex discrete AWGN process with variance $N_0/2$. Usually, $c(t)$ and c_k are modeled as correlated complex Gaussian random processes with Rayleigh distributed amplitudes and uniform phases [5, 16]. Several adaptive channel estimation methods have been developed by using this statistical description to estimate rapidly varying

fading coefficients (e.g. [19, 20, 21, 22, 23, 24, 25, 26, 27, 28, 29, 30, 31]). However, the performance of these methods degrades when the fading rate increases due to large estimation error. More recently, estimating the fading signal by decomposing it along a deterministic basis was addressed in [32, 33, 34]. In contrast, our work focuses on predicting the future behavior of the fading coefficient, rather than estimating its current value. Of course a current estimate of $c(t)$ can serve to predict its behavior over a time period sufficiently small such that $c(t)$ is not expected to change significantly. A common measure of this time period is the coherence time as defined in Chapter 2. However, even prediction for this time interval is challenging when previously proposed methods are used. The key novelty of our approach is to accurately predict $c(t)$ over a much longer time scale, by exploiting the fact that $c(t)$ consists of a small collection of sinusoidal components as explained in Section 2.4. Recalling from that section, the fading coefficient at the receiver is given by a sum of N Doppler shifted signals [16]

$$c(t) = \sum_{n=1}^{N} A_n e^{j(2\pi f_n t + \phi_n)} \tag{3.3}$$

where (for the n^{th} scatterer) A_n is the amplitude, f_n is the Doppler frequency, and ϕ_n is the phase. Also, as described earlier, the Doppler frequency is given by

$$f_n = f_c \left(\frac{v}{c}\right) \cos \alpha_n \tag{3.4}$$

where f_c is the carrier frequency, v is the speed of mobile, c is the speed of light, and α_n is the incident angle relative to the mobile's direction. Note that, the Doppler frequency is maximum when $\cos(\alpha_n) = 1$ or -1, i.e., $\alpha_n = 0$ or π. For example, in North American cellular system standards, the carrier frequency, $f_c = 900$ MHz. Therefore,

in this environment, a car traveling 80 mph experiences a maximum Doppler frequency, f_{dm} around 100 Hz.

In practice, the Doppler shifts are not known. Therefore, we address the *deterministic* prediction of the variations in c_k. By prediction we imply estimating an *entire* future block of coefficients c_k based on the observation of the received signal during an earlier time interval. To predict the fading signals (3.2) and (3.3), we employ linear prediction followed by interpolation as explained below.

3.1.1 Linear Prediction and Performance Analysis

Estimation of the power spectral density of discretely sampled deterministic and stochastic processes is usually based on procedures employing the Discrete Fourier Transform (DFT) [53]. Although this technique for spectral estimation is computationally efficient, there are some performance limitations of this approach. The most important limitation is that of frequency resolution. The frequency resolution ($\Delta f = f_s/K$) of the K-point DFT algorithm, where f_s is the sampling frequency, limits the accuracy of estimated parameters. These performance limitations cause problems especially when analyzing short data records. Therefore, many alternative Spectral Estimation Techniques have been proposed within the last three decades in an attempt to alleviate the inherent limitations of the DFT technique [53, 54, 55].

Our linear prediction (LP) method is based on the Autoregressive (AR) channel modeling. This method is also known as the All-poles Model and is widely used for spectral estimation. The reason why we chose this technique is that the it has very nice advantage of fitting sharp spectral features as we have in our fading channel due to scatterers (3.3). Furthermore, it is closely tied to Linear Prediction (LP) which we use to predict future channel coefficients. The frequency response of the AR channel

modeled is given as:

$$H(z) = \frac{1}{1 - \sum_{j=1}^{p} d_j z^{-j}}. \tag{3.5}$$

where d_j coefficients are obtained by minimizing mean squared error (MSE), min $\mathrm{E}|\hat{c}_n - c_n|^2$, and are provided by well-known Yule-Walker equations in the vector form

$$\boldsymbol{d} = \boldsymbol{R}^{-1}\boldsymbol{r} \tag{3.6}$$

where $\boldsymbol{R}$ is the autocorrelation matrix of size $p \times p$ and with the elements defined as $R_{ij} = \mathrm{E}[c_{n-i}c^*_{n-j}]$. Similarly, $\boldsymbol{r}$ is the autocorrelation vector of size $p \times 1$ and with the elements defined as $r_j = \mathrm{E}[c_n c^*_{n-j}]$. This model is obtained based on a block of samples of the fading process. Note that the samples have to be taken at least at the Nyquist rate which is twice the maximum Doppler frequency, f_{dm}. Moreover, the accuracy of the model depends on the number of samples in the given block which limits the model order, p.

The d_j coefficients in (3.5) are also the linear prediction coefficients. The estimates of the future samples of the fading channel can be determined as:

$$\hat{c}_n = \sum_{j=1}^{p} d_j c_{n-j}, \tag{3.7}$$

Note that $\hat{c}_n$ is a linear combination of the values of c_n over the interval $[n-p, n-1]$. By Central Limit Theorem (CLT), since c_n has complex Gaussian distribution, $\hat{c}_n$ has also complex Gaussian distribution. Furthermore, if $\hat{c}_n$ is a unbiased estimate of c_n, i.e., $\sum_{j=1}^{p} d_j = 1$, then $E(\hat{c}_n) = E(c_n)$. Also note that the channel sampling rate utilized for LP is much lower than the symbol rate, $1/T$. Therefore, to predict the fading coefficients, c_k, from (3.2), associated with transmitted symbols, interpolation is employed. Interpolation will be discussed later in this chapter. To date, most

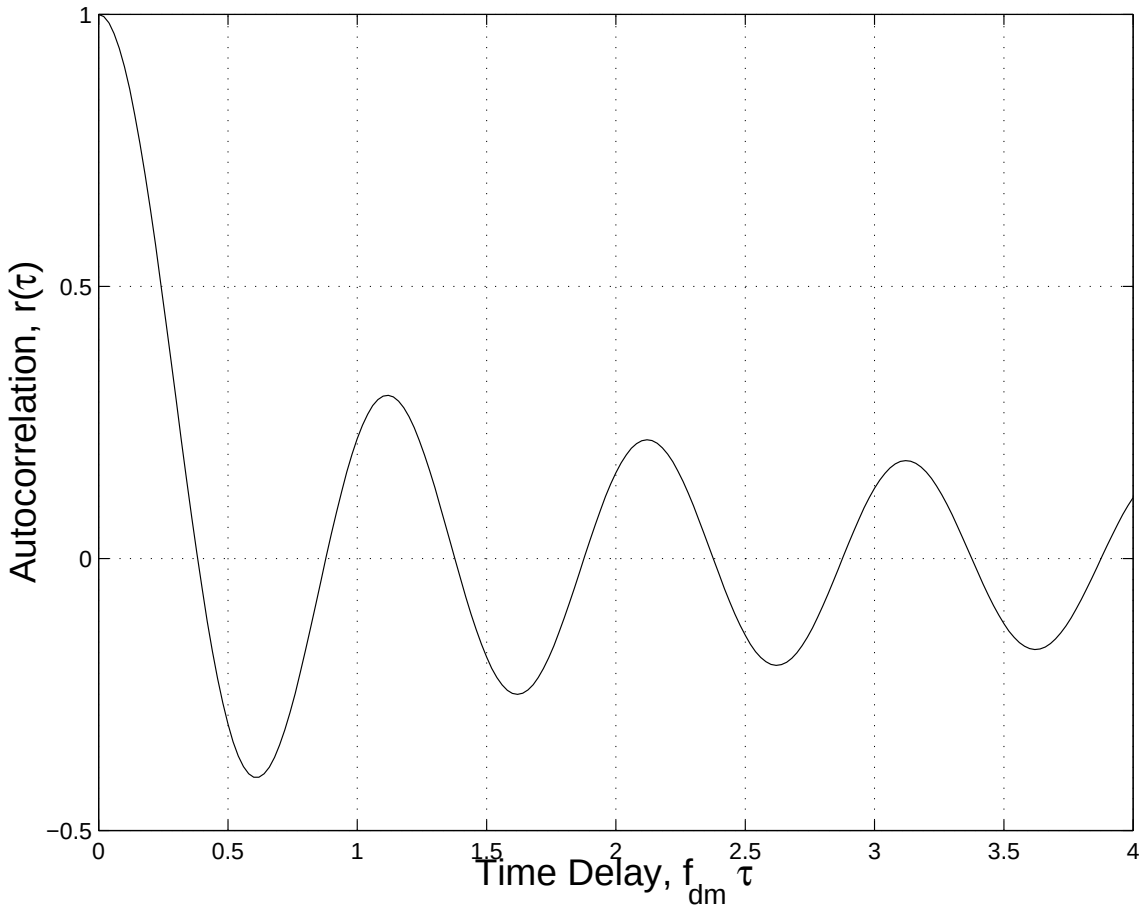

Figure 3.1: The theoretical autocorrelation function for the Rayleigh fading channel

investigations of fading channel modeling and estimation assume sampling at the data rate (e.g., [20]). As a result, even with very accurate coefficient adjustment, it is impossible to specify future channel coefficients from past observations - the filter length is not long enough. This can be illustrated by considering the parameters involved in the MMSE prediction.

We start with the case when N in (3.3) is infinite (Rayleigh fading), although the discussion below also applies to the more practical case of a modest number of

scatterers with the underlying channel parameters varying slowly. The channel is modeled as the complex stationary Gaussian process with the normalized autocorrelation function

$$r(\tau) = J_0(2\pi f_{dm}\tau) \tag{3.8}$$

where $J_0(.)$ is the zero-order Bessel function of the first kind [16]. The plot of this function is shown in Figure 3.1. For illustration, let us fix the maximum Doppler frequency at 100 Hz. Then the low sampling rate of 500 Hz would correspond to 5 samples/unit of the $x-$axis of Figure 3.1, whereas the data rate of 25 KHz results in 250 samples/unit. When the model order p in (3.7) is fixed, the observation samples taken at the low sampling rate span much larger time interval than the samples at the data rate. This translates into exploitation of the sidelobes of the autocorrelation function in the prediction [36, 37] and lower MMSE when low rate sampling is employed.

This observation can be quantified by considering a general channel prediction problem. For a given sampling rate $1/T_s$, the objective is to find the LP filter coefficients d_j which minimize the MSE, $\mathrm{E}[|e(\tau)|^2] = \mathrm{E}[|c(\tau) - \hat{c}(\tau)|^2]$, where τ is a prediction range, and $\hat{c}(\tau)$ is an estimate of the future channel coefficient, $c(\tau)$, given by the linear combination of p past samples $c_{-j} = c(-jT_s)$ (0 is the reference time, so the observations are taken for $t \leq 0$):

$$\hat{c}(\tau) = \sum_{j=0}^{p-1} d_j c_{-j} \tag{3.9}$$

Note that equation (3.7) applies prediction one sample ahead, whereas in (3.9) we compute the predicted value of the future sample separated from the observations by τ seconds. Thus, the coefficients d_j are not the same in (3.7) and (3.9) unless τ is the

sampling interval. The optimal coefficients d_j are computed as

$$\boldsymbol{d} = \boldsymbol{R}^{-1}\boldsymbol{r} \tag{3.10}$$

where $\boldsymbol{d}$= $(d_0 \ldots d_{p-1})$. $\boldsymbol{R}$ is the autocorrelation matrix $(p \times p)$ with coefficients $R_{ij} = \mathrm{E}[c_{-i}c^*_{-j}]$ and $\boldsymbol{r}$ is the autocorrelation vector $(p \times 1)$ with coefficients $r_j = \mathrm{E}[c(\tau)c^*_{-j}]$. Note that when noisy observation are used in (3.9) (e.g., as in (3.2 with $b_k = 1$), the effect of the noise is incorporated into $\boldsymbol{R}$ by adding $(N_0/2)\boldsymbol{I}$ where $\boldsymbol{I}$ is the $p \times p$ identity matrix. The resulting minimum MSE is given by

$$E[|e(\tau)|^2] = r(0) - \sum_{j=0}^{p-1} d_j r(\tau + jT_s), \tag{3.11}$$

where $r(\tau) = E[c(t)c^*(t+\tau)]$ (see Figure 3.1).

The MMSE performance of the long range prediction with various sampling rates is compared in Figure 3.2. A moderate model order, $p = 20$, and a very high SNR = 140 dB are chosen to illustrate the performance comparison, although, later, the results will be generalized for any p and SNR values. In this figure, the theoretical MMSE curves (3.11) for a given prediction range are plotted. For example, assuming $f_{dm} = 100$ Hz, the range of 0.2 on the $x-$axis corresponds to 50 data points ahead with the data rate of 25 kHz and 1 sampling point ahead with a lower sampling rate of 500 Hz. As seen from the figure, the same future value can be predicted with much greater accuracy by using the low sampling rates. Thus, when the sampling rate is reduced greatly relative to the data rate, but the filter length p remains the same, prediction much further ahead becomes feasible.

The effect of the sampling rate is explored further in Figure 3.3. In this figure, the MMSE vs sampling rate, f_s, is plotted for various model orders, p, at the prediction range, $f_{dm}\tau = 0.4$. As seen from the figure, for each model order there is an optimal

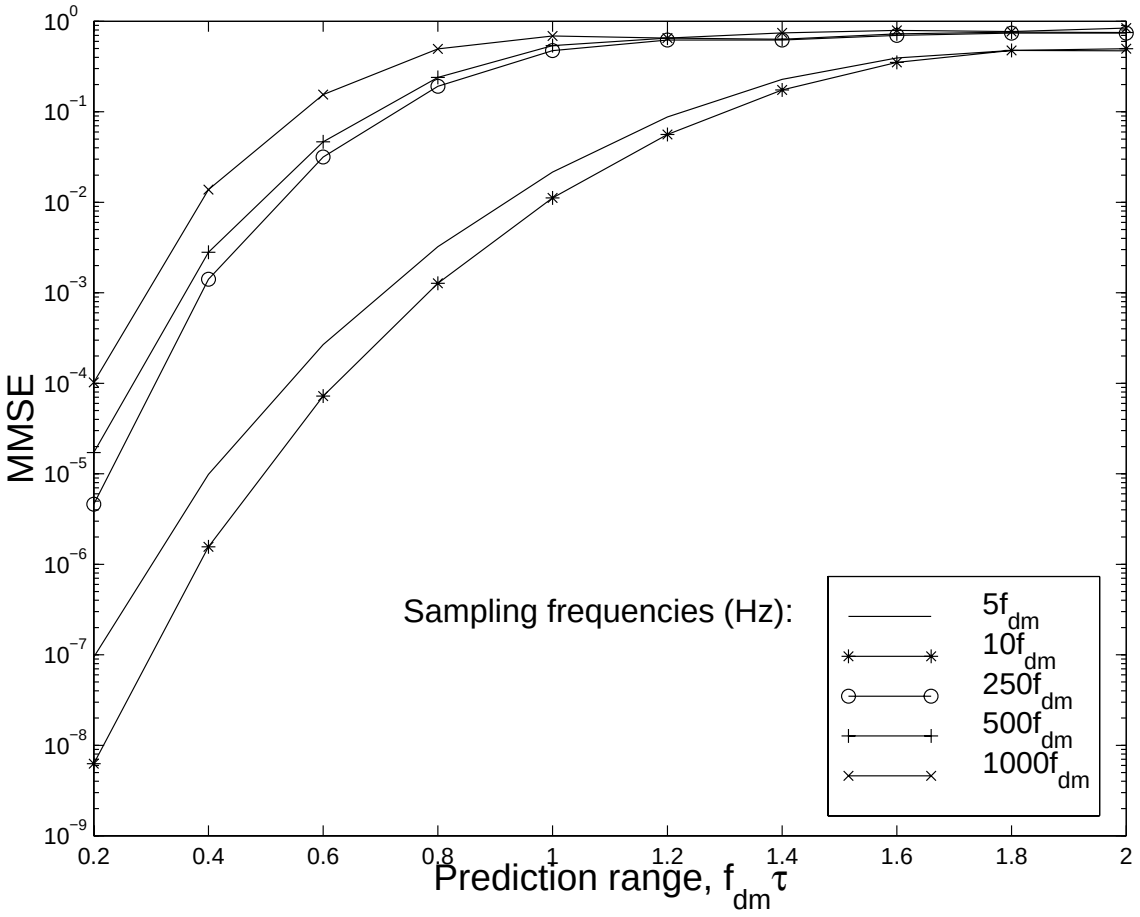

Figure 3.2: MMSE for long term prediction for different values of sampling rate, f_s, with the model order, $p = 20$, and SNR = 140 dB.

low sampling rate that minimizes the MMSE. This optimal rate is close to 1 KHz for moderate to high p. These results are obtained for an infinite number of scatterers, N. In this case, the lower sampling rate of 500 Hz is not the optimum rate. However, as we will see later in this chapter, in the important practical case when the number of effective scatterers is modest, the MMSE decreases with the sampling rate for a fixed p, and the sampling rate of 500 Hz gives the best performance among the rates

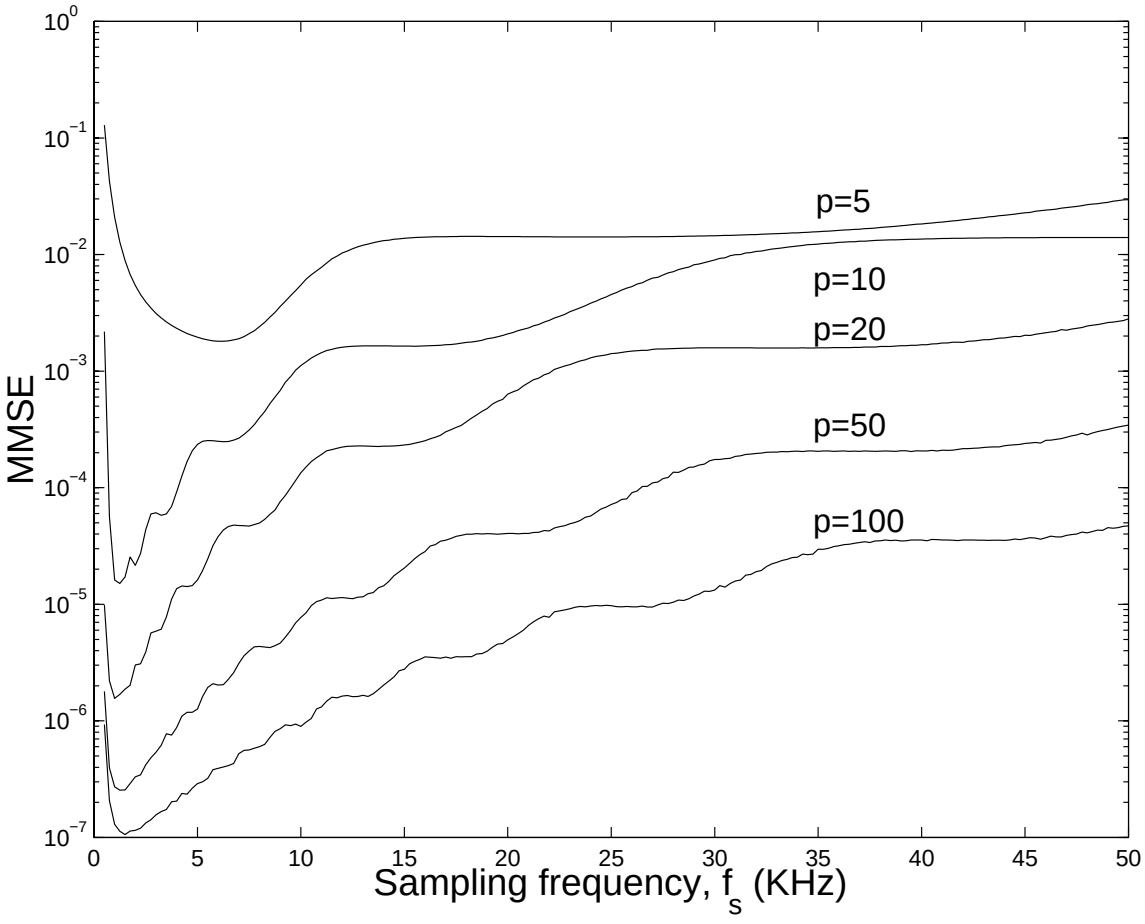

Figure 3.3: MMSE vs sampling rate, f_s, for various model orders p; prediction range $\tau = 4$ ms, SNR = 140 dB and $f_{dm} = 100$ Hz.

examined in Figure 3.3. Hence, we use $f_s = 500$ Hz as a low sampling rate below to illustrate the performance of the MMSE with respect to SNR and p. In Figure 3.4, we demonstrate our MMSE results for different SNR values at the data rate of 25 KHz and at the low sampling rate of 500 Hz. Since the prediction range, $f_{dm}\tau = 0.4$ is chosen for these curves, for the data rate of 25 KHz, 100 bits ahead are predicted. This range also corresponds to 2 low rate samples ahead. Since the sampling rate of

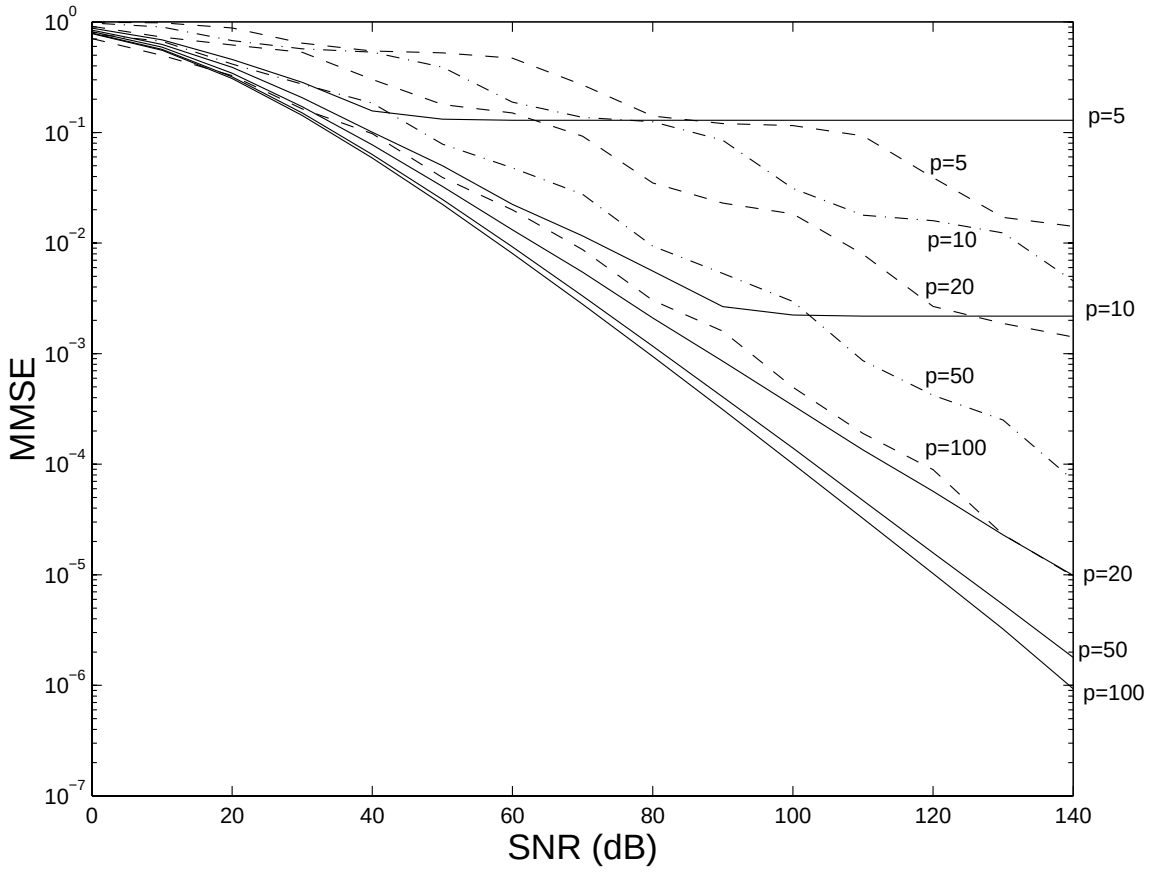

Figure 3.4: MMSE vs SNR for different values of model order, p, at data rate of 25 KHz (dashed lines) and $f_s = 500$ Hz (solid lines) for prediction range $\tau = 4$ ms, $f_{dm} = 100$ Hz

500 Hz is not the optimal rate for Rayleigh fading, for some values of SNR and p, high data rate might perform better. However, most of the time, the performance of the lower sampling rate is better than that of the high sampling rate. For lower sampling rates, we observe the saturation of the MMSE as the SNR increases. This MMSE floor can be found from (3.11) for a given value of p by setting $N_0 = 0$.

In Figure 3.5, the MMSE vs p is plotted in solid lines for $f_{dm}\tau = 0.2$ and the sampling rate of $5f_{dm}$, for different values of SNR. As p increases the MMSE saturation

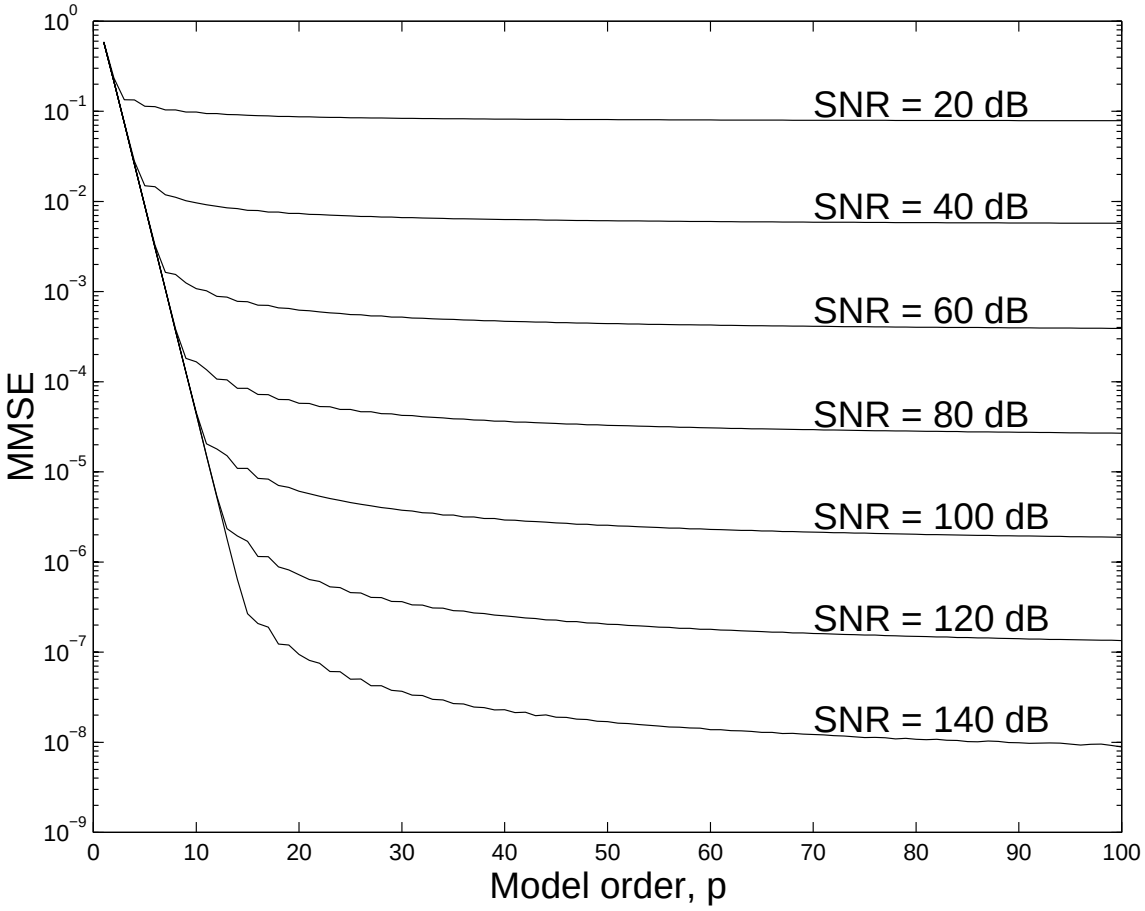

Figure 3.5: MMSE vs. model order, p, for different values of SNR for the sampling rate of 500 Hz, $\tau = 2$ ms, $f_{dm} = 100$ Hz.

level is approached. This MMSE floor corresponds to the prediction error given an infinite number of past observations for the fading process sampled at $5f_{dm}$ in the presence of noise.

Given desired prediction range $f_{dm}\tau$, the MMSE solution is found by solving for the filter taps in (3.32). However, in practice, this approach might be computationally expensive if several future samples have to be predicted at once. Instead, we use the one-step prediction at a given sampling rate (as in (3.7)) and then iterate equation

(3.7) to predict more then one sample ahead by using previously predicted samples or their estimates when the observations are not available. Obviously, the MSE of this iterative prediction technique is lower bounded by (3.11).

So far, we investigated the case of the infinite number of scatterers in creating the Rayleigh fading environment. In Figure 3.6, the theoretical autocorrelation functions are plotted for the infinite number of oscillators, as well as for $N = 3$ and 9. For the infinite number of oscillators, the autocorrelation function is given by (3.8), whereas for finite N, the autocorrelation function is found as [16]:

$$r(\tau) = \frac{4}{N_a} \sum_{n=1}^{N-1} \cos\left(2\pi f_{dm}\tau \cos\frac{2\pi n}{N_a}\right) + \frac{2}{N_a}\cos(2\pi f_{dm}\tau) \tag{3.12}$$

where $N_a = 4N - 2$. Note that the autocorrelation values for the finite values of N initially approximate the autocorrelation values of the Rayleigh fading. For large $f_{dm}\tau$, the autocorrelation functions diverge, and for finite N much larger sidelobes are present. These larger sidelobes help to reduce the MMSE as illustrated in Figure 3.7. In this figure, the solid lines represent the MMSE curves using the theoretical autocorrelation functions for different N values. These theoretical MMSE values are closely approximated as the observation interval used to calculate the empirical autocorrelation values (and the resulting linear predictor coefficients) increases. Figure 3.7 depicts these simulation results for different number of oscillators and observation intervals. We have found that adaptive techniques can significantly improve prediction accuracy shown in Figure 3.7 for short observation intervals. The MMSE values in Figure 3.7 are high due to large additive noise in the observation. The effect of the noise can be greatly reduced by using adaptive processing. The adaptive processing and tracking issues will be addressed later in this chapter.

We mentioned earlier that the low sampling rate of 500 Hz (assuming $f_{dm} = 100$

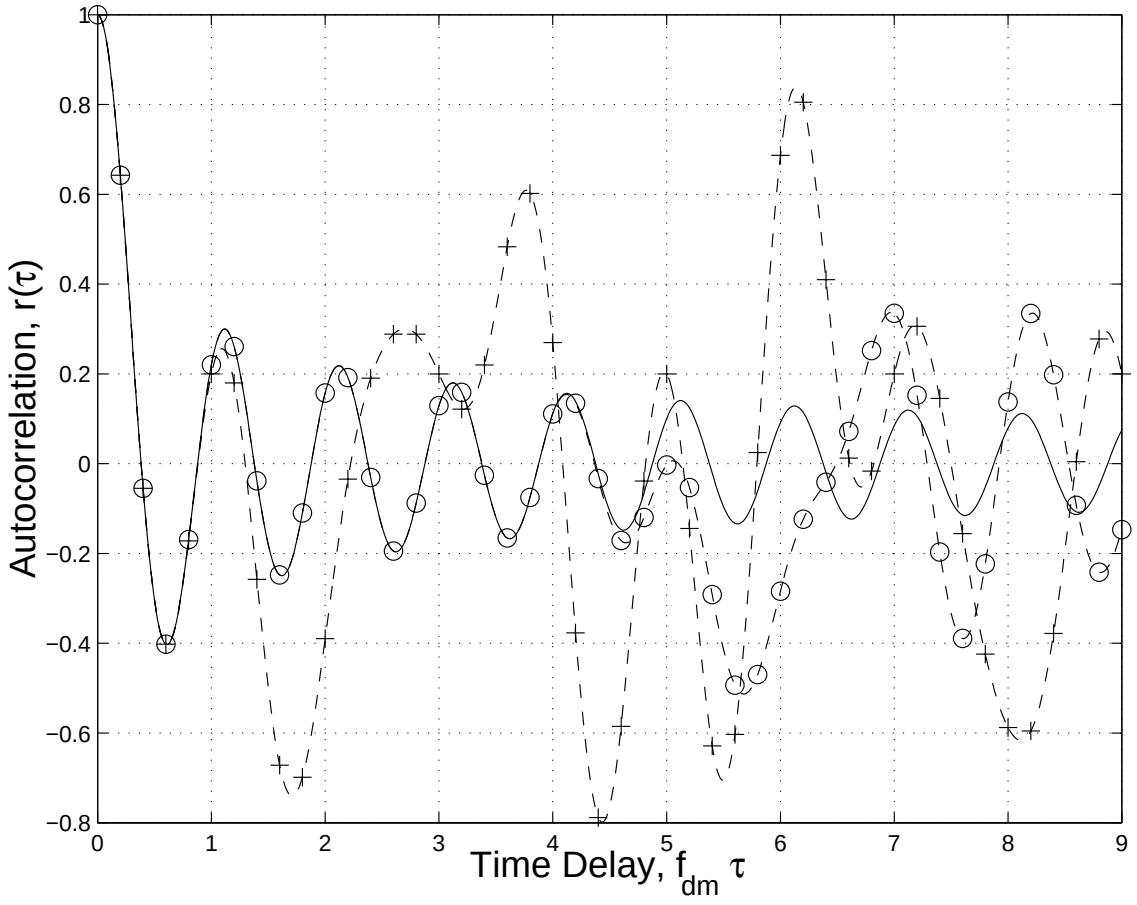

Figure 3.6: Theoretical autocorrelation functions for the infinite number of oscillators (Rayleigh fading) (solid line) and for a finite number of oscillators, $N = 3$ $(+ - - - +)$ and $N = 9$ $(o - - - o)$.

Hz) does not result in the best performance for the infinite number of oscillators. However, when the number of oscillators is modest, the sampling rate of 500 Hz results in the smallest MMSE among the rates considered in Figure 3.8. We limit ourselves to lowest sampling rate of 500 Hz although we could decrease the sampling rate to the Nyquist rate of 200 Hz that is twice the maximum Doppler frequency. In practice, interpolation and adaptive tracking accuracy benefit from a higher sampling

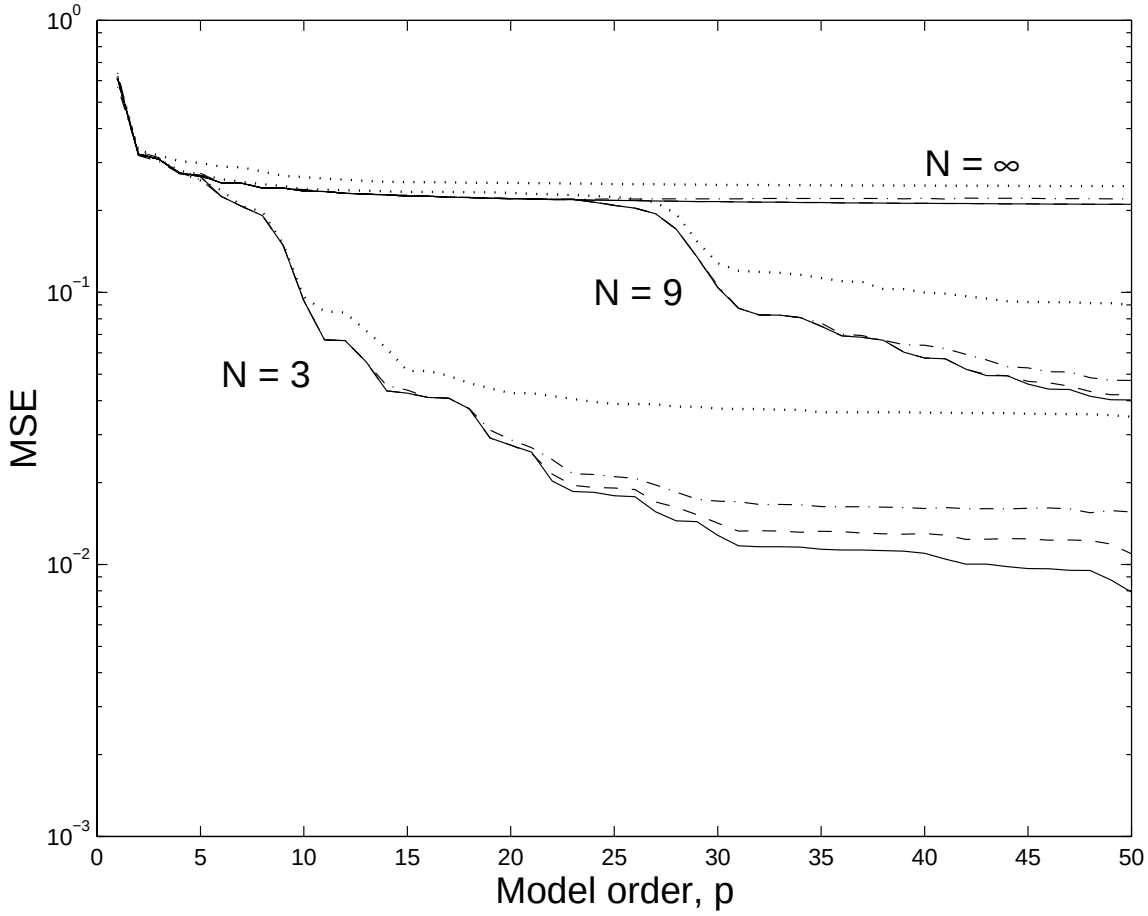

Figure 3.7: Theoretical MMSE vs model order, p, for Rayleigh fading ($N = \infty$) and $N = 3$ and 9 (solid lines) at SNR = 11.9 dB for prediction range of 2 ms, $f_{dm} = 100$ Hz. Also, for each N, simulated average MSE for various observation intervals: 200 samples (.....), 1000 samples ($-.-.-$), and 2000 samples ($---$).

rate. These considerations need to be taken into account in selecting the optimal sampling rate.

Both Figures 3.7 and 3.8 illustrate the fact that the advantages of using longer memory in the prediction are more pronounced for smaller values of N. For a given model order p and sampling rate, the total memory span is given by p/f_s. For a

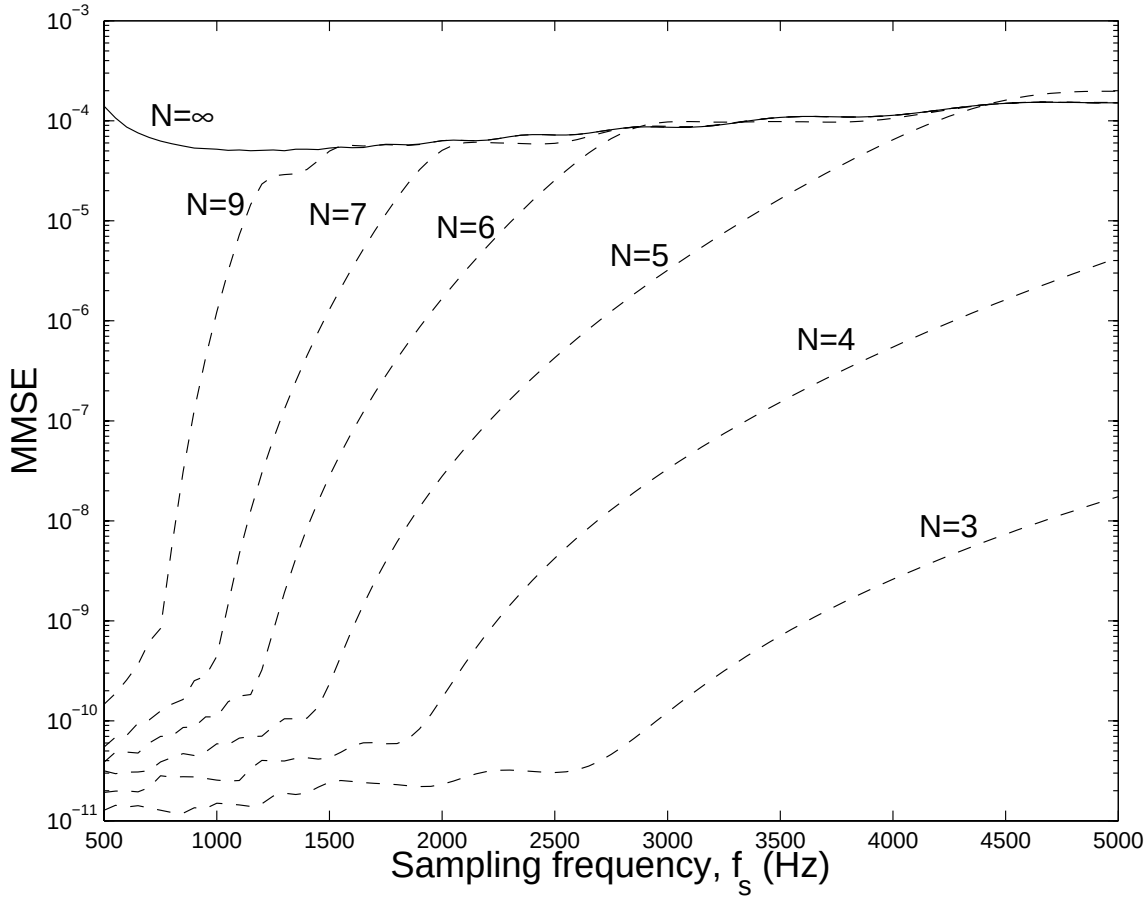

Figure 3.8: MMSE vs f_s for different values of N and for prediction range of 4 ms, $f_{dm} = 100$ Hz at SNR=100 dB and p=50.

fixed p, lower f_s implies longer memory. Thus, as f_s decreases, greater utilization of the sidelobes of the autocorrelation function becomes possible. Since the sidelobes are larger for smaller values of N, lower MMSE results when f_s is low and p is sufficiently large as N decreases. On the other hand, as f_s increases for fixed p, the prediction MMSE for any N converges to the MMSE of the Rayleigh fading. This is due to the reduction of the memory span of the prediction to the region where the autocorrelation functions are similar for all N (Figure 3.6). Similarly, for low

model order p, the advantage in the MMSE due to the lower number of oscillators diminishes. When short range prediction or channel estimation is the objective, short memory span is sufficient to generate reliable estimates. Thus, the MMSE in this case is not sensitive to the number of oscillators.

3.1.2 Experimental Results

Several numerical results presented below illustrate performance characteristics of early development of our long range prediction technique. In the examples, we assume that the maximum Doppler frequency is 100 Hz, and the data rate is 25 Kbps. Initially, we sample the channel at the rate of 250 Hz. Thus, there are 100 data points between adjacent sampling points. To determine the observations of the fading coefficients, c_n, at the sampling points, one can send training symbols b_n at the channel sampling rate of 250 Hz (see (3.2)). This overhead affects the throughput only by 1%.

In order to give a better insight into the performance of this technique, we will first demonstrate the case of three scatterers ($N = 3$ in (3.3)). In Figure 3.9, the pole-zero plot of the frequency response of the channel is illustrated. Note that the three poles corresponding to the three oscillators are placed very close to the unit circle. The angles of these poles correspond to the oscillator frequencies. With the sampling frequency, $f_s = 250$ Hz, these three Doppler frequencies correspond to $100, 50$, and 30 Hz. The plot of the envelope due to these scatterers is drawn in Figure 3.10. The channel is observed for the first 25 samples. Then, by employing Linear Prediction, the future values of the channel envelope are estimated and plotted using dotted lines for the next 25 samples (roughly ten times the coherence time) in the figure. The estimates agree with actual values and we can detect when the channel will enter

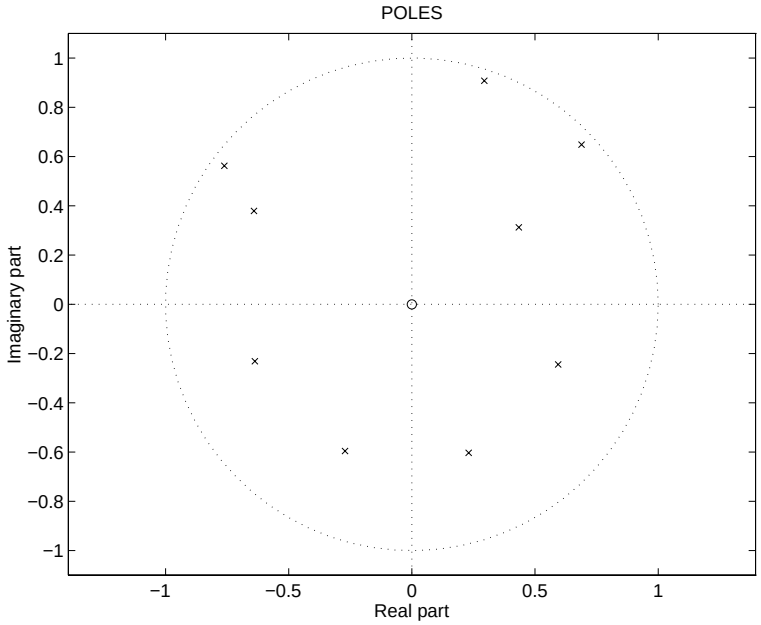

Figure 3.9: Pole-zero locations of the frequency response of the channel for three scatterers, $f_{dm} = 100$ Hz

deep fades in the future. The same experiment is repeated in the presence of additive white Gaussian noise and the result is plotted in Figure 3.11. Note that the predicted values still follow very closely the actual channel envelope which is plotted in solid lines.

We also performed simulations for a greater number of scatterers. In Figures 3.12 and 3.13, the original Jakes channel model with nine oscillators (scatterers) is examined [16]. In Figure 3.12, the pole-zero plot of the frequency response of the Jakes channel model with a maximum Doppler frequency, $f_{dm} = 100$ Hz, is illustrated. As the number of oscillators increases, we need a greater number of poles. Note that the poles corresponding to the oscillators are still very close to the unit circle. The channel is observed for the first 150 samples. We plotted the predicted channel envelope in

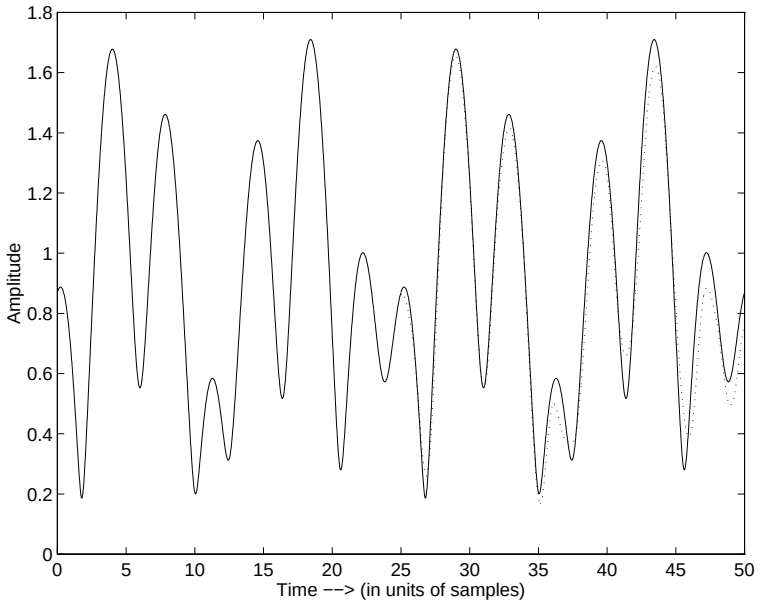

Figure 3.10: Actual (—) and estimated (...) fading channel envelopes for 3 scatterers, $f_{dm} = 100$ Hz

dotted lines and the actual channel envelope in solid lines after the observation interval in Figure 3.13. It can be seen that the predicted values still follow very closely the actual channel envelope. However, since actual channel coefficients are not available beyond the observation interval, the estimates (previously predicted values) $\hat{c}_{n-j}$ were used to form future predicted values $\hat{c}_n$ in (3.7). Therefore, later in the prediction, the accuracy decreases because of the cumulative effect of the LP error. This error propagation problem can be solved by combining adaptive tracking at the receiver with prediction as described later in Section 3.3. Using adaptive channel estimation combined with transmitter pre-compensation (see Section 3.2) more reliable data-aided estimates of fading coefficients can be obtained at the receiver, and fed back to the transmitter at the channel sampling rate. Our results (section 3.3 and [36]) indi-

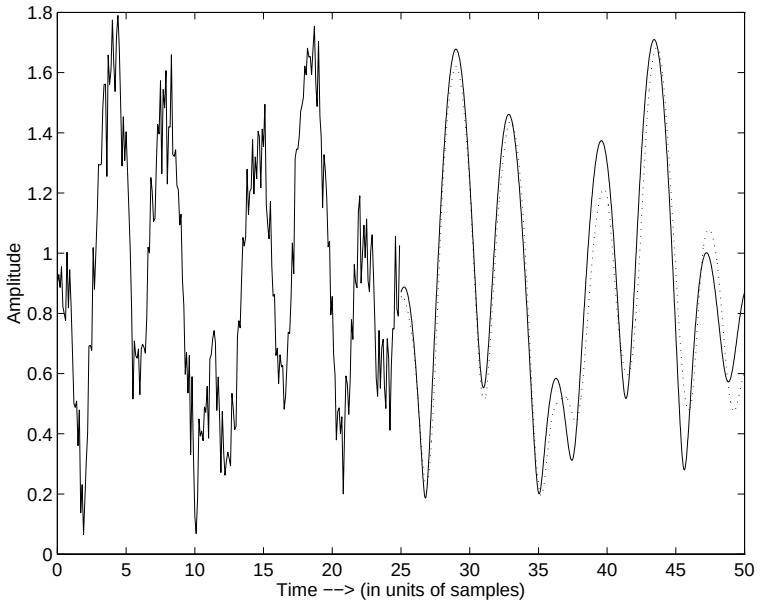

Figure 3.11: Actual (—) and estimated (...) fading channel envelopes for 3 scatterers in the presence of AWGN, SNR = 20 dB

cate that this technique significantly reduces error propagation, and that the channel can be accurately forecasted for several hundred of future data symbols. Therefore, for the rest of our performance analysis in this report we are assuming that perfect estimates of fading coefficients c_{n-j} are available in (3.7).

3.1.3 Interpolation

Since the sampling rate for the fading channel is much lower than the data rate, we perform interpolation between predicted channel coefficients to forecast fading coefficients for all data points [56, 57]. In this interpolation process, four consecutively predicted channel coefficients are interpolated by a Raised Cosine (RC) filter to generate estimates of the fading coefficients, $\hat{c}_k$, between two adjacent predicted

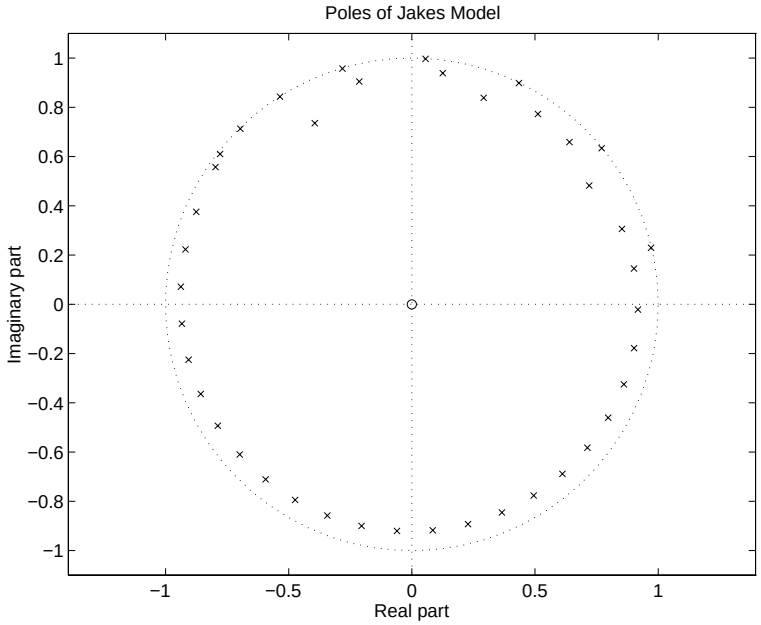

Figure 3.12: Pole-zero locations of the frequency response of the Jakes channel model, $f_{dm} = 100$ Hz

samples at the data rate [58, 59]. We searched for the suitable channel sampling rate for our system. Note that, initially, we used channel sampling rate, $f_s = 250$ Hz. Lets define normalized channel sampling rate as $f_s' = f_s/(2f_{dm})$, where f_{dm} is the maximum Doppler frequency. In order to satisfy the Nyquist's criteria fs' should be at least 1. However, it does not give the best performance for interpolation purposes where we use only four fading coefficients at the low sampling rate. Figure 3.14 shows interpolation MSE vs rolloff factor of the RC interpolator for f_s'=1.25 (dashed line) and for f_s'=2.5 (solid line). MSE is defined by $\mathrm{E}|\hat{c}_n - c_n|^2$ at data rate. Obviously interpolator with rolloff factor of 0.64 at f_s'=2.5 has the best performance and we used these values for the rest of our analysis. In theory, optimum rolloff factor could be found for a given f_s as $(1-1/f_s')$. The optimum rolloff value is 0.6 for f_s'=2.5. The

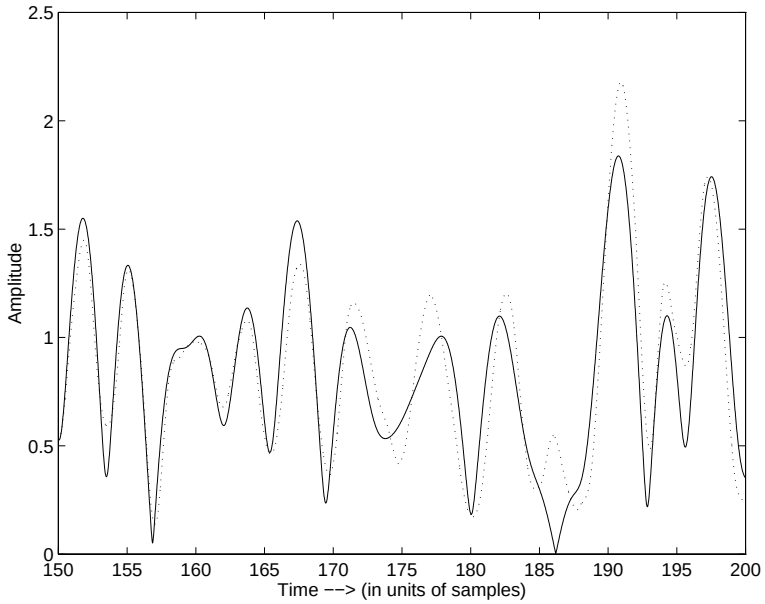

Figure 3.13: Actual (—) and estimated (...) fading channel envelopes for the Jakes channel model, $f_{dm} = 100$ Hz

result we get by simulations, 0.64, is reasonable because ripple distortion at the edge of passband requires more rolloff to smooth out. Although f'_s=2.5 results in oversampling, it produces much more accurate interpolated values than lower values of f'_s. Therefore, for the rest of our simulations we fixed the normalized channel sampling rate, f'_s, to 2.5 and used RC interpolator filter with rolloff factor of 0.64.

3.1.4 Dependency on the Observation Interval

In this section, we explore the sensitivity of our prediction method to the observation interval. We used channel sampling rate, $f_s = 500$ Hz, and the number of oscillators (scatterers), $N = 9$. When the observation interval is long enough, e.g., 200 channel sampling points (0.4 sec), the predicted values are very close to the actual

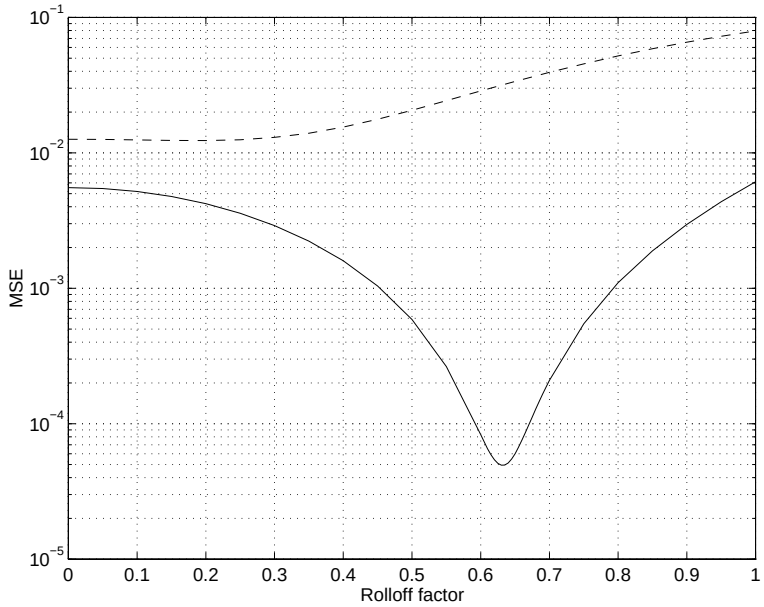

Figure 3.14: Interpolation MSE vs rolloff factor of the Raised Cosine interpolator for normalized channel sampling rate, f_s', 1.25 (dashed line) and 2.5 (solid line)

values as seen in Figure 3.15. As we reduce the observation interval, the prediction accuracy reduces gradually as illustrated in Figures 3.16, 3.17, 3.18 for the observation intervals of 100 (0.2 sec), 50 (0.1 sec), 10 (0.02 sec) respectively. The model order, p, is chosen 60 for the observation interval of 100 and 200 because of the complexity constraints. But, there is not much improvement by choosing higher order, p. On the other hand, the observation interval is the upper limit in determining the value of p. Therefore, we chose the maximum values for the observation intervals of 50 and 10 as of 49 and 9 respectively. Moreover, the dependency on the observation interval can be observed numerically in Figure 3.19 where the average MSE, $\mathrm{E}(|\hat{c}_n - c_n|^2)$, between the predicted values and the actual values are illustrated for different observation intervals and number of oscillators (scatterers). For all the oscillators, the

prediction accuracy reduces as the observation interval gets shorter. The dependency of the number of oscillators will be explained in the next section. Furthermore, the effect of the observation interval on the BER is discussed later in Section 3.2.1.

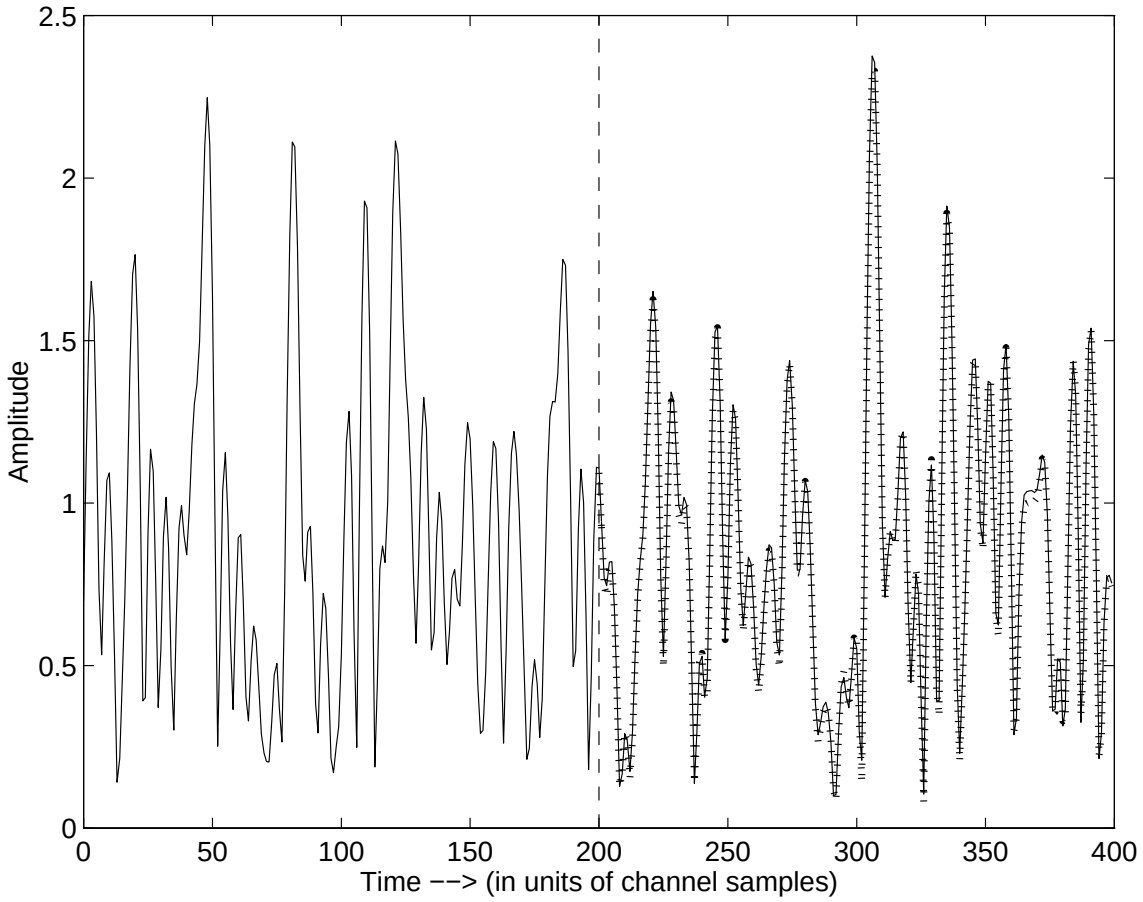

Figure 3.15: First half: The actual channel envelope (solid line) is observed. Second half: The actual future (solid line) and the predicted (dotted line) fading channel envelope for observation interval of 200 channel sampling points (0.4 sec) with N= 9, $f_{dm} = 100$ Hz

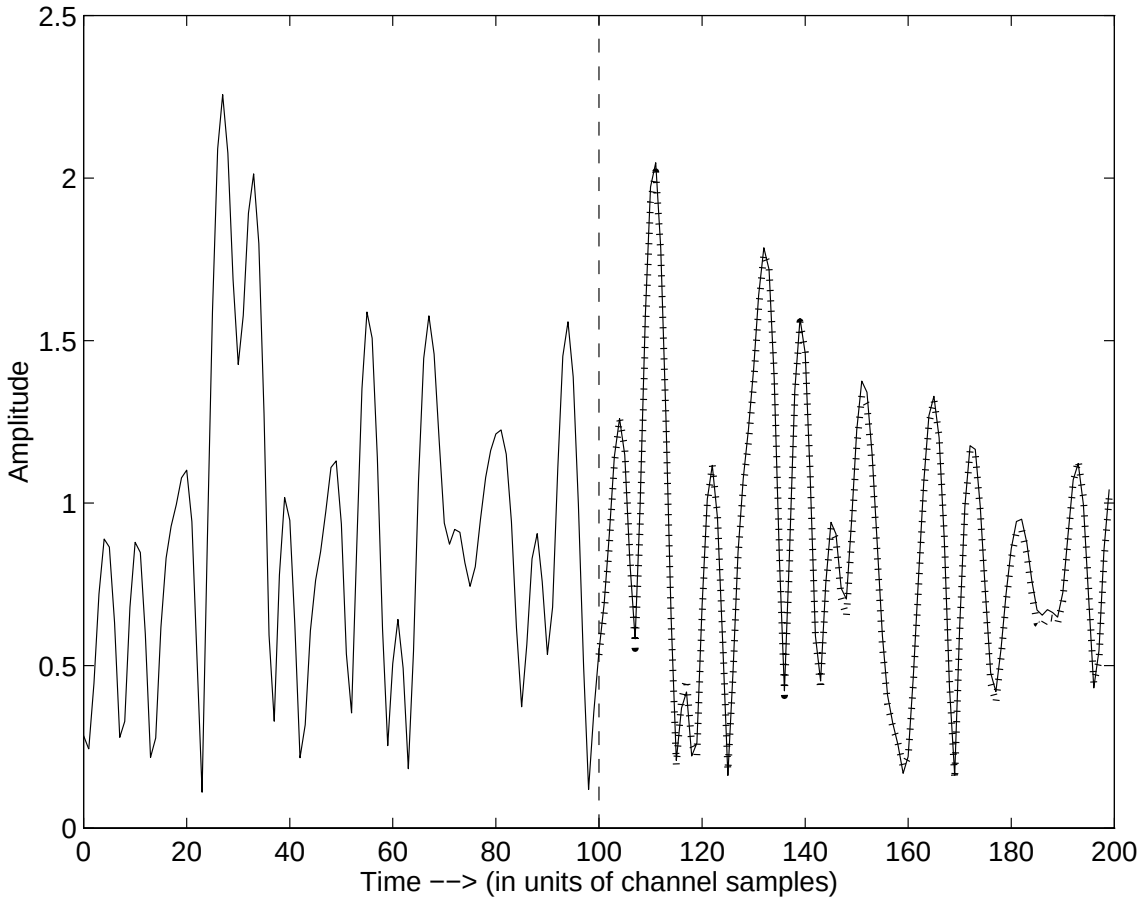

Figure 3.16: First half: The actual channel envelope (solid line) is observed. Second half: The actual future (solid line) and the predicted (dotted line) fading channel envelope for observation interval of 100 channel sampling points (0.2 sec) with N= 9, $f_{dm} = 100$ Hz

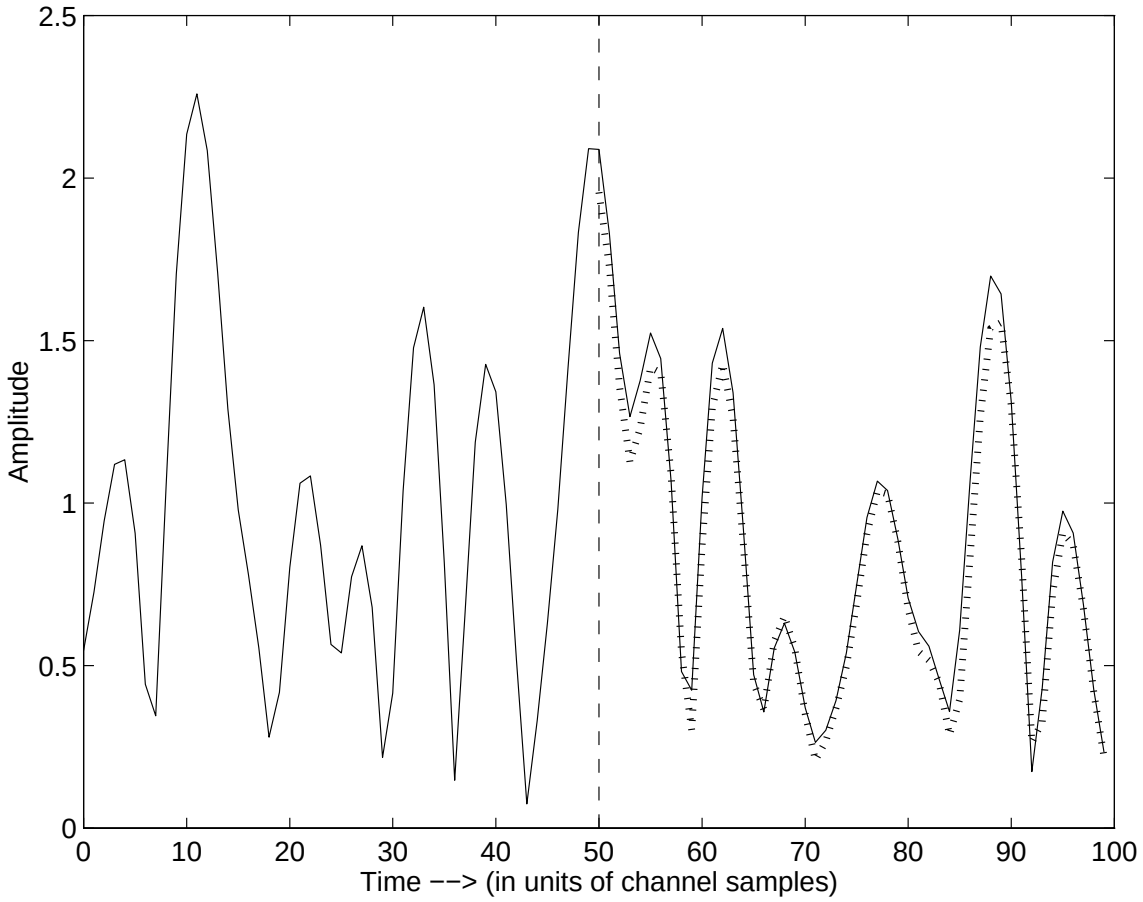

Figure 3.17: First half: The actual channel envelope (solid line) is observed. Second half: The actual future (solid line) and the predicted (dotted line) fading channel envelope for observation interval of 50 channel sampling points (0.1 sec) with N= 9, $f_{dm} = 100$ Hz

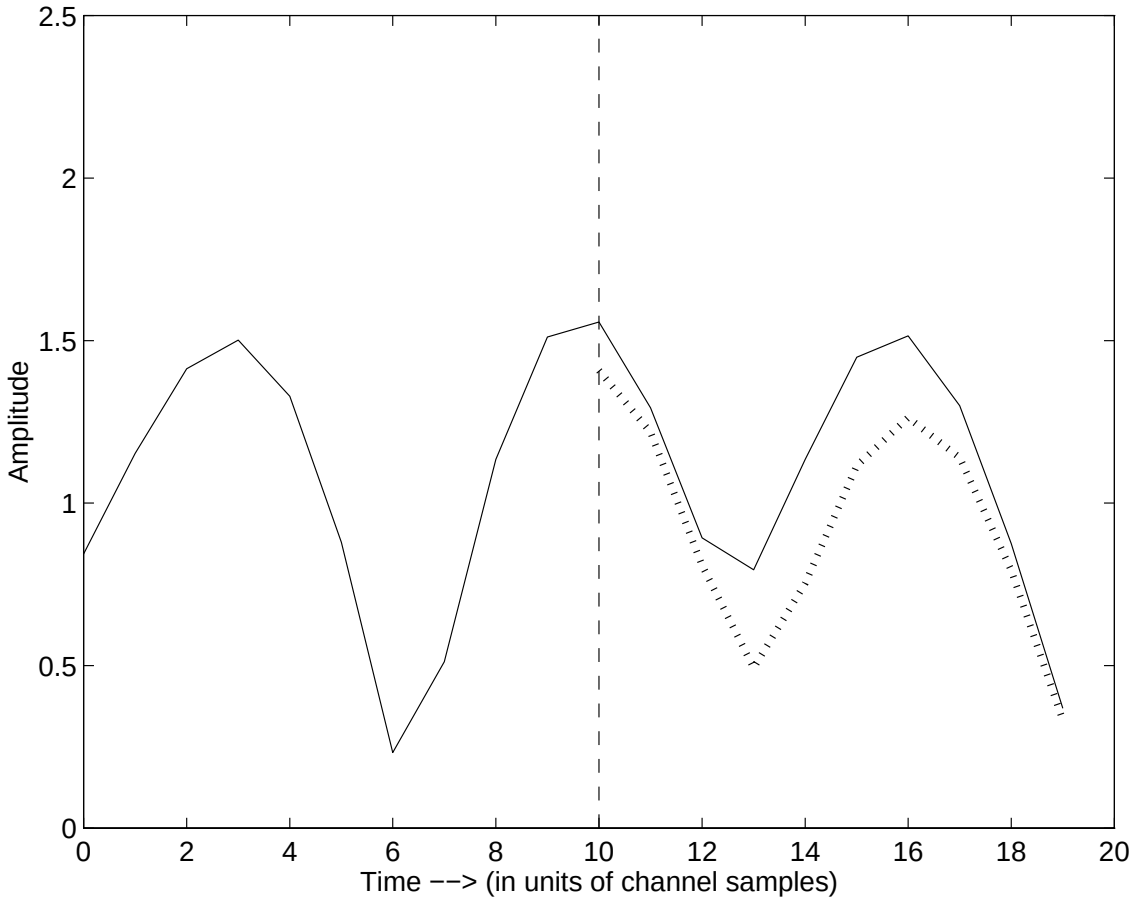

Figure 3.18: First half: The actual channel envelope (solid line) is observed. Second half: The actual future (solid line) and the predicted (dotted line) fading channel envelope for observation interval of 10 channel sampling points (0.02 sec) with N= 9, $f_{dm} = 100$ Hz

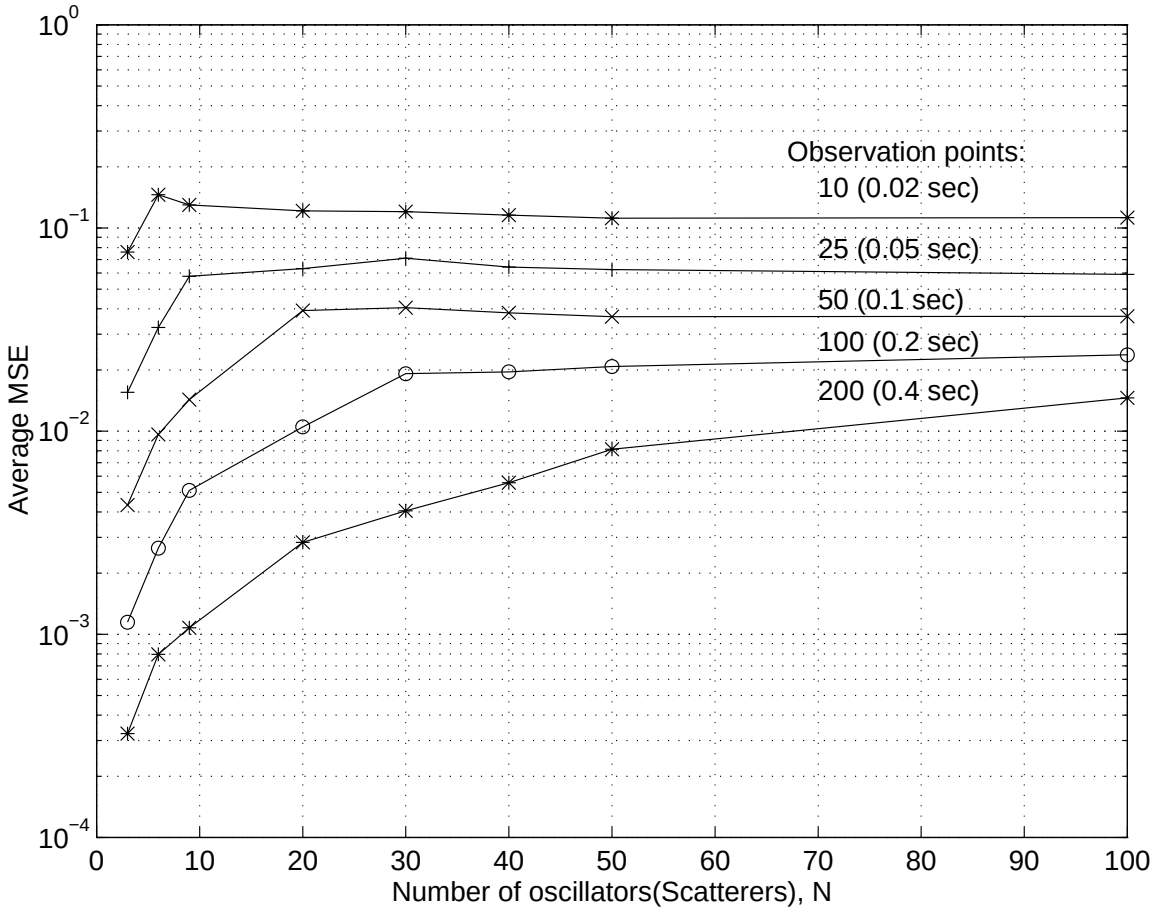

Figure 3.19: Dependency on the number of oscillators, N, and the observation interval length

3.1.5 Dependency on the Number of Oscillators (Scatterers)

In this section, we show the change in the prediction accuracy with increasing the number of oscillators (scatterers). We fixed our observation interval to 100 channel sampling point and the model order, $p = 60$, for the plots in this section. The actual and the predicted values can be seen in Figures 3.20, 3.21, 3.22, 3.23 for the number of oscillators, $N = 3, 20, 100, 1000$ respectively. As seen from the these figures, the prediction accuracy decreases very little as N gets larger. However, note that our prediction method can handle up to 1000 (or more) scatters with a reasonable accuracy. This number of scatterers dependency can also be observed from the Figure 3.19 for different observation interval by reaching the same conclusion explained above.

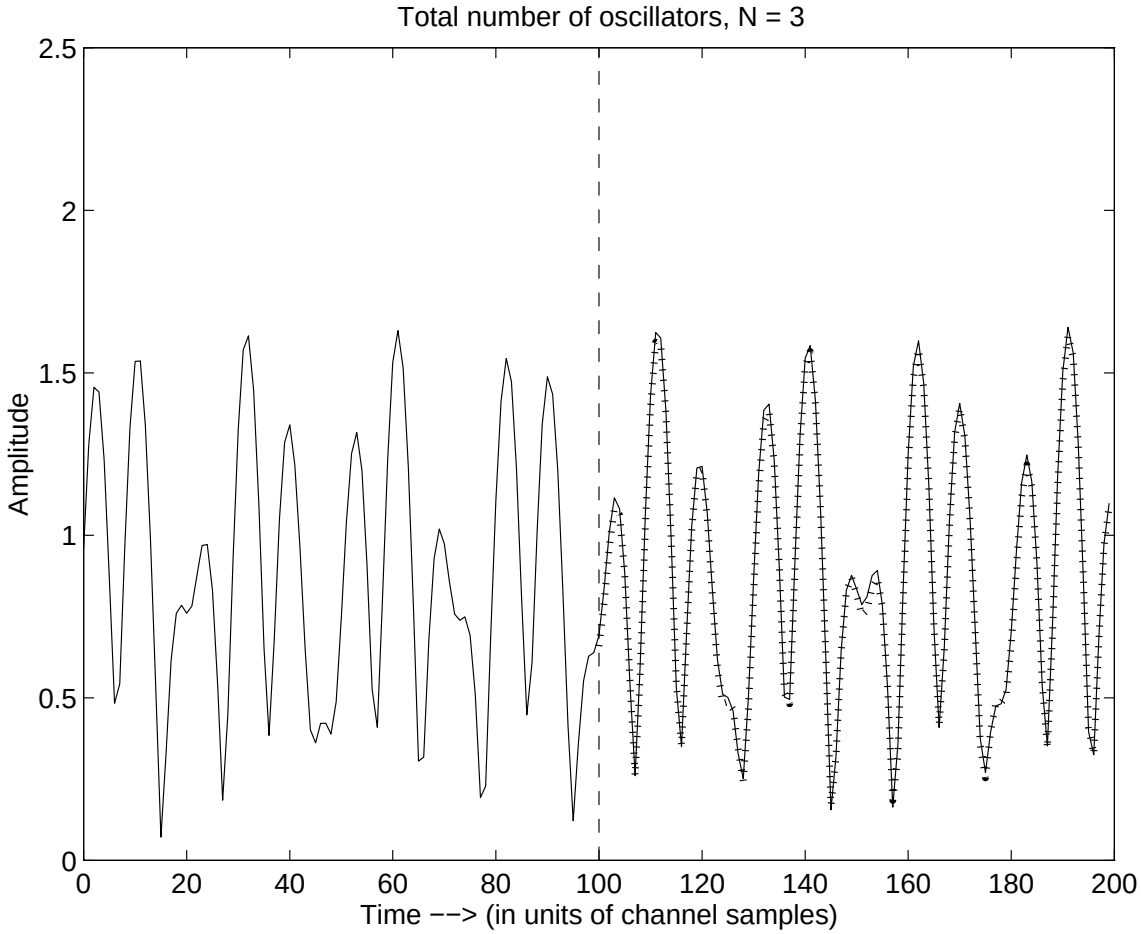

Figure 3.20: First half: The actual channel envelope (solid line) is observed. Second half: The actual future (solid line) and the predicted (dotted line) fading channel envelope for N= 3 oscillators (scatterers), and the observation interval of 100 channel sampling points (0.2 sec) with $f_{dm} = 100$ Hz

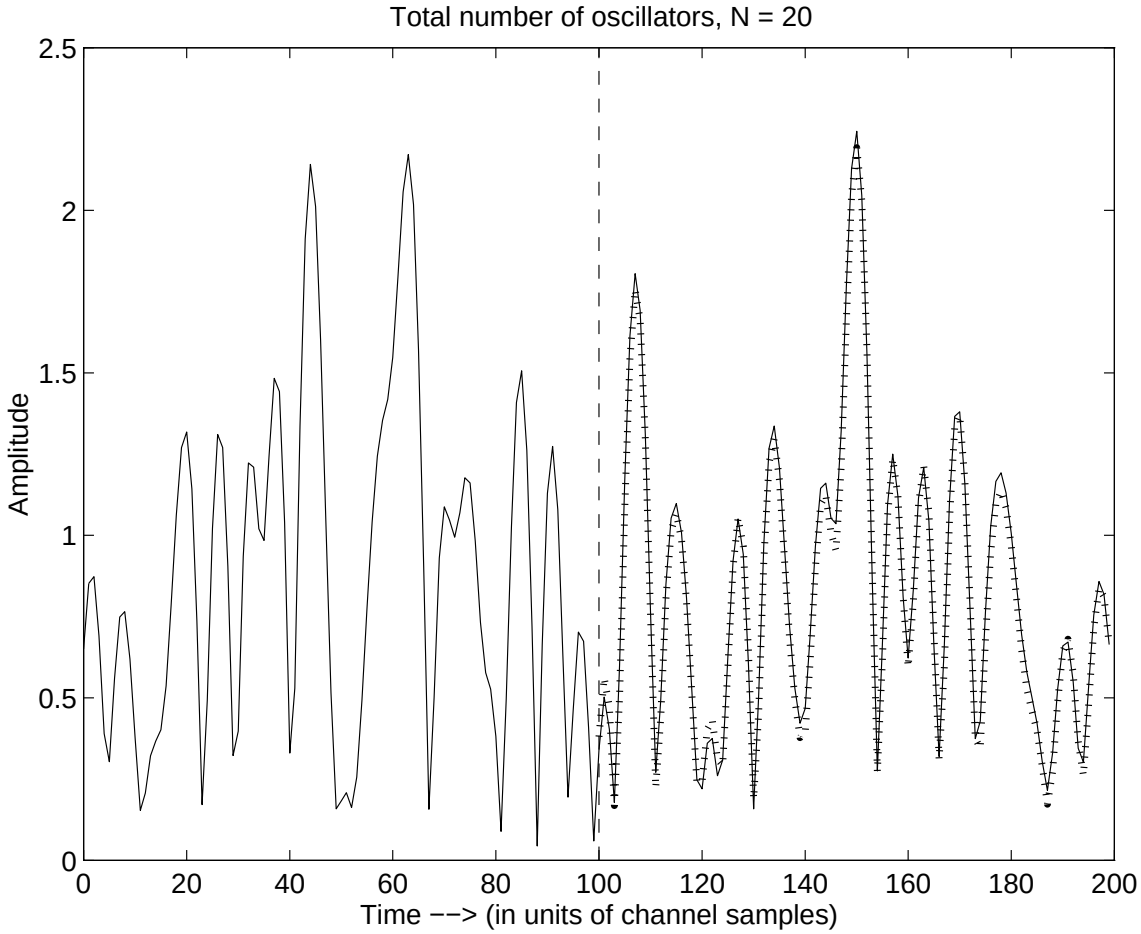

Figure 3.21: First half: The actual channel envelope (solid line) is observed. Second half: The actual future (solid line) and the predicted (dotted line) fading channel envelope for N= 20 oscillators (scatterers), and the observation interval of 100 channel sampling points (0.2 sec) with $f_{dm} = 100$ Hz

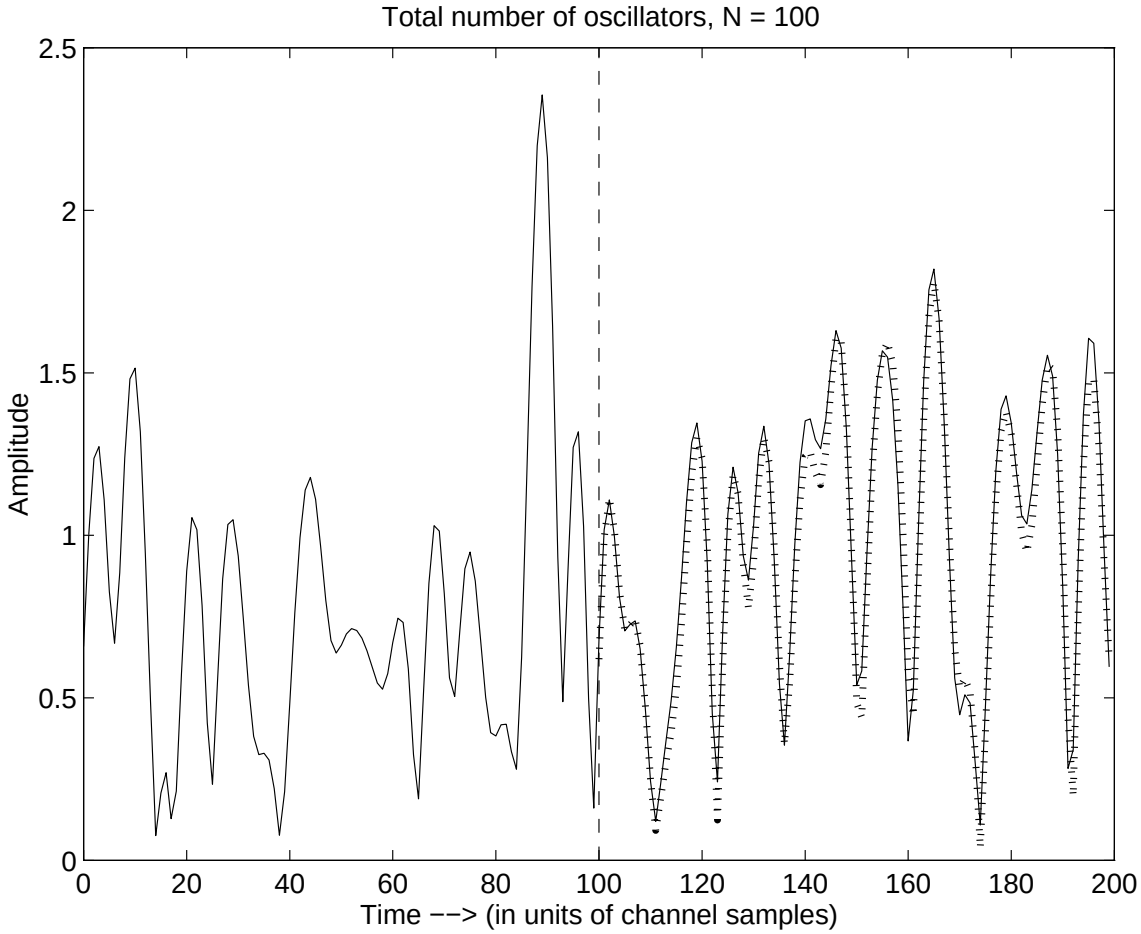

Figure 3.22: First half: The actual channel envelope (solid line) is observed. Second half: The actual future (solid line) and the predicted (dotted line) fading channel envelope for N= 100 oscillators (scatterers), and the observation interval of 100 channel sampling points (0.2 sec) with $f_{dm} = 100$ Hz

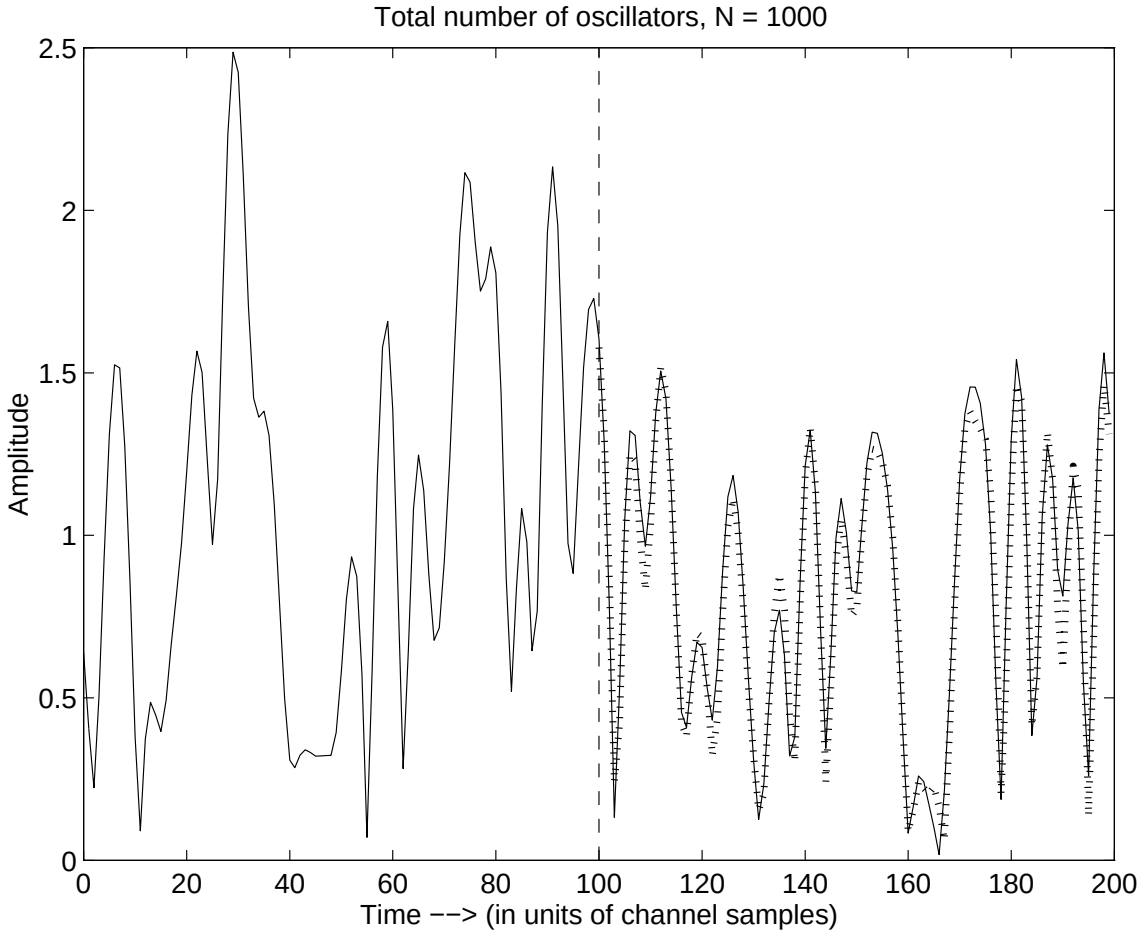

Figure 3.23: First half: The actual channel envelope (solid line) is observed. Second half: The actual future (solid line) and the predicted (dotted line) fading channel envelope for N= 1000 oscillators (scatterers), and the observation interval of 100 channel sampling points (0.2 sec) with $f_{dm} = 100$ Hz

3.2 BER Analysis with Channel Inversion

As mentioned earlier, we propose to combine prediction with tracking and transmitter optimization. To illustrate the potential of this approach, consider the following communication system example. Note that, similar power control strategies have been proposed in [60, 61, 62, 63, 64]. This power adjustment is not proposed as a practical solution, since it will result in large transmitter power fluctuations. It is considered here to illustrate the performance advantages of the proposed prediction technique. In our simulations, we assumed coherent detection and used Binary Phase Shift Keying (BPSK) modulation scheme. Given a binary signal b_k and assuming $\mathrm{E}(|c_k|^2) = 2\sigma^2 = 1$, the signal to noise ratio (SNR) is $\gamma_b = \mathrm{E}(b_k^2)/N_0$. The channel samples taken at the receiver during the observation interval (e.g., using training) are sent to the transmitter, which applies linear prediction and interpolates to produce predicted fading values $\hat{c}_k$ at the data rate for the next frame (a few hundred data symbols). Note that we are assuming a reliable feedback path to the transmitter to send back the predicted fading values. This is a valid assumption considering the base station (transmitter), where more complex detection methods, diversity and antenna array can be utilized because of the availability of more space and hardware compared to the mobile unit. After receiving the predicted values, the transmitter uses the following encoding algorithm: it interrupts the transmission if the power level, $|\hat{c}_k|^2$ is below a previously chosen threshold value, ρ. Furthermore, if $|\hat{c}_k|^2$ is above the threshold, the transmitter sends the data bits, b_k, by multiplying them with the inverse of the predicted $\hat{c}_k$ values (3.7). That is, with the channel inversion, at the output of the matched filter and sampler, the new modified discrete-time received

signal is given by

$$y_k = \frac{c_k}{\hat{c}_k} b_k + z_k. \tag{3.13}$$

where z_k is discrete-time AWGN.

Now, lets investigate the theory and the limitations of this technique. Recalling from chapter 2, when there are large number of closely time-spaced propagation paths in the medium, the time-variant impulse response $c(t)$ can be modeled as a complex-valued gaussian random process. Then, by the central limit theorem, the real and imaginary parts of c, c_I and c_Q, are independent, zero-mean Gaussian random processes [1] [5, 7, 9, 16]

$$c = c_I + jc_Q = \alpha e^{j\theta}. \tag{3.14}$$

The components c_I and c_Q each have the mean power (or variance), σ^2 resulting in $E[|c|^2] = 2\sigma^2 (= E[\alpha^2])$. From the discussion in Appendix A, it follows that $\alpha = |c|$ and has a Rayleigh probability density function (pdf):

$$p(\alpha) = \frac{\alpha}{\sigma^2} e^{-\frac{\alpha^2}{2\sigma^2}}, \qquad 0 \leq \alpha < \infty \tag{3.15}$$

with $E(\alpha) = \sqrt{\frac{\pi}{2}}\sigma$ and $E(\alpha^2) = 2\sigma^2$. Moreover, the pdf of the power of fading channel, α^2 is given by an exponential distribution. (Appendix A)

$$p(\alpha^2) = \frac{1}{2\sigma^2} e^{-\frac{\alpha^2}{2\sigma^2}}, \qquad 0 \leq \alpha^2 < \infty \tag{3.16}$$

again with $E(\alpha^2) = 2\sigma^2$.

Furthermore, when the channel inversion technique is applied as explained above, we need to know the pdf of the inverted power to investigate the effect of power

[1] the time dependence of channel impulse response is implicit.

inversion process. As calculated in Appendix A, the pdf of the inverted power is given as

$$p\left(\frac{1}{\alpha^2}\right) = \frac{\alpha^4}{2\sigma^2} e^{-\frac{\alpha^2}{2\sigma^2}}, \qquad 0 \leq \frac{1}{\alpha^2} < \infty \tag{3.17}$$

However, $E(\frac{1}{\alpha^2}) = \infty$ which makes channel inversion impossible to apply. In order to overcome this limitation we introduce the concept of the threshold, ρ, in our encoding algorithm described above. From now on we will assume average channel power, $E(\alpha^2) = 2\sigma^2 = 1$. With the given ρ, the new pdf of the inverted power becomes

$$p\left(\frac{1}{\alpha^2} \mid \frac{1}{\alpha^2} < \frac{1}{\rho}\right) = \frac{\alpha^4}{e^{-\rho}} e^{-\alpha^2}, \qquad 0 \leq \frac{1}{\alpha^2} < \frac{1}{\rho} \tag{3.18}$$

with the finite average power calculated as in Appendix A

$$E\left(\frac{1}{\alpha^2} \mid \frac{1}{\alpha^2} < \frac{1}{\rho}\right) = \frac{1}{e^{-\rho}} \Gamma_{inc}(0, \rho) \tag{3.19}$$

Where Γ_{inc} is the incomplete gamma function defined as $\Gamma_{inc}(0, \rho) = \int_0^{1/\rho} \frac{e^{-1/x}}{x} dx$.

When neither threshold nor channel inversion is applied, the channel exhibits Rayleigh fading characteristics, and the bit error rate (BER) is given by [5]

$$P_e = \frac{1}{2}\left(1 - \sqrt{\frac{\gamma_b}{1+\gamma_b}}\right) \tag{3.20}$$

where γ_b is the average signal to noise ratio (SNR). This Rayleigh BER which is the upper bound corresponds to the top curve in Figure 3.24. In this figure we used an observation interval of 100 and the model order, $p = 60$. When our prediction method is applied and the channel inversion technique is utilized, we obtain the performance results given in the same figure. By increasing the threshold from 0.1 to 0.6, we

observe performance improvement. However, the spectral efficiency decreases with the increasing thresholds (or equivalently, the bandwidth increases). The throughputs are calculated for a given ρ as

$$Pr(|c_k|^2 > \rho) = \int_{\rho}^{\infty} e^{-y} dy = e^{-\rho} \tag{3.21}$$

and confirmed by simulations. The spectral efficiencies and the average power of inverted channel (also the power boost at the transmitter), $E(\frac{1}{\alpha^2} \mid \frac{1}{\alpha^2} < \frac{1}{\rho})$, are summarized in Table 3.1 for different values of thresholds as follows:

Threshold, ρ	Throughput	$E(\frac{1}{\alpha^2} \mid \frac{1}{\alpha^2} < \frac{1}{\rho})$ (dB)
0.1	90.5%	3
0.2	82%	1.76
0.4	67%	0
0.6	55%	-0.82

Table 3.1: Throughput and the average power of inverted channel values with corresponding threshold values

In Figure 3.24, the simulation results slightly deviate from the theoretical values due to the prediction and the interpolation errors. However, the agreement with the theoretical results is very good, despite the fact that Rayleigh fading and perfect prediction is assumed in power calculations, while the actual channel has only 9 oscillators. Since the power of the transmitted signal is greater than E$[b_k^2]$ for thresholds $\rho < 0.4$, the BERs for these threshold values are above the AWGN channel BER. For the threshold, $\rho = 0.4$, the transmitted power is equal to E$[b_k^2]$, and the analytical curve in this case is also the BER of the AWGN channel [5]

$$P_e = Q(\sqrt{2\gamma_b}) \tag{3.22}$$

where γ_b is the signal to noise (SNR) and $Q(x)$ is defined as $Q(x) = \frac{1}{\sqrt{2\pi}} \int_x^\infty e^{-t^2/2} dt$. Moreover, for thresholds greater than 0.4, the BER is lower than for the AWGN channel. This is due to the fact that for these thresholds the most favorable channel conditions are chosen for transmission, i.e., the data is sent only when the channel is strong. Thus, by using the proposed prediction method, we were able to reduce the BER to and beyond the level of the AWGN channel.

In Figure 3.24, performance of the channel inversion algorithm for threshold level 0.1 is also shown for the case when the channel coefficient c_n is fed back to the transmitter as the same sampling rate (500 Hz) and used as an estimate of the channel coefficient c_k (at the data rate) between the samples c_n and c_{n+1}. This estimate is used to adjust the power for all data points on the interval $[n, n+1]$. This method was simulated for other thresholds, and the degradation relative to the results with prediction is similar to the case shown. Note that the performance of the feedback without prediction method is optimistic, since the delay is assumed to be zero. This result illustrates the importance of long range prediction for reliable performance of adaptive modulation and coding techniques.

Remember as mentioned at the end of the Section 3.1.1, we are assuming that the perfect estimates of fading coefficients c_{n-j} are available in (3.7). We will discuss adaptive tracking which can approach such performance in Section 3.3. But before that, we would like to examine more on our results in this section by exploring the dependency of BER on the observation interval in the next section.

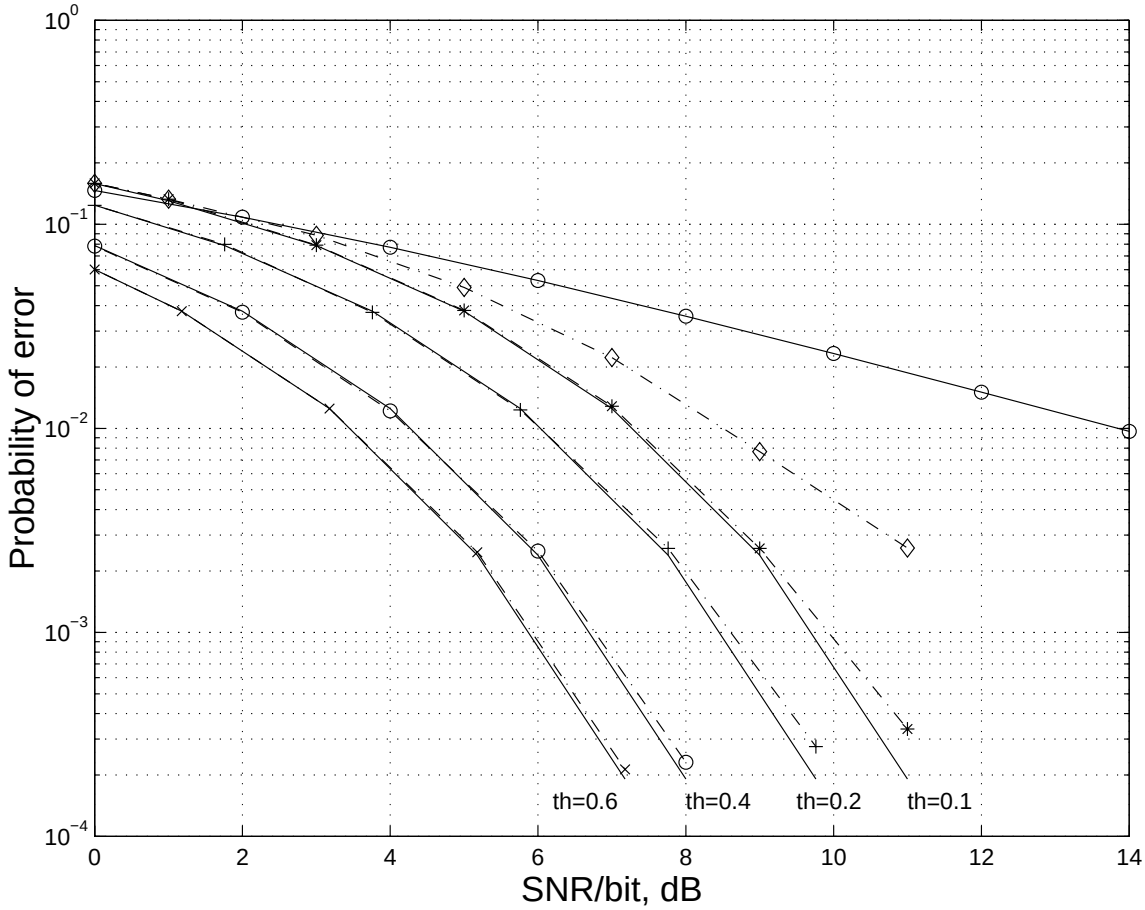

Figure 3.24: Probability of bit error vs SNR for Rayleigh fading channel with no threshold and no compensation at the transmitter (o——o); channel inversion with prediction for thresholds 0.1 ($*---*$), 0.2 ($+---+$), 0.4 (o $---$ o) (also Gaussian channel BER), and 0.6 (x $---$ x). Channel inversion (thr. 0.1) for feedback without prediction ($\diamond - - - \diamond$). The dashed lines are the simulations and the solid lines are the theoretical results for the each threshold level.

3.2.1 Effect of the Observation Interval on BER

The observation interval plays an important role in our analysis. As we reduce the observation interval, the performance of our system deviates more from the theoretical curves for every threshold value as seen in Figure 3.25. Note that we eliminate the deep fades by introducing thresholds. When we have higher threshold values, we observe less deep fades and consequently less abrupt changes in the fading channel. We also observe that most of the interpolation error occurs in the deep fades. Therefore, this explains the reason why there are more deviations for the lower threshold values. From the figure, we can see that the observation interval of 100 channel sampling points has very reasonable performance. The difference between theoretical curves and the simulated curves can be reduced by incorporating an adaptive tracking of the LP coefficients, d, as studied by a collegue working on the same project, Shengquan Hu [36].

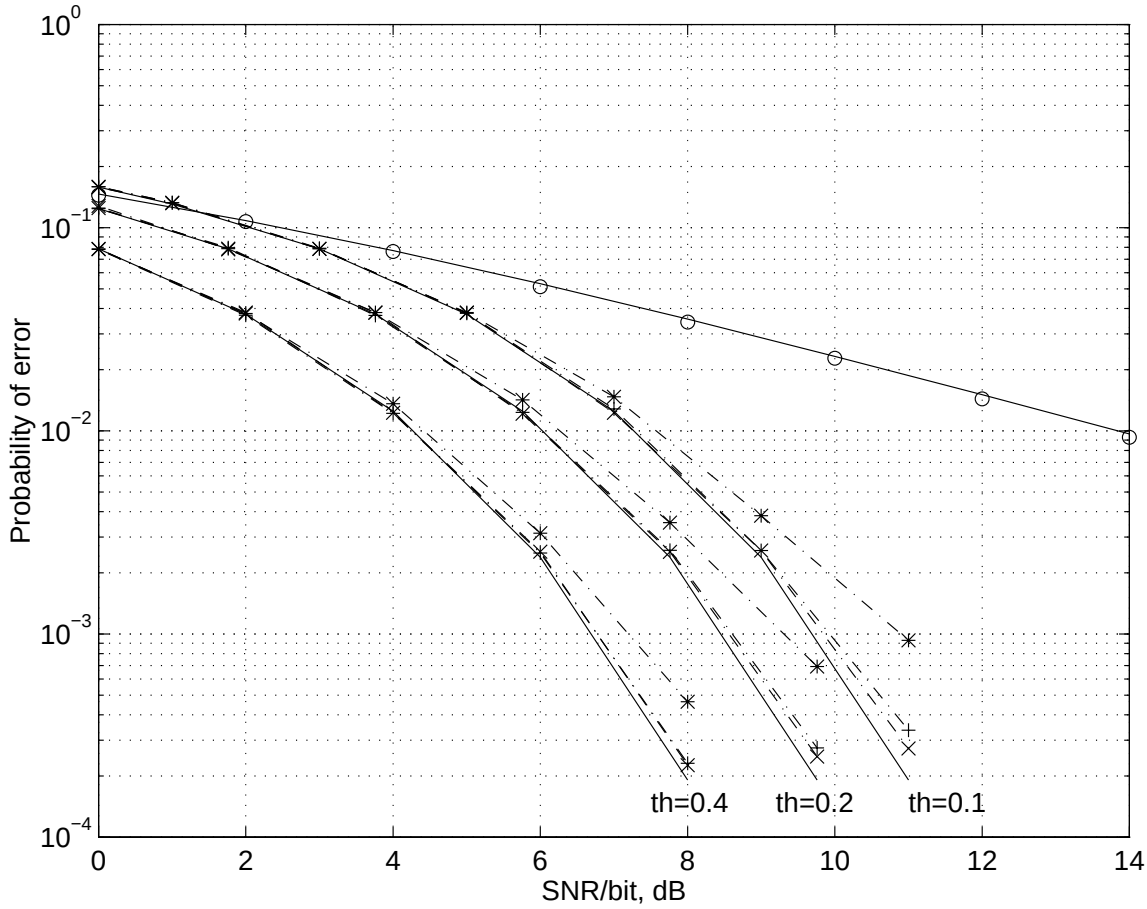

Figure 3.25: Dependency of BER on the observation interval: Rayleigh fading channel without feedback to transmitter (o——o); Solid lines - theoretical and the dashed lines - simulation results for each observation interval: $(*---*)$ 50 points (0.1 sec), $(+---+)$ 100 points (0.2 sec), (x − − − x) 200 points (0.4 sec).

3.3 Adaptive Tracking

(The adaptive tracking techniques described in this Section is jointly developed and studied by Hu [36])

We described how channel parameters d_j and future estimates $\hat{c}_n$ are obtained from the initial observations of the fading channel. We refer to the number of observation samples as the observation interval. The main factors which affect the prediction accuracy of this algorithm can be summarized as: (a) previously predicted values used to predict the future fading coefficients (in (3.7), $\hat{c}_{n-j}$ is used instead of c_{n-j} later in the prediction); (b) additive noise and decision - directed tracking. (c) limited number of observations used in initial acquisition of the LP coefficients (short observation interval); (d) limited order p of the AR model; (e) fixed LP coefficients d_j used throughout the entire future prediction block;

Factor (a) causes error propagation later in the prediction and often makes prediction accuracy unacceptable as shown in Figure 3.13. In practice, it is not necessary to predict ahead further than a few samples (several hundred of data bits). As new actual observations are collected, they can be used in the LP equation. Moreover, the additive noise and decision-directed tracking (b) result in poor prediction accuracy. Therefore, Least Mean Squares (LMS) adaptive tracking method is employed in conjunction with the channel inversion algorithm to eliminate the error propagation and to improve prediction accuracy. When the prediction and the channel inversion techniques are employed at the transmitter, at the output of the matched filter and sampler, the new modified discrete-time received signal is given by

$$y_k = \frac{c_k}{\hat{c}_k} b_k + z_k. \tag{3.23}$$

where z_k is discrete-time AWGN.

Lets define prediction accuracy factor, $a_k \triangleq c_k/\hat{c}_k$. When the prediction accuracy gets better, the value of a_k approaches 1. We use Least Mean Squares (LMS) adaptive algorithm to track the variations in a_k. Given the received signal (3.23), the LMS algorithm is performed at the data rate at the receiver as

$$\tilde{a}_{k+1} = \tilde{a}_k + \mu \hat{b}_k (y_k - \tilde{y}_k)^* \tag{3.24}$$

where μ is the step size controlling the convergence rate, $\hat{b}_k$ is the decision of b_k, and $\tilde{y}_k = \tilde{a}_k \hat{b}_k$. Adaptive tracking of a_k is beneficial when noise is non-negligible and/or decision-directed operation is desired. Since variation of a_k is not significant, the convergence is better than for channels without inversion. The estimate $\tilde{a}_k$ is used for coherent detection. In addition, the updated factor $\tilde{a}_n$ is sent back to transmitter at the low sampling rate and used to update previously predicted fading channel coefficient $\hat{c}_n$ as

$$\tilde{c}_n = \tilde{a}_n \hat{c}_n. \tag{3.25}$$

Since the transmitter uses this updated estimates in (3.7) to predict future fading values, rather than relying on previous estimates, this adaptive algorithm enables us to reduce the prediction error described earlier and to approximate the performance of the theoretical curves.

In Section 3.2, it was shown that long range channel prediction benefits from choosing lower sampling rate,f_s, given model order p. When received samples are corrupted by noise, prediction accuracy greatly decreases. In this case, noisy received signals sampled at the high data rate can be used to reduce the noise effect in the prediction, even if lower sampling rate is employed in the autoregressive filter. As new received signals y_k become available, we utilize them to update previously pre-

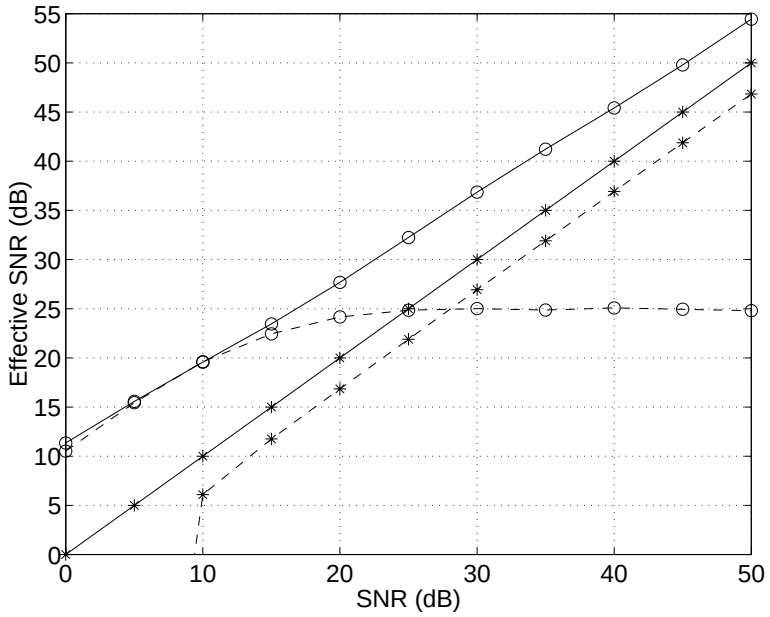

Figure 3.26: Effective SNR comparison for different prediction approaches. o—o: Wiener filtering; o - - - o: adaptive tracking of factor a_k; *—*: ideal SNR using noisy samples; * - - - *: measured SNR using noisy samples; prediction range of 2 ms, $f_{dm} = 100$ Hz.

dicted channel values $\hat{c}_n$. This update results in improved future predictions. In the following discussion, we assume that the sampling rate f_s is 500 Hz, the data rate is 25 Kbits/second and $f_{dm} = 100$ Hz. Thus, there are 49 data bits between the two adjacent low rate samples. Since we often refer to two different rates in this paper, we use the index k for the samples at the data rate, and index n for the lower sampling rate throughout. We utilize channel inversion with threshold, ρ, and assume the average transmitter power is normalized to 1.

The MMSE estimate of the channel coefficient c_n (at the lower sampling rate) using Wiener filtering based on 50 previous noisy samples at the data rate results in the minimum mean squared estimation error ξ_{min}. This error can be viewed as

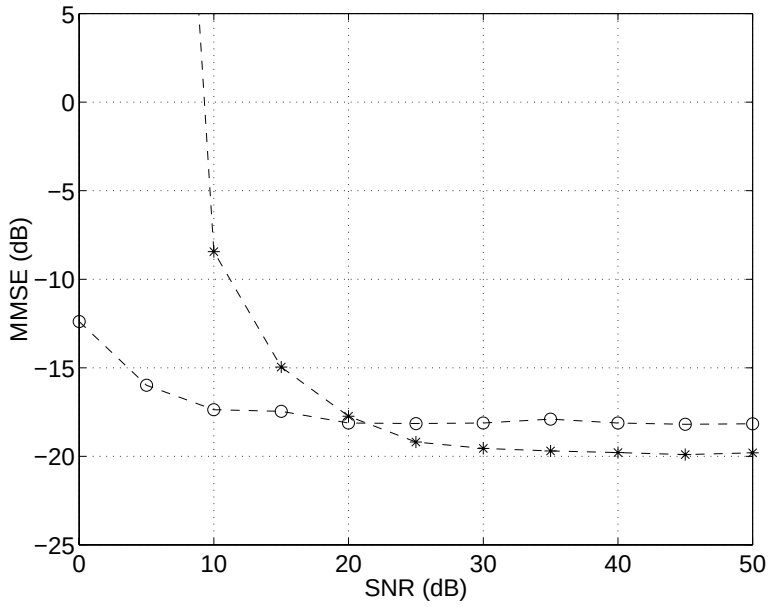

Figure 3.27: MMSE performance comparison: o - - - o: adaptive tracking of factor a_k; * - - - *: using noisy samples.

the variance of the effective noise added to the actual channel sample to obtain the estimate. Then, the effective SNR for the estimated channel samples is given by $E(|c_n|^2 \mid |c_n|^2 > \rho)/(2\xi_{min}) = (1+\rho)/(2\xi_{min})$. This effective SNR is shown by solid curve (circles) in Figure 3.26 and can be viewed as an upper bound on the SNR enhancement in the low rate samples using received signal sampled at the data rate. When by adaptively tracking a_k (3.24) with the step size, $\mu = 0.1$, the effective SNR is examined through simulation. We use the number of scatterers $N = 9$, the observation interval of 100 samples, very low noise during the intitial observation interval, and model order $p = 60$. The prediction range is 2 ms, and the SNR is computed using 50 low rate samples following the initial observation interval. Here we just consider the updated channel coefficient $\tilde{c}_n$ (3.25) in the calculation of SNR, corresponding to the

part of the channel above the threshold. The SNR is shown as dashed line (circles) in Figure 3.26 and the corresponding prediction MSE is shown in Figure 3.27. The performance of this method is very good for low-to-moderate SNR, but the effective SNR and the MMSE saturate for high SNR. In practice, one will have to take into account the effect of interrupted transmission (when the channel power is below the threshold) on the performance of the adaptive algorithm and the issues associated with the decision-directed tracking (e.g., phase ambiguity, propagation error, etc). Furthermore, if we had just used noisy samples at low sampling rate without any decision directed adaptation, our effective SNR would be the same as SNR ($= 1/N_0$). This is shown as a linear line (solid-stars) in Figure 3.26. The measured SNR (from simulations) is lower due to prediction error and is shown as the dashed line (stars) in the same figure. This approach gives poor prediction performance for moderate SNR, and the performance degrades significantly when the SNR is less than 10 dB due to the noise enhancement resulting from unacceptable prediction. The comparison of the MSE for the second and third methods is shown in Figure 3.27.

In addition to the error propagation (a) and the additive noise (b) problems, short observation interval and the time-variant channel model also significantly affect the prediction accuracy (Factors (c),(d), and (e)). In particular, the constant parameter assumption in the deterministic model, e.g., the incident angle of radio wave (and the Doppler shift), are assumed constant during a data block) is not strictly true. For example, as mentioned in [65], for the mobile moving at 30 m/s ($\approx$ 67.5 miles/h), the incidence angle changes at the rate of 4.2°/sec (with respect to a base station 3 km away). Consequently, learning the fast fading channel using just the observation samples is not sufficient. Therefore, slowly changing channel parameters, the limited number of observations used in initial acquisition of the LP coefficients (short obser-

vation interval), the limited order p of the AR model, and the fixing LP coefficients, d_j, used throughout the entire future prediction block affect the performance and are needed to be considered. These factors are mainly reflected in the LP coefficients, d_j, in (3.7). This is investigated by implementing the LMS algorithm for updating the LP coefficients, d_j,

$$\boldsymbol{d}(n+1) = \boldsymbol{d}(n) + \eta e_n \tilde{\boldsymbol{c}}_n^* \tag{3.26}$$

where η is the step-size, $\boldsymbol{d}(n) = (d_1(n), \ldots, d_p(n))$ is the time-dependent vector of channel model parameters (see (3.7)), $\tilde{\boldsymbol{c}}(n) = (c_{n-1}, \ldots, c_{n-p})$ is the vector of updated channel estimates, and the error signal, $e_n = \tilde{c}_n - \hat{c}_n$.

A combined improvement in prediction accuracy using joint adaptive tracking of a_k's and d_j's enhances the proposed prediction method in combating the problems described earlier. Simulation results show that the predicted values using adaptive tracking method follow very closely the actual channel envelope [36]. Again, in practice, the parameters d_j could be updated with a delay of several samples without significantly degrading performance.

3.4 Prediction of Power in the Presence of Phase Ambiguity

The results we provided so far are based on several ideal assumptions. For example, we used binary shift keying signaling (BPSK) and assumed the knowledge of the phases of training bits. In practice, phase ambiguity necessitates the use of differential encoding [5]. In the presence of phase ambiguity, the prediction of power of the fading coefficients, $\Omega(t) = |c(t)|^2$, without the phase information is one alternative. The power is the most important parameter to predict, since it reveals the locations of deep fades and other channel power variations. With our proposed technique, the

power prediction is possible as illustrated in Figure 3.28. The actual channel power (solid line) is observed for the first 100 channel sampling points. Then, we predicted the fading channel power for the next 100 points. It can be seen that our predicted values follow very closely the actual values. Here, we assumed maximum Doppler frequency of 100 Hz and the total number of scatterers are 9. We used the channel sampling rate, $f_s = 500$ Hz. Although the fading signal, $c(t)$, can be described by 9 oscillators, i.e., N= 9 in (3.3), the power of the fading signal can not be simply defined by 9 oscillators. Since the power, $\Omega(t) = c(t)c^*(t)$, by simple arithmetic it can be shown that $\Omega(t)$ consists of a DC term and the sum of the cosines of the pairwise differences of all possible frequencies. Therefore, there exist a combination of $\begin{pmatrix} N \\ 2 \end{pmatrix}$ cosine terms. For example, for $N = 9$, the power, $\Omega(t)$, consists of $\begin{pmatrix} 9 \\ 2 \end{pmatrix} = 36$ cosine terms. This number can go up to thousands depending on the number of scatterers, N. However, our simulation results show that our prediction method can handle even the number of scatterers is on the order of thousands.

Now, we will present the theoretical analysis of the MMSE of long range prediction of the power envelope as a function of several parameters such as: model order, sampling rate, prediction range and the Signal-to-Noise ratio (SNR). We start with the case when number of scatterrs, N, is infinite (Rayleigh fading). The channel is modeled as the complex stationary Gaussian process. Assuming isotropic scattering, the autocorrelation function of the power of the fading coefficient is given for the noiseless observations [4],

$$r(\tau) = E[\Omega(t)\Omega(t+\tau)] = (\Omega_0)^2 + (\Omega_0)^2 J_0^2(2\pi f_{dm}\tau) \tag{3.27}$$

where $J_0(.)$ is the zero-order Bessel function of the first kind and $\Omega_0 = E[|c(t)|^2] =$

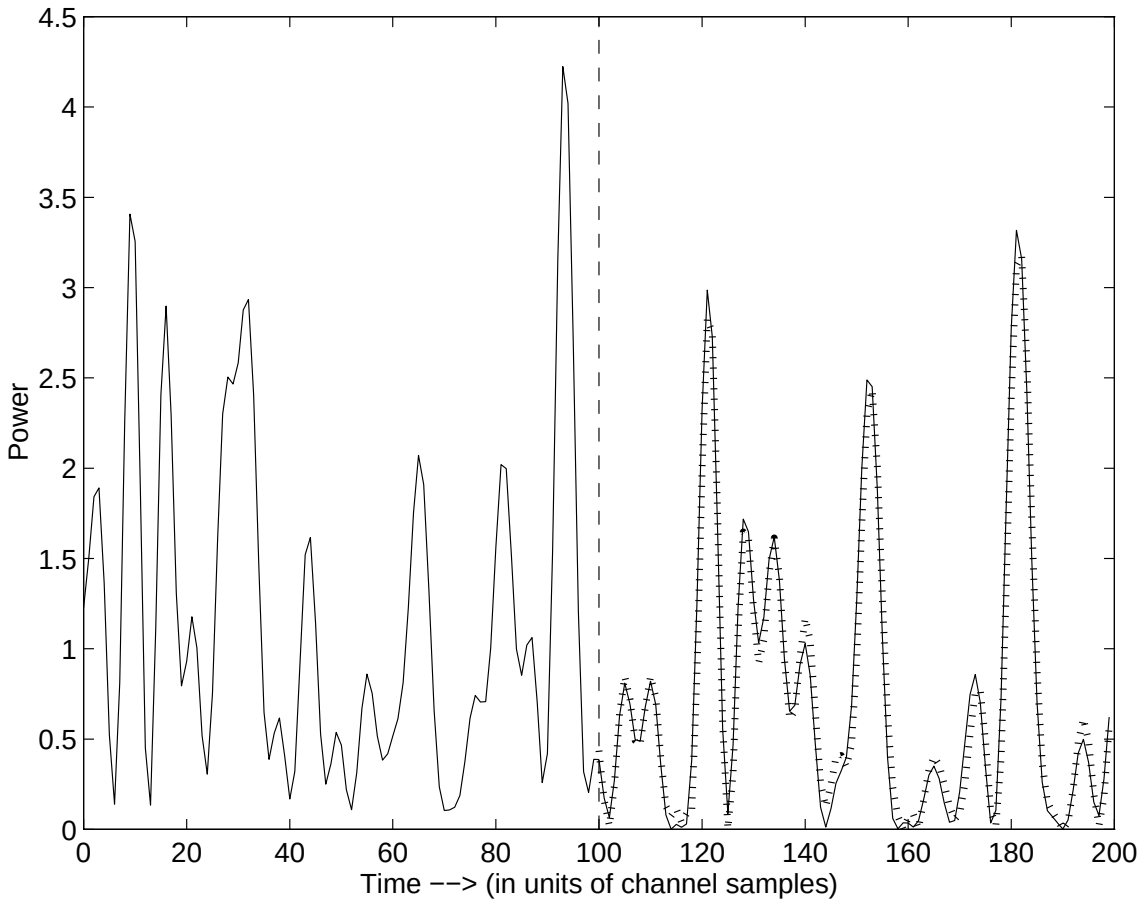

Figure 3.28: First half: The actual channel power (solid line) is observed. Second half: The actual (solid line) and the predicted (dotted line) fading channel power for N= 9 and $f_{dm} = 100$ Hz

$E[\Omega(t)]$. However, the autocorrelation function including the noise terms can be calculated as follows: Let the observed channel samples are $c(t) + n(t)$, where $n(t)$ is AWGN. Therefore, by definition

$$r(\tau) = E[\Omega(t)\Omega(t+\tau)] = E[|c(t) + n(t)|^2 |c(t+\tau) + n(t+\tau)|^2] \tag{3.28}$$

By writing right hand side more explicitely, and using $E[c(t)] = 0$; $E[n(t)] = 0$;

$c(t)$ and $n(t)$ are uncorrelated therefore $E[c(t)n(t)] = E[c(t)]E[n(t)]$; $E[|c(t)|^2] = E[|c(t+\tau)|^2] = \Omega_0$; $E[|n(t)|^2] = E[|n(t+\tau)|^2] = N_0/2$; since $n(t)$ has a complex gaussian distribution with $E[|n(t)|^2] = N_0/2$, then $E[|n(t)|^4] = 2(N_0/2)^2 = N_0^2/2$; $E[|c(t)|^2|c(t+\tau)|^2] = (\Omega_0)^2 + (\Omega_0)^2 J_0^2(2\pi f_{dm}\tau)$; $E[c(t)c^*(t+\tau)] = (\Omega_0/2)J_0(2\pi f_{dm}\tau)$; equation (3.28) is given as:

$$r(\tau) = (\Omega_0^2 + N_0) + \Omega_0^2 J_0^2(2\pi f_{dm}\tau) + N_0\Omega_0 J_0(2\pi f_{dm}\tau) + (N_0^2/2)\delta(\tau) \tag{3.29}$$

This autocorrelation function includes both dc and continuous components. The dc component gives rise to the discrete spectral component. However, we are primarily interested in the continuous portion which describes the variations in the channel. Therefore, the autocovariance function will be used instead of the autocorrelation function. As a convenience in notation, we will also refer to autocovariance function with $r(\tau)$ which is given as:

$$r(\tau) = \Omega_0^2 J_0^2(2\pi f_{dm}\tau) + N_0\Omega_0 J_0(2\pi f_{dm}\tau) + (N_0^2/2)\delta(\tau) \tag{3.30}$$

Note that for low N_0 values, the second term is negligible with respect to the first term. The plot of the autocovariance is shown in Figure 3.29 for $N_0 = 0$. For illustration, let us fix the maximum Doppler frequency at 100 Hz. Then the low sampling rate of 500 Hz would correspond to 5 samples/unit of the $x-$axis of Figure 3.29, whereas the data rate of 25 KHz results in 250 samples/unit. When the model order p is fixed, the observation samples taken at the low sampling rate span much larger time interval than the samples at the data rate. This translates into exploitation of the sidelobes of the autocorrelation function in the prediction and lower MMSE when low rate sampling is employed.

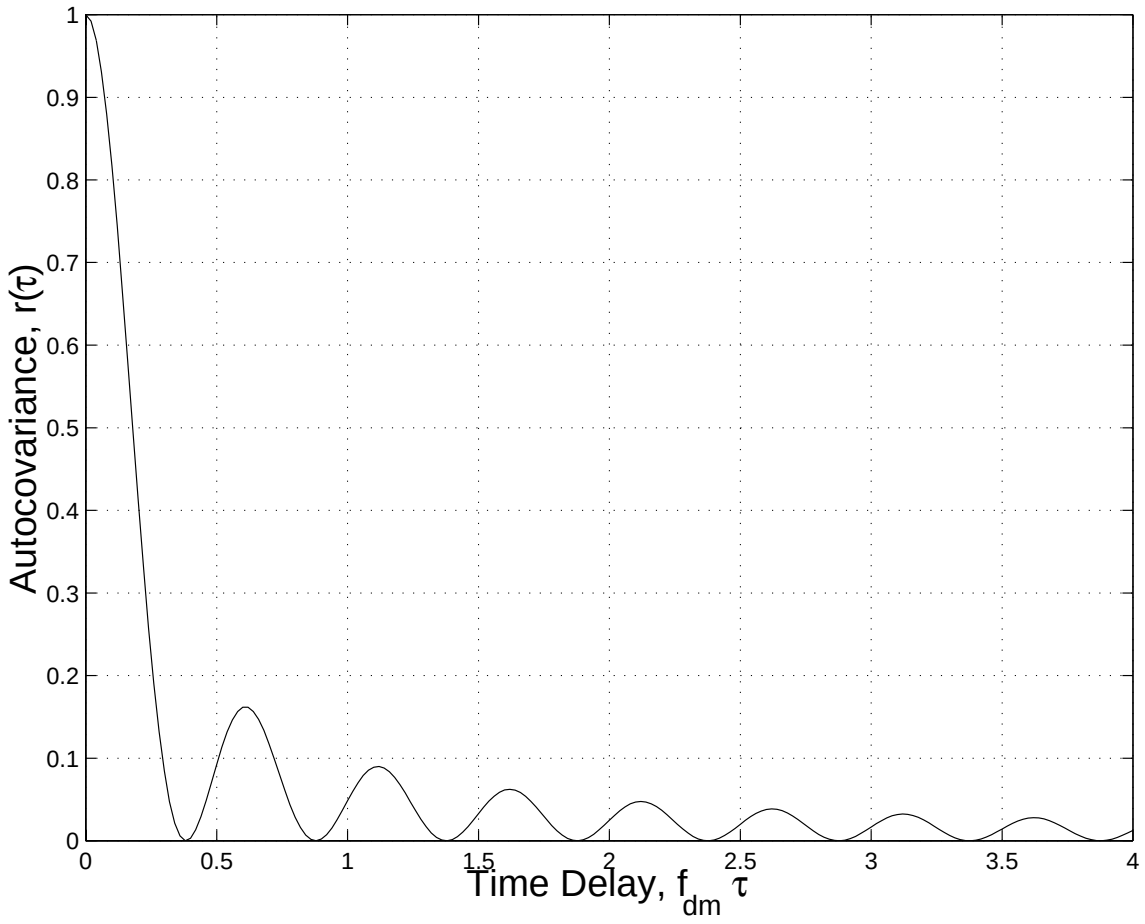

Figure 3.29: The theoretical autocovariance function of the power of the fading coefficient for the Rayleigh fading channel

This observation can be quantified by considering a general channel prediction problem. For a given sampling rate $1/T_s$, the objective is to find the LP filter coefficients d_j which minimize the MSE, $\mathrm{E}[|e(\tau)|^2]$ =$\mathrm{E}[|\Omega(\tau) - \hat{\Omega}(\tau)|^2]$, where τ is a prediction range, and $\hat{\Omega}(\tau)$ is an estimate of the future channel power, $\Omega(\tau)$, given by the linear combination of p past samples $\Omega_{-j} = \Omega(-jT_s)$ (0 is the reference time, so

the observations are taken for $t \leq 0$):

$$\hat{\Omega}(\tau) = \sum_{j=0}^{p-1} d_j \Omega_{-j} \tag{3.31}$$

Using this formula, it is possible to predict the value of the future sample separated from the observations by τ seconds. The optimal coefficients d_j are computed as

$$\boldsymbol{d} = \boldsymbol{R^{-1}r} \tag{3.32}$$

where $\boldsymbol{d}$= $(d_0 \dots d_{p-1})$. $\boldsymbol{R}$ is the autocorrelation matrix $(p \times p)$ with coefficients $R_{ij} = \mathrm{E}[\Omega_{-i}\Omega^*_{-j}]$ and $\boldsymbol{r}$ is the autocorrelation vector $(p \times 1)$ with coefficients $r_j = \mathrm{E}[\Omega(\tau)\Omega^*_{-j}]$. The resulting minimum MSE is given by

$$E[|e(\tau)|^2] = r(0) - \sum_{j=0}^{p-1} d_j r(\tau + jT_s), \tag{3.33}$$

where $r(\tau) = E[\Omega(t)\Omega^*(t+\tau)]$ (see Equation (3.30)).

The MMSE performance of the long range prediction with various sampling rates is compared in Figure 3.30. A moderate model order, $p = 20$, and a very high SNR = 140 dB are chosen to illustrate the performance comparison, although, later, the results will be generalized for any p and SNR values. In this figure, the theoretical MMSE curves (3.33) for a given prediction range are plotted. For example, assuming $f_{dm} = 100$ Hz, the range of 0.2 on the $x-$axis corresponds to 50 data points ahead with the data rate of 25 kHz and 2 sampling point ahead with a lower sampling rate of 1 KHz. As seen from the figure, the same future value can be predicted with much greater accuracy by using the low sampling rates (1 and 2 KHz). Thus, when the sampling rate is reduced greatly relative to the data rate, but the filter length p remains the same, prediction much further ahead becomes feasible.

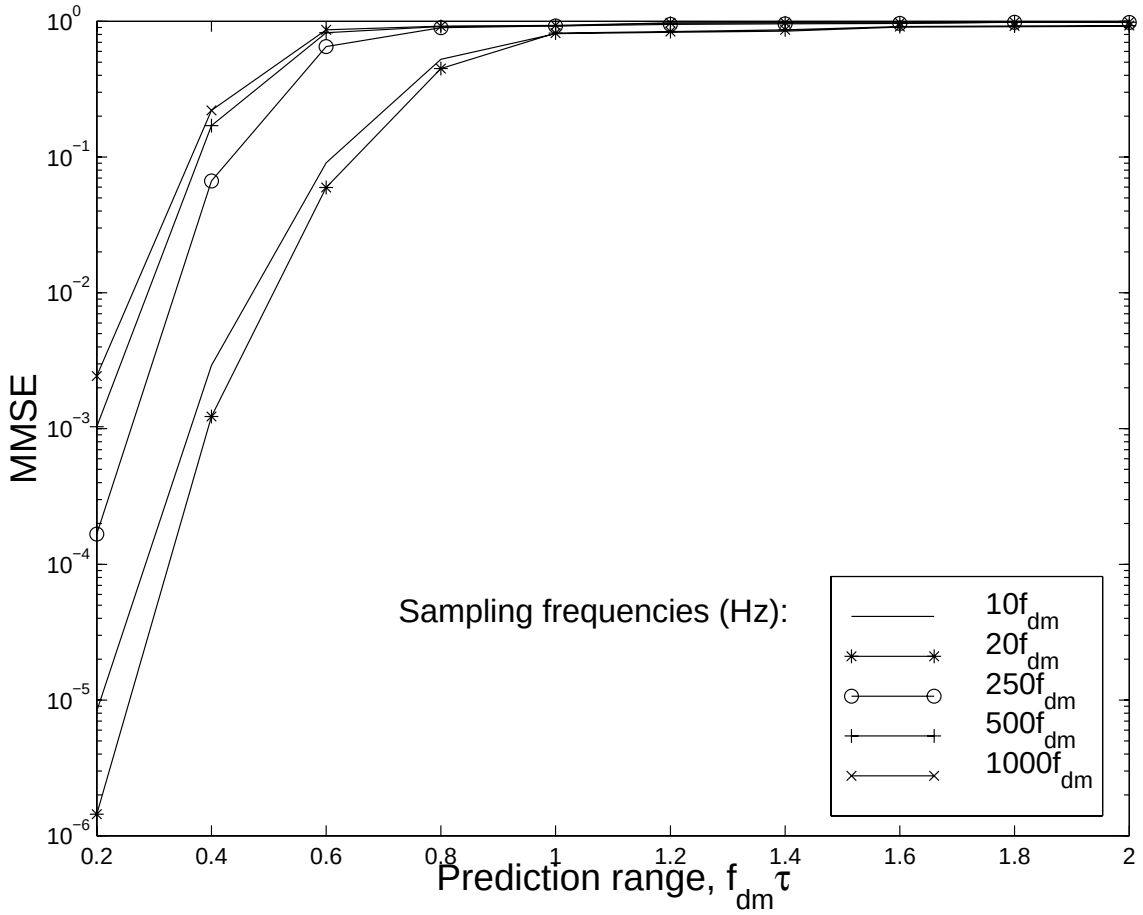

Figure 3.30: MMSE for long range prediction for different values of sampling rate, f_s, with the model order, $p = 20$, and SNR = 140 dB.

The effect of the sampling rate is explored further in Figure 3.31. In this figure, the MMSE vs f_s is plotted for various model orders, p, at the prediction range, $f_{dm}\tau = 0.4$. As seen from the figure, for each model order there is an optimal low sampling rate that minimizes the MMSE. This optimal rate is close to 1-2 KHz range for moderate to high p. These results are obtained for an infinite number of scatterers, N. In this case, the lower sampling rate of 500 Hz is not the optimum rate. Furthermore, in the

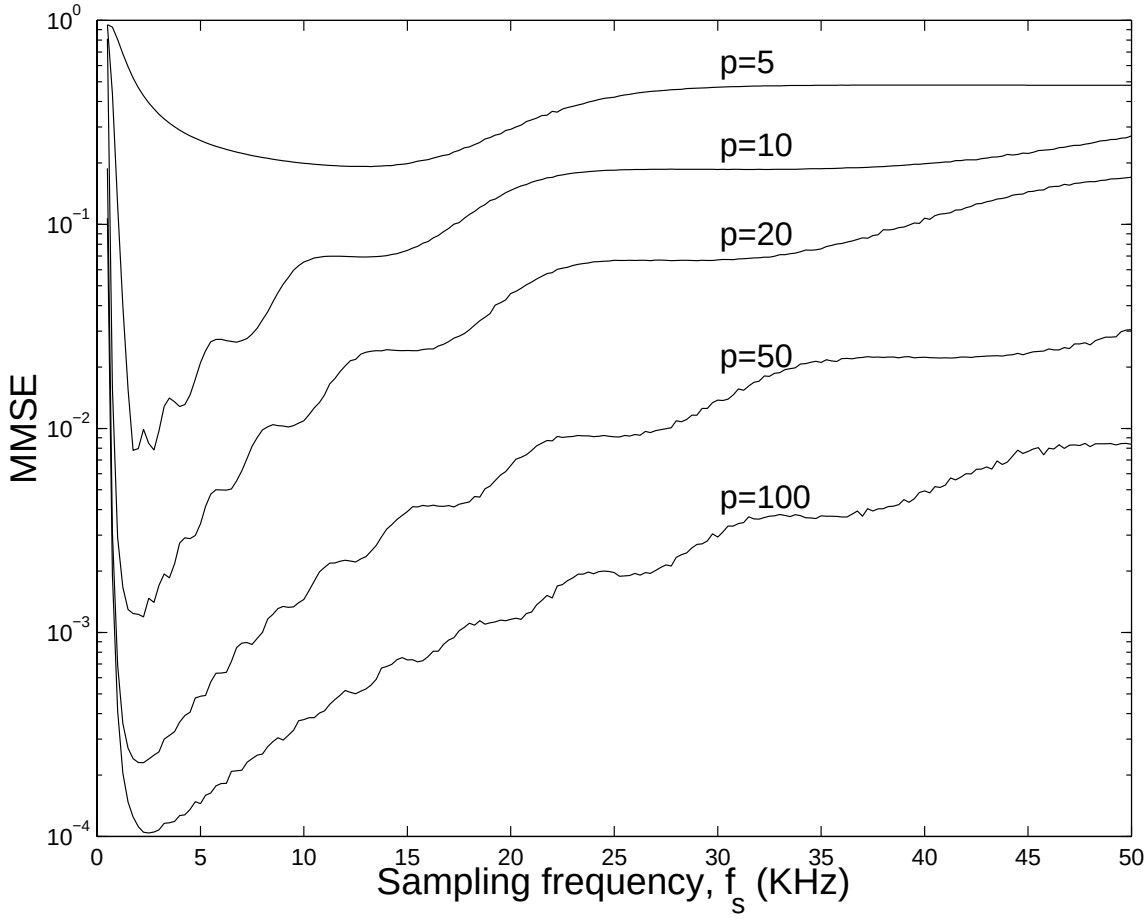

Figure 3.31: MMSE vs sampling rate, f_s, for various model orders p; prediction range $\tau = 4$ ms, SNR = 140 dB and $f_{dm} = 100$ Hz.

practical case, when the number of effective scatterers, N, is low (less than 5), the MMSE decreases with the sampling rate for a fixed p, and the sampling rate of 500 Hz gives the best performance among the rates as shown in Figure 3.32. However, when the number of effective scatterers are greater than 5, the best performance is obtained for the sampling rate around 1 KHz. Hence, we use $f_s = 1$ KHz as a low sampling rate below to illustrate the performance of the MMSE with respect to SNR

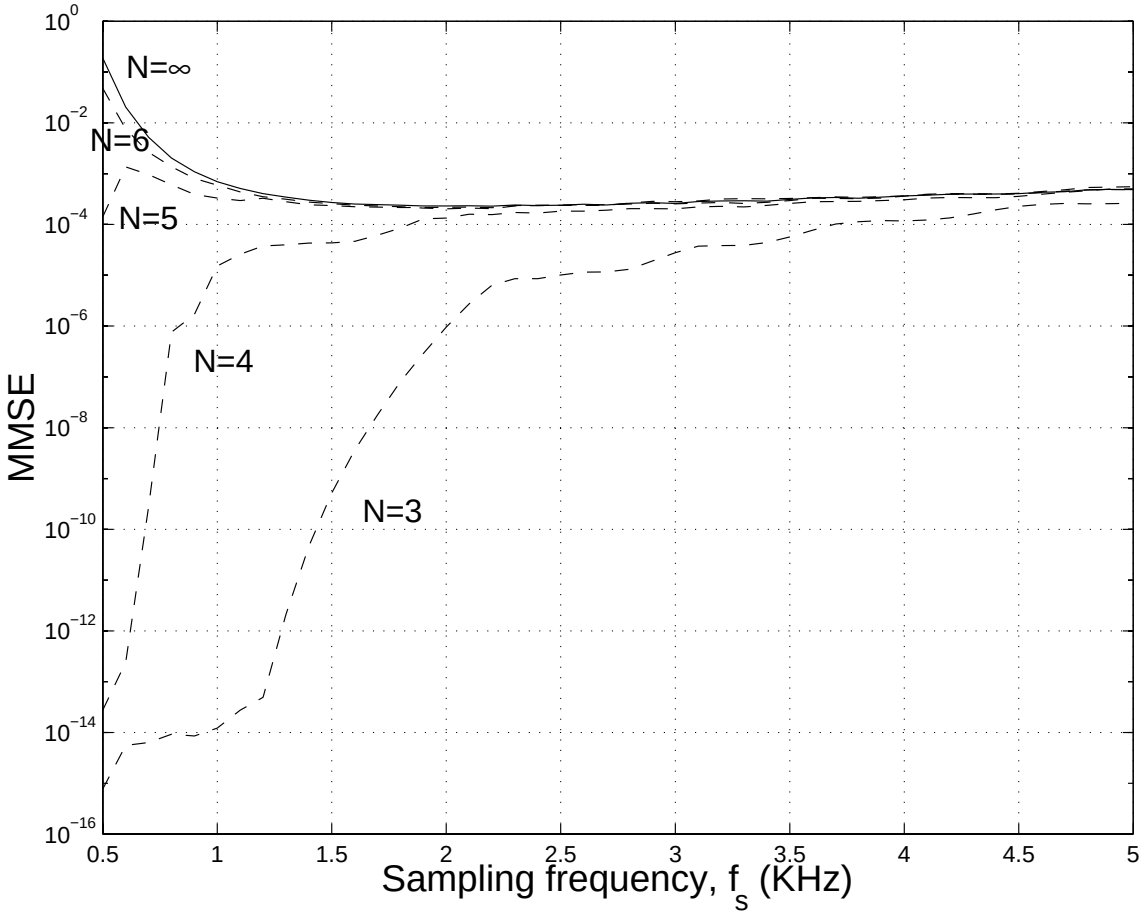

Figure 3.32: MMSE vs f_s for different values of N and for prediction range of 4 ms, $f_{dm} = 100$ Hz at SNR = 100 dB and $p = 50$.

and p. In Figure 3.33, we demonstrate our MMSE results for different SNR values at the data rate of 25 KHz and at the low sampling rate of 1 KHz. Since the prediction range, $f_{dm}\tau = 0.4$ is chosen for these curves, for the data rate of 25 KHz, 100 bits ahead are predicted. This range also corresponds to 4 low rate samples ahead. It can be seen from the figure that the performance of the lower sampling rate is better than that of the high sampling rate for different values of model order, p. For lower

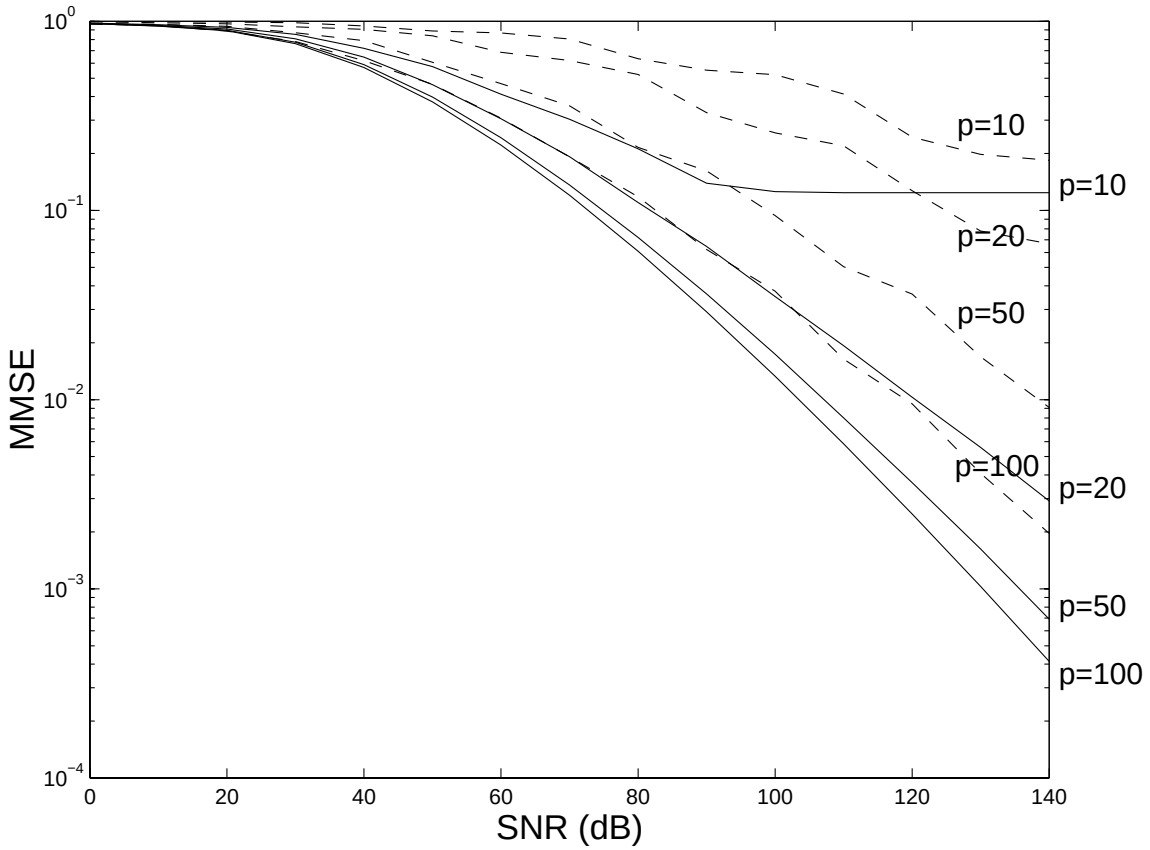

Figure 3.33: MMSE vs SNR for different values of model order, p, at data rate of 25 KHz (dashed lines) and $f_s = 1$ KHz (solid lines) for prediction range τ= 4 ms, $f_{dm} = 100$ Hz.

sampling rates, we observe the saturation of the MMSE as the SNR increases. This MMSE floor can be found from (3.33) for a given value of p by setting $N_0 = 0$. In Figure 3.34, the MMSE vs p is plotted in solid lines for $f_{dm}\tau = 0.1$ and the sampling rate of $10f_{dm}$, for different values of SNR. As p increases the MMSE saturation level is approached. This MMSE floor corresponds to the prediction error given an infinite number of past observations for the fading process sampled at $10f_{dm}$ in the presence of noise.

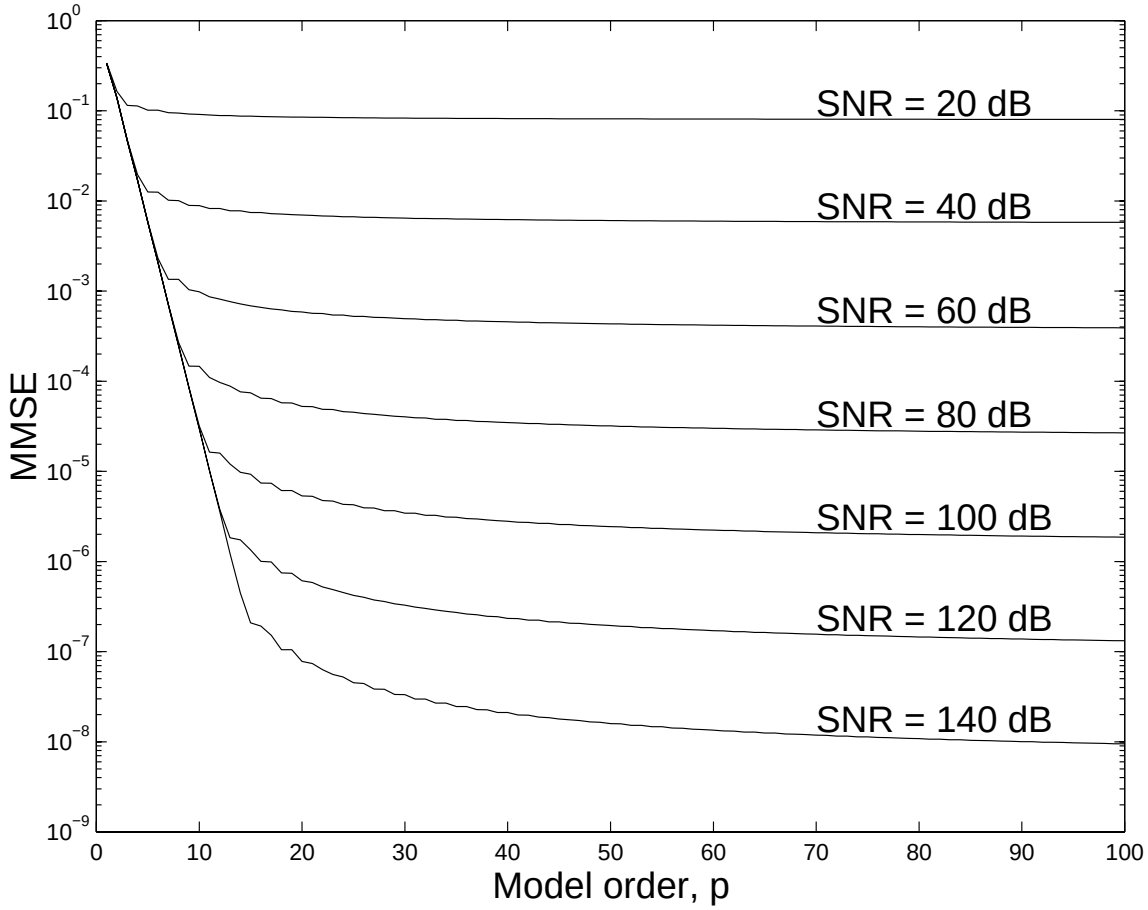

Figure 3.34: MMSE vs. model order, p, for different values of SNR for the sampling rate of 1 KHz, $\tau = 1$ ms, $f_{dm} = 100$ Hz.

Chapter 4

Performance Results in the Presence of ISI - Frequency Selective Fading Channel

So far we examined the flat fading channel where the multipath spread, T_m, is relatively small compared to the signaling interval, T. For example, in North American Cellular System standards the signaling interval, T, is 40 μsec. Assuming the local scatterers around the mobile are in 1 mi radius, the corresponding multipath spread is around 4 μsec which is one tenth of the signaling interval. Since this is the common multipath spread observed in real environment, the actual systems are mostly considered flat. However, there are sometimes very distant scatterers such as a mountain, a hill or a large building. These scatterers act as an another transmitter and the signal comes to the receiver with a delay, e.g., as seen in the Figure 4.1. The delayed received signals cause intersymbol interference (ISI) and result in large multipath spread which is comparable to T [66, 67], i.e., when the multipath delay spread exceeds about 10 percent of the symbol duration, significant ISI can occur. Therefore, channel is considered frequency selective. In this chapter, we will extend our long range prediction technique and results to the frequency selective case. We will show how to utilize the frequency selectivity of the channel into our advantage by using a matched filter (MF) followed by an equalizer. Basically, an equalizer is used

to compensate and reduce the ISI introduced by the frequency selective channels. The combination of MF and an equalizer is a way to gain diversity.

In the next section, we first review the frequency selective channel model used in our analysis. Then, we derive the Matched Filter Bounds (MFB) for the frequency selective fading channels. First, we derive the MFB for 2-path frequency selective channel model and analyze the dependency of the path delay on the MFB. Then, we extend our MFB analysis for more general frequency selective channel with arbitrary number of distinct paths, delays and path strengths. Once we find the MFB for a given channel model, we use this MFB as a reference performance bound in our analysis.

In Section 4.3, the estimation of the channel impulse response is investigated by using pilot signaling. Then, we demonstrated the feasibility of the long range prediction of the channel impulse response of the frequency selective fading channels by using these estimated channel impulse response coefficients. Two different approaches used for the long range prediction are also discussed in this section. The first approach is the optimal approach in the Minimum Mean Squared Error (MMSE) sense. The second approach is a subobtimal approach but it has less computational complexity than the first approach. Performance comparisons of both approaches are also provided in this section.

The time-variant multipath propagation of the signal through the frequency selective channel results in intersymbol interference (ISI). Therefore, the digital transmission at a rate exceeding the coherence bandwidth of the frequency selective fading channel requires equalization at the receiver to compensate and to reduce the ISI [5, 68]. In most communication systems that employ equalizers, the channel characteristics are unknown a priori. Furthermore, in many cases, the channel response

is time-variant, as we experience in wireless communication channels. In that case, the equalizers are designed to be adjustable to the channel response and, for time variant channels, to be adaptive to the time variations in the channel response. The adjustment of equalizer coefficients is usually performed adaptively during the transmission of information by using the decisions at the output of the detector in forming the error signal for the adaptation. Some of these decision directed adaptive techniques, such as LMS, track the variations of the slowly varying channels efficiently, but their performance reduces considerably under the rapidly varying fading conditions. The RLS technique works better under rapidly varying channel conditions but it introduces more computational complexity. Another Adaptive Equalization technique, known as block adaptation scheme, is initially introduced by [69, 59] and developed by [70, 71]. Originally, the start of each data frame contains a known training sequence or pilot symbols which are used to estimate the channel impulse response (CIR). Instead of explicitly tracking the time-varying CIR by using a continuous, decision-directed adaptive algorithm like LMS or RLS, block-adaptive strategy computes the time-varying CIR by interpolating a set of estimated CIR values. This technique has been proven to work well under fast fading conditions for the frequency selective channels. However, it has drawback of an inherent processing delay. Therefore, In Section 4.4, we investigated how the novel long range prediction technique enabled more efficient equalizer techniques at the receiver.

In Section 4.5, we expanded our research on how we utilize the prior knowledge of the predicted channel impulse response at the transmitter. It has been shown that there is a big potential for this technique to be used in more efficient transmitter antenna diversity [38, 72, 73, 74], adaptive modulation and adaptive coding [63, 64, 75, 76, 77, 78, 79, 80, 81, 82] (and the references therein). Our work on the long range

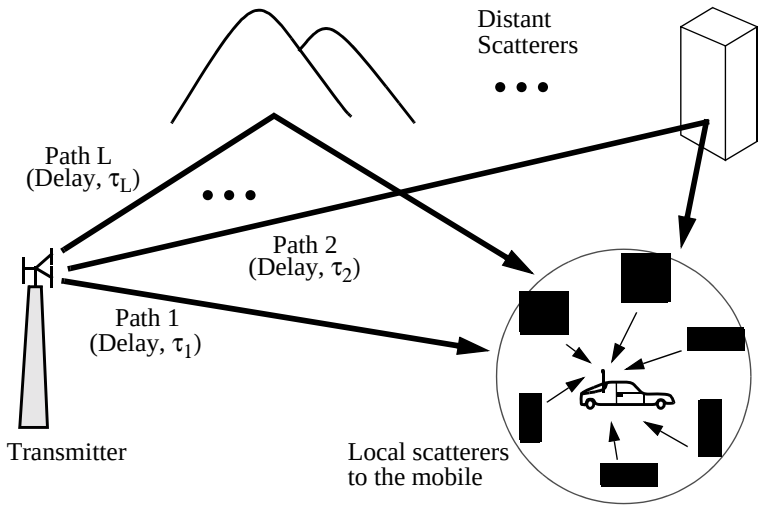

Figure 4.1: The frequency selective fading channel with $L-$paths

prediction of the generalized frequency selective channels provides more insights and flexibility for these transmitter adaptive techniques. In this section, we concentrate on a transmitter precoder (preequalizer) to combat the ISI at the transmitter [83, 84]. It has been shown that the transmitter precoder works well under slowly varying fading channel conditions [85, 86, 87, 88]. However, these transmitter precoder designs work only with the slowly varying fading channels and they fail to track the variations of the rapidly varying fading channels. In this thesis, we also demonstrate how our novel long range prediction algorithm enables powerful transmitter precoders for the rapidly varying fading channels as well. The new design of the transmitter precoder with the long range prediction algorithm for the rapidly varying fading channels is discussed in detail in Section 4.5.

4.1 Frequency Selective Fading Channel Model

As a frequency selective channel model, a general $L-$path model is considered as seen in Figure 4.1. The first path is the main path (Path 1) to the local scatterers

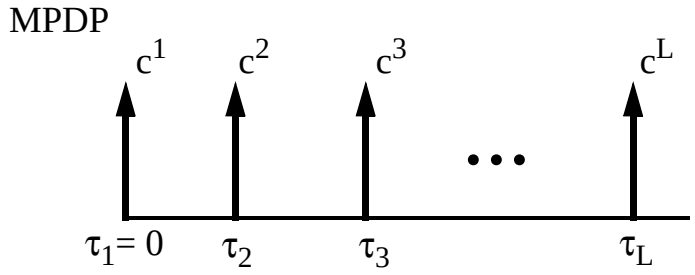

Figure 4.2: Multipath Power Delay Profile (MPDP) of the $L-$path fading channel model

around the mobile. The other paths that are due to the distant scatterers, e.g., a mountain, a building or a large object, cause the signal to arrive to the vicinity of the mobile with different delays, τ_i. Therefore, the impulse response of the channel is given by

$$c(t) = \sum_{i=1}^{L} c^i(t)\delta(t - \tau_i). \tag{4.1}$$

The corresponding Multipath Power Delay Profile (MPDP) is illustrated in Figure 4.2. This channel model results in the received signal in the form of

$$r(t) = \sum_{i=1}^{L} c^i(t)s(t - \tau_i) + n(t), \tag{4.2}$$

where $s(t)$ is the transmitted signal, $n(t)$ is additive white Gaussian noise (AWGN), and the coefficients c^is are independent identically distributed (iid) Rayleigh fading coefficients [1]. Furthermore, for the consistency in the BER calculations, the total average power is set to be the same as in the flat fading case which is $2\sigma^2$. That is

[1] the time dependence is implicit.

$\sum_{i=1}^{L} E(|c^i|^2) = 2\sigma^2$. It follows that each path has envelope, α_i, phase, θ_i, and instantaneous power, $|c^i|^2 = \alpha_i^2$, with Rayleigh, uniform and exponential distributions, respectively

$$p(\alpha_i) = \frac{\alpha_i}{\sigma_i^2} e^{-\frac{\alpha_i^2}{2\sigma_i^2}}, \qquad 0 \leq \alpha_i < \infty \tag{4.3}$$

$$p(\theta_i) = \frac{1}{2\pi}, \qquad 0 \leq \theta_i \leq 2\pi \tag{4.4}$$

$$p(\alpha_i^2) = p(|c^i|^2) = \frac{1}{2\sigma_i^2} e^{-\frac{|c^i|^2}{2\sigma_i^2}}, \qquad 0 \leq |c^i|^2 < \infty \tag{4.5}$$

4.2 Matched Filter Bounds (MFB)

In this section, we first derive the MFB for 2-path model and analyze the dependency of the path delay on the MFB. Then, in the following section, we extend our MFB analysis for more general frequency selective channel with arbitrary number of distinct paths, delays and path strengths. Once the MFB is found for a given channel model, this MFB is used as a reference performance bound in our analysis.

4.2.1 MFB for 2-path model

The matched filter bound (MFB) is a bound on the optimal performance over a communication channel which assumes that the transmitted pulses are sufficiently separated (or simply assume that one data pulse is transmitted) so that no intersymbol interference (ISI) occurs and the channel is perfectly known. The identification of the best performance is generally accepted as being useful in setting a goal for the practical realization of the communication system.

The exact MFB is evaluated for a channel modeled by the sum of two delayed

and independently Rayleigh fading paths in [89] The two path-model is used as a benchmark in the North American Digital Cellular standard IS−54 [90]. Therefore, initially, we review the MFB for 2-path model to show the performance characteristics. In the next section, we will discuss the general case for $L-$path frequency selective fading channel.

The derivation of MFB for 2-path model is as follows. Let the differential delay between two paths be τ. Recalling the equation (4.2), the received signal is given as

$$r(t) = c^1(t)s(t) + c^2(t)s(t-\tau) + n(t), \tag{4.6}$$

where $s(t)$ is the transmitted signal, $n(t)$ is additive white Gaussian noise (AWGN), and the coefficients c^1 and c^2 are Rayleigh distributed fading coefficients with equal average power for each path. Let the transmitted signal be $s(t) = \sum_k b_k g(t-kT)$, where b_k is the data sequence, T is the symbol delay, and $g(t)$ is the pulse shape of the cascaded combination of the transmit and the receive filters. Having the transmit and the receive filters with the Square Root Raised Cosine (SRRC) frequency responses, the overall frequency response is given as the Raised Cosine (RC) response satisfying Nyquist's criterion for zero ISI. The corresponding impulse response of RC filter with the unit energy is given as (see Figure 4.3)

$$g(t) = \frac{\sin(\pi t/T)}{\pi t/T} \frac{\cos(\pi\beta t/T)}{1-4\beta^2 t^2/T^2}, \tag{4.7}$$

where β is called the *rolloff factor*, and takes values in the range $0 \leq \beta \leq 1$. Assuming that the $g(t)$ is sufficiently concentrated in time, and τ is sufficiently short, so that the $c^1(t)$ and $c^2(t)$ can be regarded as constants c^1 and c^2 over a combined duration of $g(t)$ and $g(t-\tau)$. If we denote the Fourier transform of $g(t)$ by $G(\omega)$, then, within

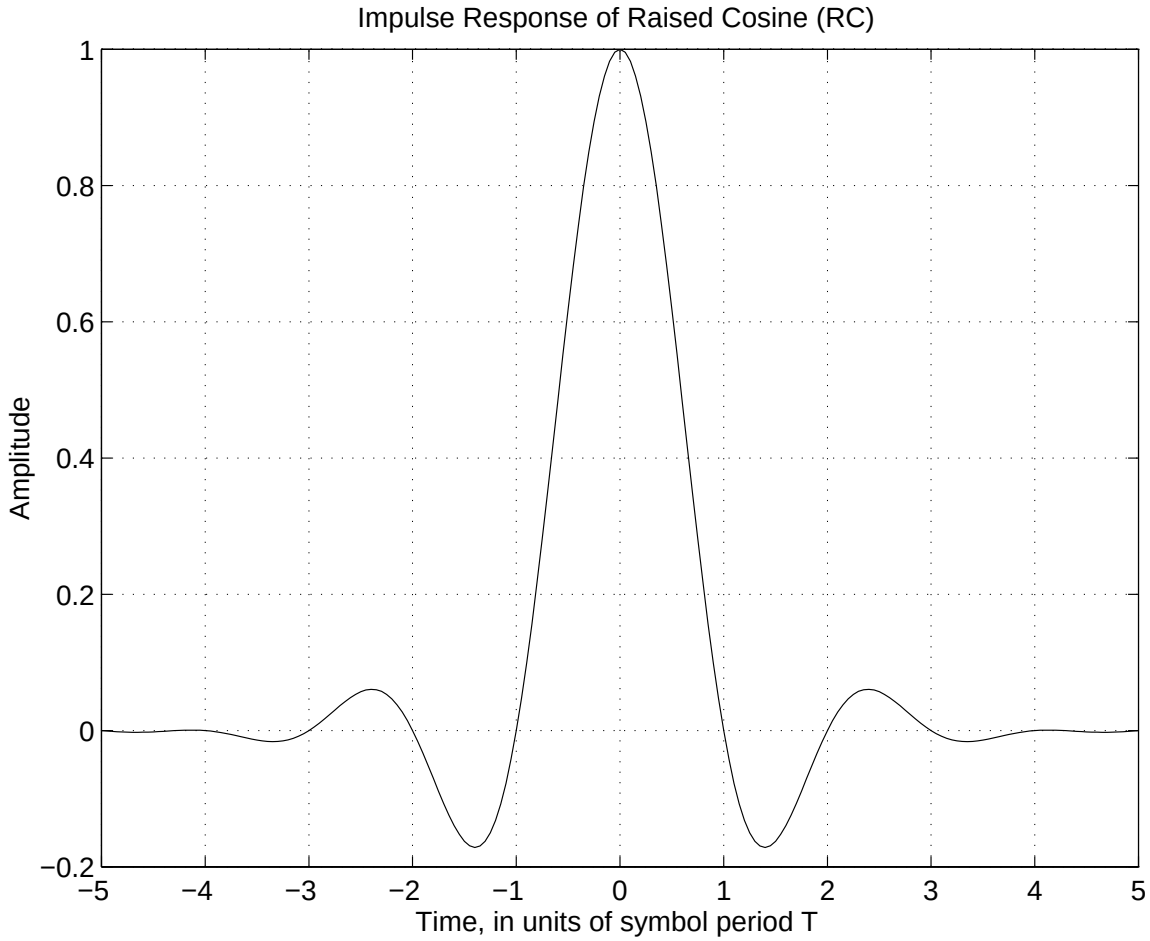

Figure 4.3: Impulse response of a raised cosine (RC) filter

this approximation, the Fourier transform, $G_r(\omega)$ of the received pulse is

$$G_r(\omega) = G(\omega)[c^1 + c^2 e^{-j\omega\tau}]. \tag{4.8}$$

The matched filter (MF) to be used for optimum reception has $G_r^*(\omega)$ for its frequency characteristics. When the filter's output is appropriately sampled, the signal

contribution to the sample value is the energy E_r in the received pulse as

$$E_r = \frac{1}{2\pi} \int_{-\infty}^{\infty} |G_r(\omega)|^2 d\omega. \tag{4.9}$$

Then, at the output of the MF, E_r evaluates to

$$E_r = |c^1|^2 + |c^2|^2 + 2Re[(c^1)(c^2)^* g(\tau)]. \tag{4.10}$$

Therefore, the corresponding BER which is also MFB in this case is given by [89]

$$P_e = \frac{1}{2} \left[1 - \frac{1}{d_1 - d_2} \left(\frac{\sqrt{\gamma_b} d_1}{\sqrt{\gamma_b + \frac{1}{d_1}}} - \frac{\sqrt{\gamma_b} d_2}{\sqrt{\gamma_b + \frac{1}{d_2}}} \right) \right] \tag{4.11}$$

where γ_b is the average signal to noise ration (SNR), and the parameter d_i is defined as

$$d_i = \frac{1 - (-1)^i g(\tau)}{2}, \qquad i = 1, 2. \tag{4.12}$$

The equation (4.11) is valid as long as $d_1 \neq d_2$. The case $d_1 = d_2$ can only occur when $g(\tau) = 0$, resulting in $d_1 = d_2 = \frac{1}{2}$. Then, we obtain

$$P_e = \frac{1}{2} \left[1 - \frac{\sqrt{\gamma_b}}{\sqrt{2 + \gamma_b}} - \frac{\sqrt{\gamma_b}}{(\sqrt{2 + \gamma_b})^3} \right]. \tag{4.13}$$

It is obvious from the equations (4.11)-(4.13) that the BER depends on the relative delay τ. This dependency can be seen in Figure 4.4 for a fixed SNR= 10 dB. When $\tau = 0$, i.e, $g(\tau) = 1$, the delayed path coincides with the main path and due to the assumed independence of the fading process the path powers add, resulting in one main path with power increased by a factor of 2. The corresponding $d_1 = 1$ and $d_2 = 0$ for this case. Therefore, BER reduces to the case same as to the flat fading channel (3.20). When $\tau = kT$, i.e, $g(\tau) = 0$, the MF detector is equivalent to optimal

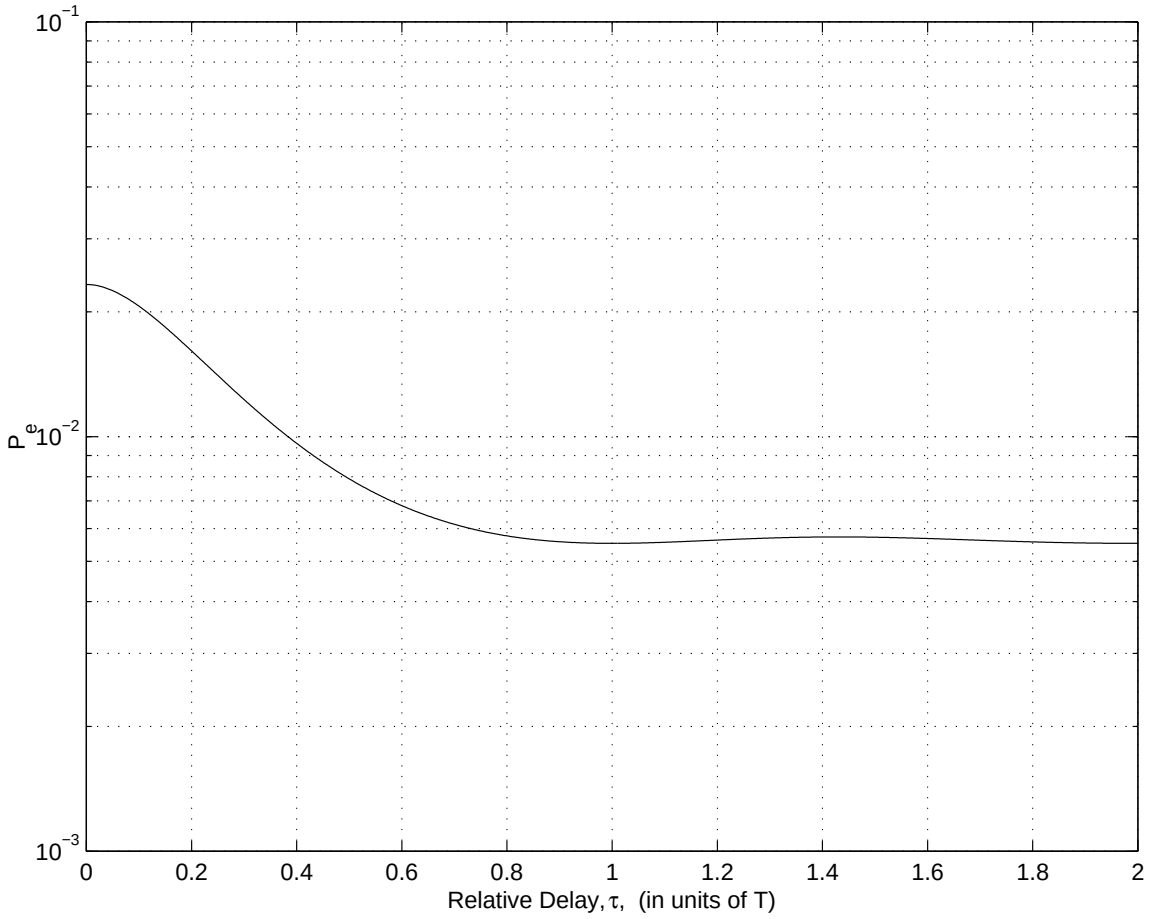

Figure 4.4: Matched filter bound vs relative delay, τ, for SNR= 10 dB

diversity combining. Explicitly, we could have used a received filter matched to the undistorted pulse, $g(t)$, and sampled the output both at $t = 0$ and $t = \tau$. There would be no interference between the signal components, and the two noise samples would be independent. This is equivalent to two separate beams with independent noise backgrounds. The corresponding $d_1 = 1/2$ and $d_2 = 1/2$ for this case. Therefore, the BER is given by (4.13) which is the same as the equation given for two branch diversity [5]. Figure 4.4 provides the MFB vs τ where we have taken $g(\tau)$ having a RC impulse

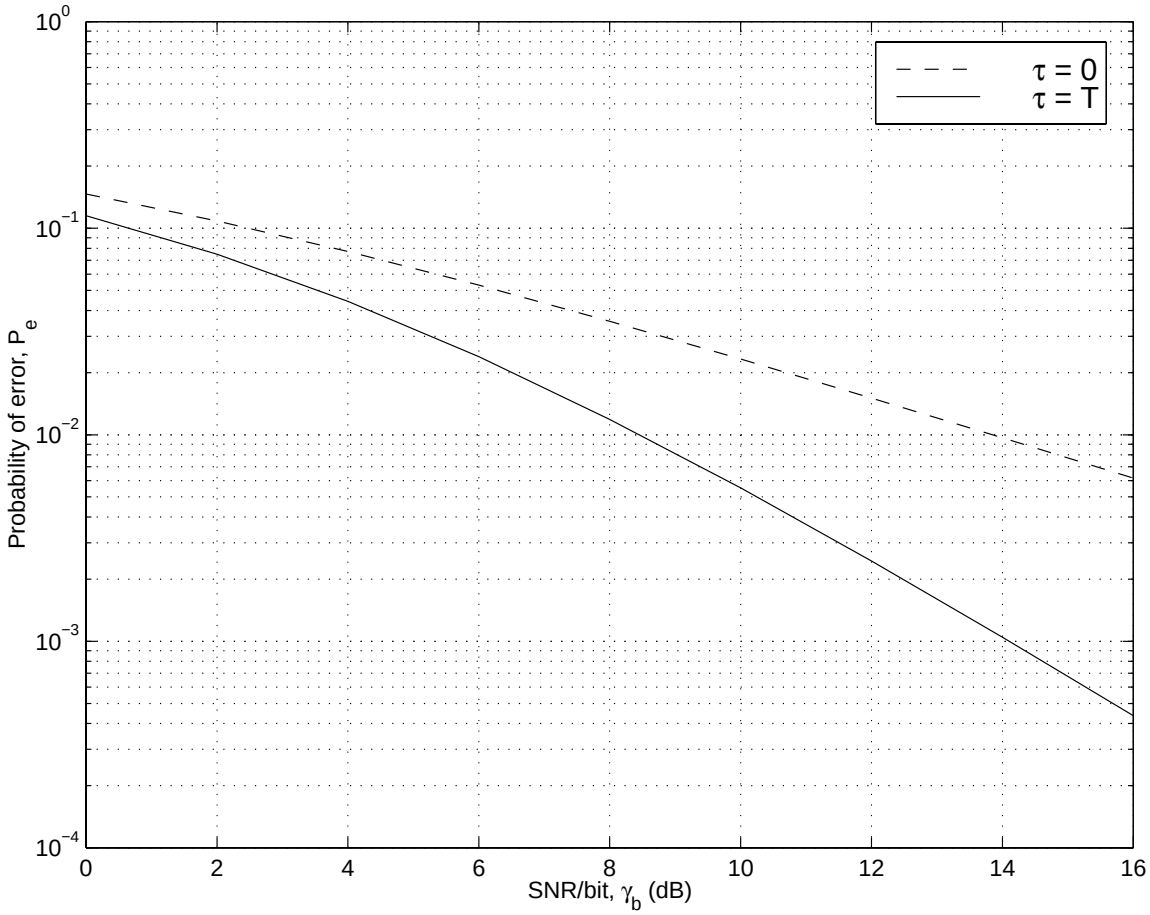

Figure 4.5: BER vs SNR for $\tau = 0$ and $\tau = T$

response with $\beta = 35\%$ (however, it is noted in [89] that the bounds are insensitive to the β.) The diversity like improvement is observed. The performance is very close to the dual diversity case for $\tau > 0.8T$. The probability of bit error is plotted with respect to the SNR for $\tau = 0$ and $\tau = T$ in Figure 4.5. When $\tau = 0$, the performance is the same as that of the Rayleigh fading channel (Flat fading). Whereas, when $\tau = T$, the performance is the same as the dual diversity performance. (Note that when $\tau > 0.8T$, the similar performance is observed as that of dual diversity case).

4.2.2 MFB with Channel Inversion

In this section, we demonstrate how to obtain the new MFB with the channel inversion methodology introduced in Chapter 3. Please note that the channel inversion method might not be practical for some applications and is analyzed here to access the performance advantages of the proposed technique. More practical implementations both at the receiver and at the transmitter for the general frequency selective channels will be discussed in details in the next Section.

The derivation has been done for 2-path model. Using the same methodology, it can easily be extended to the $L-$path model. We will also explore the MFB and estimation of the $L-$path model with arbitrary delays later along with the long range prediction and the equalization. When $\tau = T$, $g(\tau) = 0$, the output of the MF is given by (4.10)

$$|c^T|^2 = |c^1|^2 + |c^2|^2. \tag{4.14}$$

Assuming an equal power for each path 1 and 2, i.e., $\sigma_1^2 = \sigma_2^2 = \sigma_P^2$, pdf of $|c^T|^2$ is given by the convolution of the pdfs of the each path (4.5), A and B, and is found as (Appendix B):

$$p(|c^T|^2) = \frac{1}{(2\sigma_P^2)^2}|c^T|^2 e^{-\frac{|c^T|^2}{2\sigma_P^2}}, \qquad 0 \leq |c^T|^2 < \infty \tag{4.15}$$

The expected value of $|c^T|^2$ is also calculated as (Appendix B), $E(|c^T|^2) = 2(2\sigma_P^2)$. Let the average power of each path be equal, i.e., $2\sigma_1^2 = 2\sigma_2^2 = \sigma^2$. Therefore, $E(|c^T|^2) = 2\sigma^2$ which is the same as flat fading case.

The channel inversion technique introduced in Chapter 3 for flat fading case. For a frequency selective case, it is modified as follows: The transmitter interrupts the transmission if the power level, $|c^T|^2$ is below a previously chosen threshold value, ρ.

Furthermore, if $|c^T|^2$ is above the threshold, the transmitter sends the data bits, b_k, by multiplying them with the inverse of the $|c^T|$ values. Therefore, we need to know the pdf of the inverted power, $z = \frac{1}{|c^T|^2}$, to investigate the effect of power inversion process. As calculated in Appendix B, the pdf of the inverted power is given as

$$p(z) = \frac{1}{(2\sigma_P^2)^2}\frac{1}{z^3}e^{-\frac{1}{z2\sigma_P^2}}, \qquad 0 \leq z < \infty \tag{4.16}$$

or

$$p\left(\frac{1}{|c^T|^2}\right) = \frac{1}{(2\sigma_P^2)^2}(|c^T|^2)^3 e^{-\frac{|c^T|^2}{2\sigma_P^2}}, \qquad 0 \leq \frac{1}{|c^T|^2} < \infty \tag{4.17}$$

with $E(\frac{1}{|c^T|^2}) = \frac{1}{2\sigma_P^2}$. When we normalize our channel to unit power, i.e., $2\sigma = 1$ or equivalently $2\sigma_P = 1/2$, the average power of inverted channel becomes $E(\frac{1}{|c^T|^2}) = 2$. This translates to 3 dB power boost is introduced at the transmitter. However, this value is obtained without the threshold unlike the flat fading case where this value was infinity without the thresholds. We can improve the performance even more with introducing the threshold, ρ, with the expense of throughput, i.e., the throughput reduces with the increasing threshold (or equivalently, the bandwidth increases). The throughputs are calculated for a given ρ as

$$Pr(|c^T|^2 > \rho) = \int_\rho^\infty \frac{1}{(2\sigma_P^2)^2} y e^{-\frac{y}{2\sigma_P^2}} dy = e^{-\frac{\rho}{2\sigma_P^2}}\left(1 + \frac{\rho}{2\sigma_P^2}\right). \tag{4.18}$$

Moreover, for a given ρ, the new pdf of the inverted power becomes:

$$p\left(\frac{1}{|c^T|^2} \mid \frac{1}{|c^T|^2} < \frac{1}{\rho}\right) = \frac{1}{(2\sigma_P^2)^2}(|c^T|^2)^3 e^{-\frac{|c^T|^2}{2\sigma_P^2}} \frac{1}{e^{\frac{\rho}{2\sigma_P^2}}(1 + \frac{\rho}{2\sigma_P^2})}, \qquad 0 \leq \frac{1}{|c^T|^2} < \frac{1}{\rho} \tag{4.19}$$

with the average power given as

$$E\left(\frac{1}{|c^T|^2} \mid \frac{1}{|c^T|^2} < \frac{1}{\rho}\right) = \frac{1}{\rho + 2\sigma_P^2}. \tag{4.20}$$

The spectral efficiencies and the the power of inverted channel, $E(\frac{1}{|c^T|^2} \mid \frac{1}{|c^T|^2} < \frac{1}{\rho})$, are summarized in Table 4.1 for different values of thresholds. When we compare these

Threshold, ρ	Throughput	$E(\frac{1}{\lvert c^T\rvert^2} \mid \frac{1}{\lvert c^T\rvert^2} < \frac{1}{\rho})$ (dB)
0	100%	3
0.167	95.54%	1.76
0.5	73.6%	0

Table 4.1: Throughput and the average power of inverted channel values with corresponding threshold values for 2-path model with relative delay $\tau = T$

results for the frequency selective fading case with the Table 3.1 which reflects the flat fading results, we observe the same level of performance can be obtained with higher spectral efficiencies (throughputs) for the frequency selective fading case.

Furthermore, with the relative delay between two paths, $\tau = T$, MFBs are plotted with or without channel inversion for different threshold values in Figure 4.6. Solid lines reflect the theoretical results assuming the perfect prediction of the channel. By increasing the threshold from 0 to 0.5, we observe performance improvement. However, the spectral efficiency decreases with the increasing thresholds (or equivalently, the bandwidth increases). Since the power of the transmitted signal is greater than $E(b_k^2)$ for thresholds $\rho < 0.5$, the BER for these threshold values are above the AWGN channel BER. For the threshold, $\rho = 0.5$, the transmitted power is equal to $E(b_k^2)$

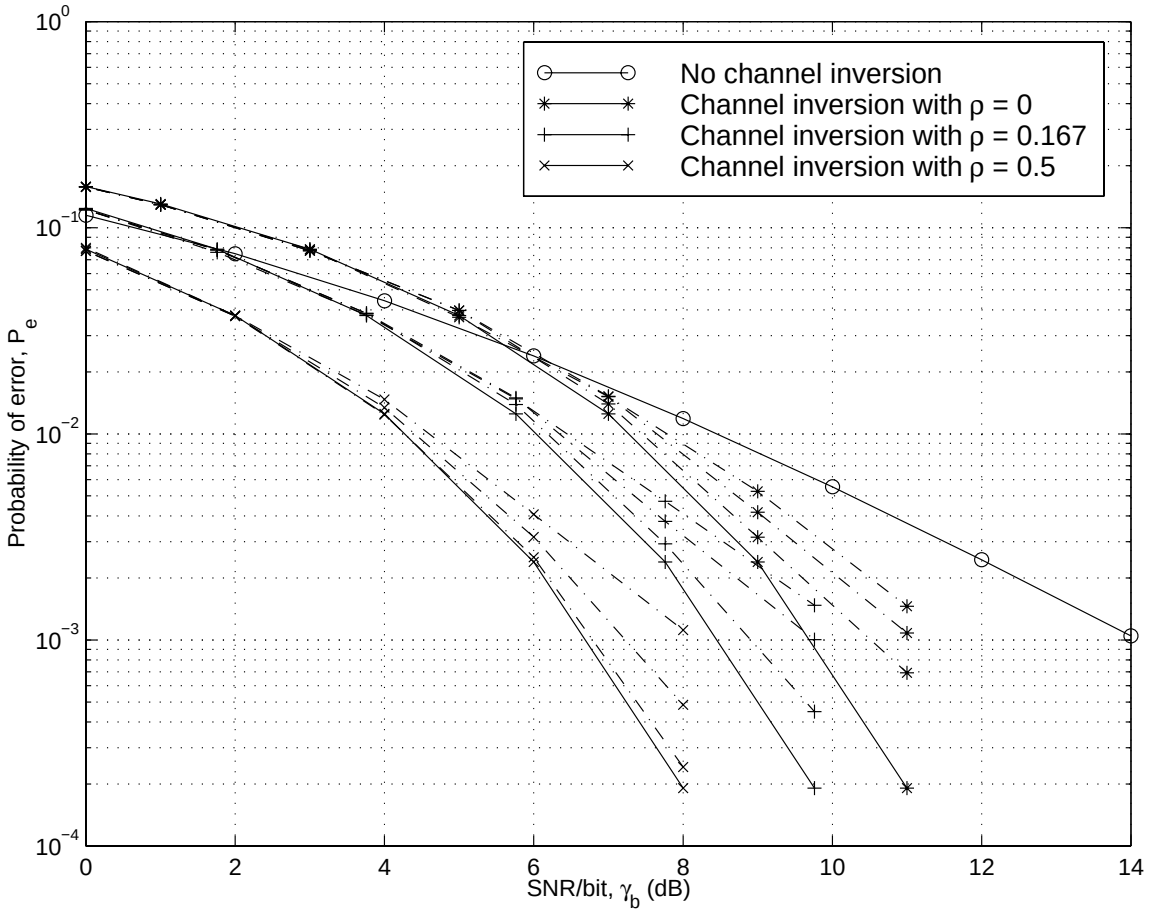

Figure 4.6: MFBs for $\tau = T$ (Solid lines are theoretical; dashed lines are simulation results for each threshold level)

and the analytical curve is also the BER of the AWGN channel given as [5]

$$P_e = Q(\sqrt{2\gamma_b}) \tag{4.21}$$

where γ_b is the signal to noise (SNR) and $Q(x)$ is defined as $Q(x) = \frac{1}{\sqrt{2\pi}} \int_x^\infty e^{-t^2/2} dt$. In this figure, the simulation results with different observation intervals are also presented with dashed lines for each threshold level. Three sets of simulation are performed with observation intervals of 50, 100, and 200 channel sampling points with

low sampling rate of 500 Hz to predict the total power, $|c^T|^2$. These observation intervals convert to time as 0.1, 0.2, and 0.4 sec respectively. As we reduce the observation interval, the performance of our system deviates more from the theoretical curves for every threshold value as seen in the figure. The closest simulation curve to the theoretical curve is the one with the longest observation interval, 200 channel samples (or 0.4 sec) for each threshold level. On the other hand, the furthest simulation curve to the theoretical curve is the one with the shortest observation interval, 50 channel samples (or 0.1 sec). Note that we eliminate the deep fades by introducing thresholds. When we have higher threshold values, we observe less deep fades and consequently less abrupt changes in the fading channel. We also observe that most of the interpolation error occurs in the deep fades. Therefore, this explains the reason why there are more deviations for the lower threshold values. Furthermore, the difference between the theoretical curves and the simulated curves can be reduced by incorporating an adaptive tracking of the LP coefficients, d, as explained in Chapter 3.

4.2.3 MFB for the general Frequency Selective Channels

The exact MFB is evaluated for a channel modeled by the sum of two delayed and independently Rayleigh fading paths in the previous section. It has been shown that if the delays are separated more than $0.8T$ where T is the symbol interval, dual-diversity (or dual antenna diversity with flat fading) performance is observed. In practical systems, there exists more than two paths with each path having its relative strength and delay. Then, the multipath channel is given by

$$c(t) = \sum_{i=1}^{L} a_i c_i(t) \delta(t - \tau_i) \tag{4.22}$$

where L is the total number of paths, $c_i(t)$ complex Gaussian random process, and a_i and τ_i are the root mean square of the magnitude and the delay of the $i-$th path. Let the baseband transmitted signal be a single pulse $m(t)b_k$ where $m(t)$ is the shaping pulse and the b_k is a complex data symbol. In our analysis, we consider Square Root Raised Cosine (SRRC) pulse shape for the transmitter pulse shape, $m(t)$ [5]. When the transmitted pulse passes through the multipath channel, (see Eq. (4.22)), the received signal is found as

$$r(t) = \sum_{i=1}^{L} a_i c_i(t) m(t - \tau_i) b_k + n(t) \tag{4.23}$$

where $n(t)$ is zero mean, additive complex white Gaussian noise (AWGN) with a power spectral density $N_0/2$. We assume that $c_i(t)$ does not change within the duration of the pulse, hence we can drop the time index t. On the other hand, over the total ensemble, c_i is complex Gaussian random variable. The Fourier transform of the signal portion in r(t) is found as

$$M_s(\omega) = M(\omega) \sum_{i=1}^{L} a_i c_i e^{-j\omega\tau_i} \tag{4.24}$$

where $M(\omega)$ is the Fourier transform of transmitter pulse shape $m(t)$. Then, the corresponding frequency response of the matched filter for $r(t)$ is given by

$$M_s^*(\omega) = M^*(\omega) \sum_{i=1}^{L} a_i^* c_i^* e^{j\omega\tau_i} \tag{4.25}$$

The Fourier transform of the received pulse at the matched filter output is given by $|M_s(\omega)|^2$. Therefore, the total received signal power per bit at the output of the

matched filter is calculated from

$$E_s = \frac{1}{2\pi}\int_{-\infty}^{\infty} |M_s(\omega)|^2 d\omega = \sum_{i=1}^{L}\sum_{j=1}^{L} a_i a_j^* c_i c_j^* g(\tau_i - \tau_j) \tag{4.26}$$

where $g(t)$ is Raised Cosine (RC) pulse shape which is also the inverse Fourier transform of $|M(\omega)|^2$ [5]. E_s is also be represented in matrix form such that $E_s = \boldsymbol{c^H G c}$ where $\boldsymbol{c}$ is a $L-$dimensional vector whose components are the random variables c_i, and the superscript H denotes Hermitian (complex conjugate transpose). $\boldsymbol{G}$ is $L \times L$ matrix with $\{g_{ij}\} = a_i a_j^* g(\tau_i - \tau_j)$. Note that since E_s is non-negative (see Eq. (4.26)), $\boldsymbol{G}$ is a non-negative definite Hermitian matrix. Therefore, it can be shown that [91]

$$\sum_{j=1}^{L} \lambda_i = Trace(\boldsymbol{G}) = g(0)\sum_{j=1}^{L} |a_i|^2 = E[E_s] \tag{4.27}$$

where λ_i's are the eigenvalues of $\boldsymbol{G}$. Therefore, E_s can be written as

$$E_s = \sum_{j=1}^{L} \lambda_i |c_i|^2 \tag{4.28}$$

Since c_i's are complex Gaussian random variables, $\lambda_i|c_i|^2$'s are Chi-Square distributed with 2 degrees of freedom. Their characteristic functions are given as $1/(1 - j\nu\lambda_i)$ [92]. Since the c_i's are independent, the characteristic function of E_s is the product

$$E(e^{j\nu E_s}) = \prod_{i=1}^{L} \frac{1}{j\nu\lambda_i} \tag{4.29}$$

Therefore, the probability density function of E_s can be found as

$$p(E_s) = \sum_{i=1}^{L} s_i \frac{e^{-E_s/\lambda_i}}{\lambda_i} \tag{4.30}$$

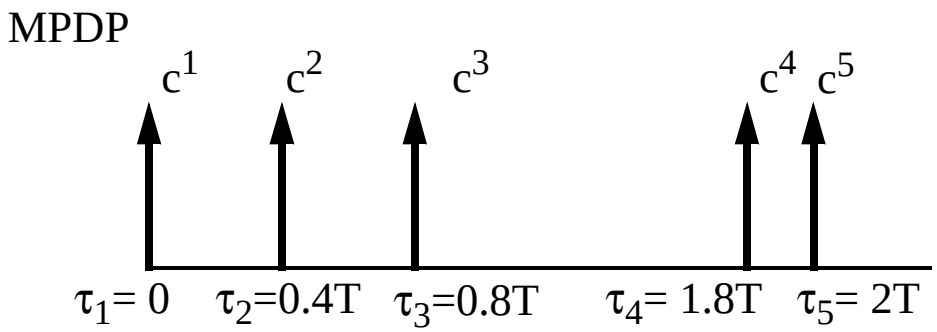

Figure 4.7: Multipath Power Delay Profile (MPDP) of the sample frequency selective channel model

where $s_i = \prod_{j=1;j\neq i}^{L} \frac{1}{1-\lambda_j/\lambda_i}$.

The bit error probability for the matched filter output for BPSK signaling is given as $P(E_s) = Q(\sqrt{2E_s/N_0})$ where the $Q(x) = \frac{1}{\sqrt{2\pi}} \int_x^\infty exp(-t^2/2)dt$ [5]. Therefore, the average bit error probability, P_e, for the general frequency selective channel can be found by averaging $P(E_s)$ over all E_s, i.e.,

$$P_e = \int_0^\infty Q(\sqrt{2E_s/N_0})p(E_s)dE_s \tag{4.31}$$

By substituting (4.30) in to (4.31), P_e can be evaluated as

$$P_e(\gamma_b) = \sum_{i=1}^{L}(s_i/2)[1 - (\bar{\lambda}_i\gamma_b/(1+\bar{\lambda}_i\gamma_b))^{1/2}] \tag{4.32}$$

where γ_b is the average signal to noise ratio (SNR), $\gamma_b = E[E_s]/N_0$, and $\bar{\lambda}_i$'s are the normalized eigenvalues, $\bar{\lambda}_i = \lambda_i / \sum_{j=1}^{L} \lambda_j$

For example, lets find the MFB of the multipath channel with Multipath Power Delay Profile (MPDP) shown in Figure 4.7. The relative delays, τ_i's, are 0, $0.4T$, $0.8T$, $1.8T$ and $2T$ for first through fifth paths respectively where T is the symbol interval.

In this example, we assume that all the paths have equal average power, a_i^2. As a transmitter filter, we used a square root raised cosine frequency response with excess bandwidth $\beta = 0.35$. We also assume that the symbols are transmitted at 25 Kbps, which corresponds to a symbol interval of $T = 40$ μsec. Therefore, the corresponding normalized eigenvalues of matrix $\boldsymbol{G}$ are found as 0.16, 0.36, 0.46, 0.017, and 0.003. Note that there are only three significant eigenvalues at this symbol rate. The MFB of this multipath channel on the average bit error probability is plotted in Figure 4.8 with the dashed lines. We observe that its performance is close to the 3-path diversity (or 3 antenna diversity receiver with flat fading) performance [5]. Intuitively, based on the study of [89] for 2 paths, we would expect this result. Basically, paths 1&2, path 3 and paths 4&5 result in the effect of 3-path diversity performance. Furthermore, the AWGN channel performance is also plotted as a reference in the figure. It has been shown that as the number of distinct paths (or number of antennas with flat fading) increases the performance approaches the AWGN performance [93].

Therefore, the MFB can be found for any frequency selective multipath channel as explained above. The MFB performance curve is mainly the function of average strengths of the distinct paths and the relative delays of each path with respect to the symbol interval, T. The MFB would be our lower performance bound for a given frequency selective channel model and would be used as a reference performance measure through this thesis.

4.3 Estimation and the Long Range prediction of the Frequency Selective Fading Channel

In this section, we first discuss the estimation of the frequency selective fading channel. The estimation is performed at the receiver by transmitting a pilot signal.

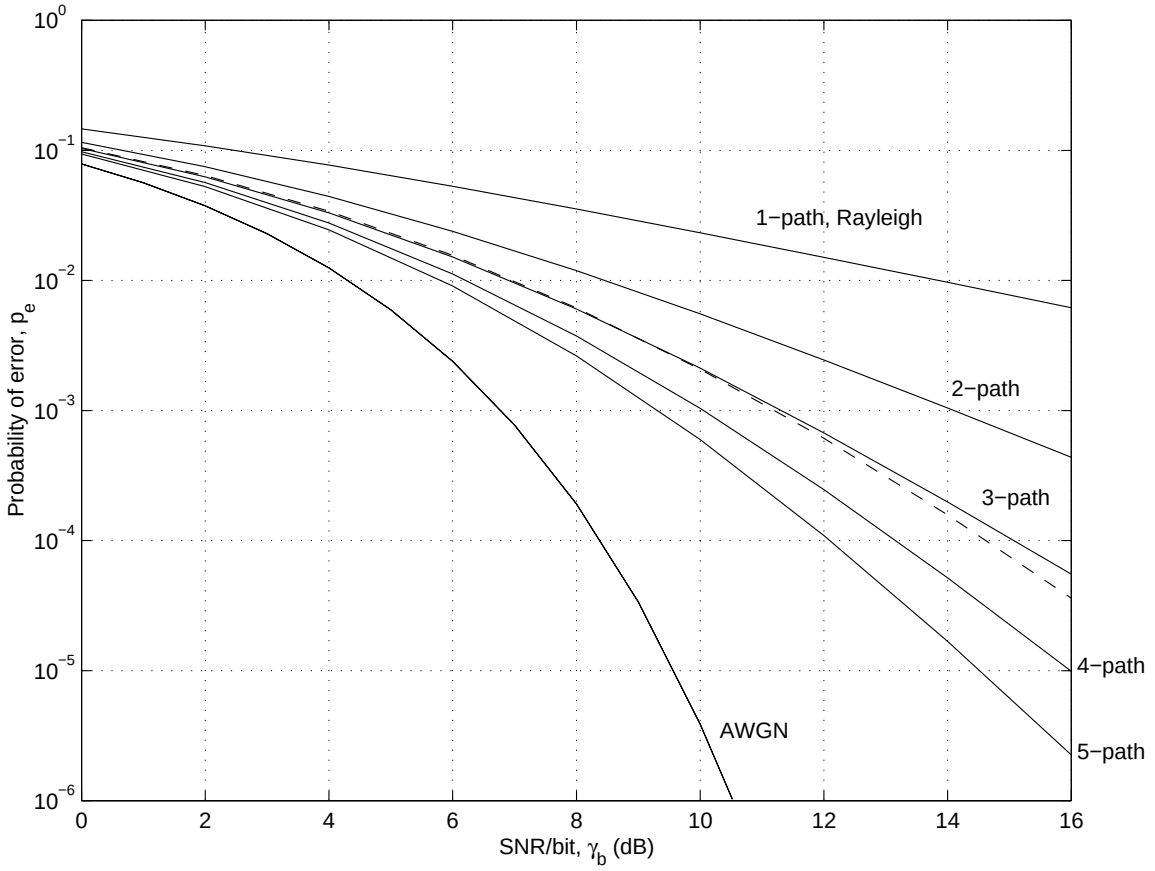

Figure 4.8: (− − −) Matched Filter Bound (MFB) of the frequency selective multipath channel given in Figure 4.7

Then, using these estimated values, we investigate the long range prediction of the impulse response of the frequency selective fading channel far beyond its coherence time. We explain how the prediction is feasible for the frequency selective multipath channels. Then, we discuss two different approaches for the long range prediction of the multipath channels. The first approach is the optimal approach in the MMSE sense, and the second approach is the less complex but suboptimal approach. Both approaches are investigated in details with comparisons of their theoretical and sim-

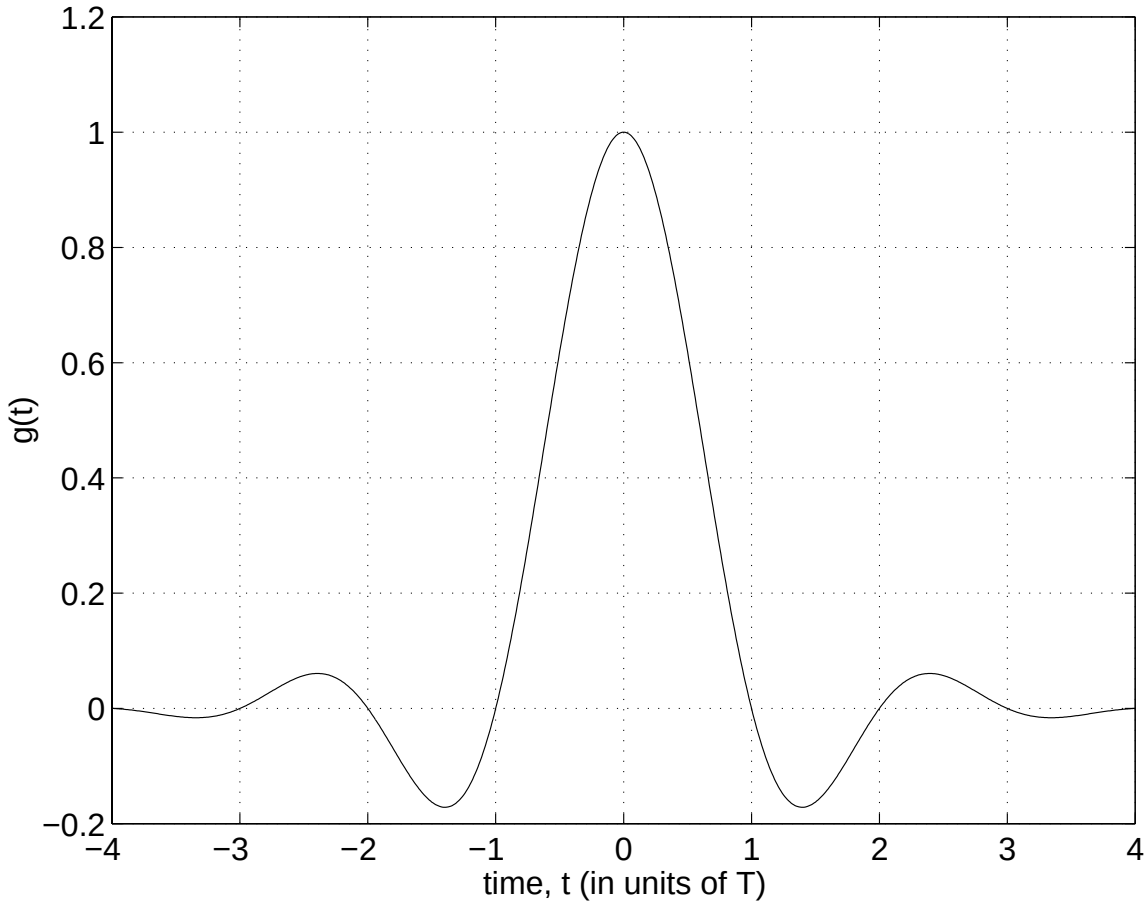

Figure 4.9: Pilot signal including the impulse response of the transmit and receive filters, $g(t)$

ulation performances below.

4.3.1 Estimation Using Pilot Signaling

In this scheme, a pilot signal is sent by the transmitter to capture the characteristics of the frequency selective fading channel. We use the transmitter filter and the receiver filter having SRRC characteristics with roll off factor of 0.35 as described in the previous section. Consequently, the cascaded transmitter and receive filters,

each having SRRC frequency response, result in overall filter having Raised Cosine (RC) frequency response characteristics. A sample pilot signal including the impulse response of the transmit and receive filters is shown in Figure 4.9. The corresponding impulse response for the RC filter, $g(t)$, is given as

$$g(t) = \frac{\sin(\pi t/T)}{\pi t/T} \frac{\cos(\pi \beta t/T)}{1 - 4\beta^2 t^2/T^2}, \tag{4.33}$$

where β is the roll off factor and T is the symbol interval. The duration of the pilot interval including the transmitter and receiver filter responses is given by $2N$ times the symbol interval, T, where N is an integer number. For example, N corresponds to 4 in Figure 4.9. We normalize the energy per symbol period to provide consistent SNR calculations. Therefore, the energy of the pulse is chosen as $2N$ times the data symbol energy. The duration of the symbol interval should be chosen long enough to capture the maximum path delay in the multipath channel and not to allow any interference from the past and previous data symbols. Since the pilot symbol has higher power level than the data symbols, our studies show that sufficiently large interval ($3 - 4$ symbols) has very minimal interference from past and previous data symbols. Therefore, in our analysis, this very small interference is considered a part of the noise given below. Hence, the noise term in this section consists of the interference as well as the thermal noise.

When a single pulse is transmitted as a pilot signal, the resulting channel impulse response at the receiver is the convolution of g(t) and frequency selective channel, $c(t)$ (see Eq.(4.22)), plus the AWGN, $n(t)$, i.e.,

$$h(t) = g(t) * c(t) + n(t). \tag{4.34}$$

Then, by substituting (4.22) into (4.34), we obtain the impulse response of the channel

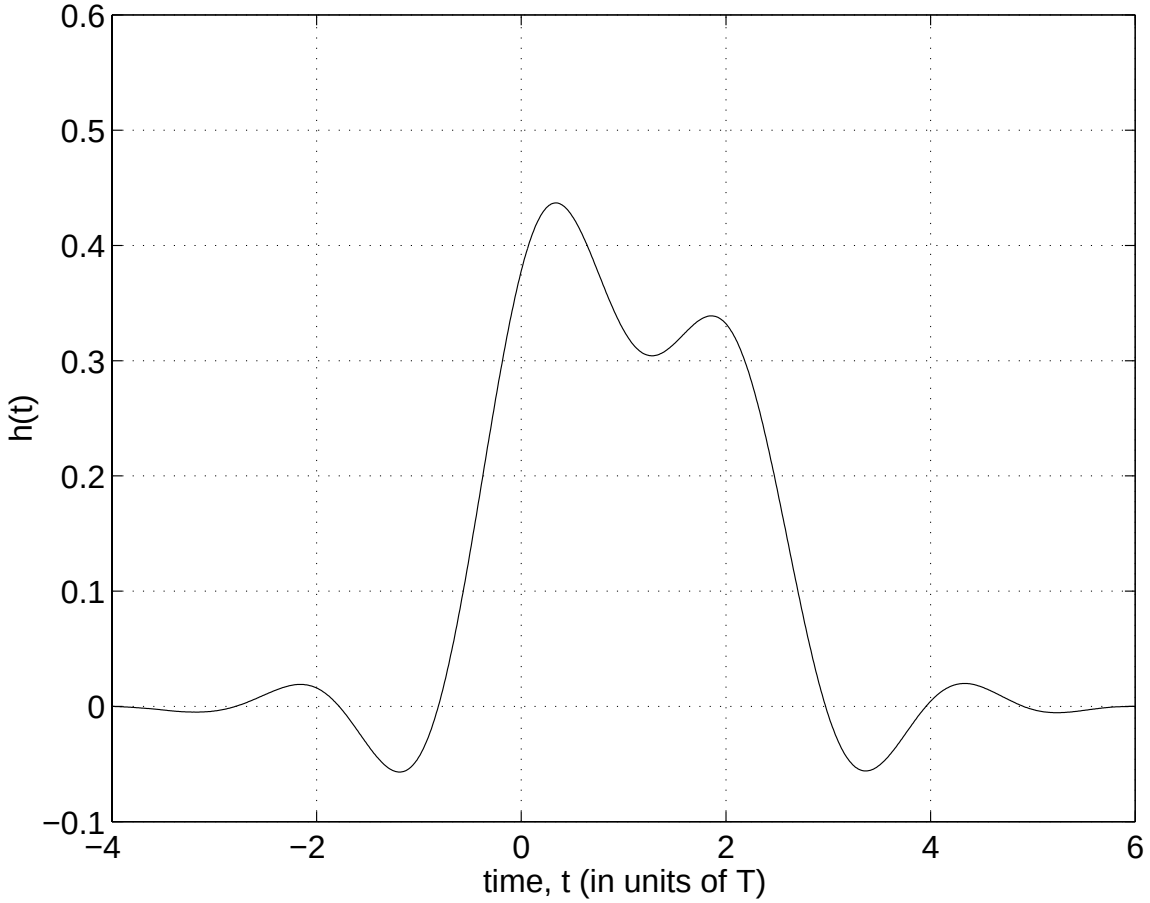

Figure 4.10: Impulse response, h(t), of the frequency selective channel given in Figure 4.7

as

$$h(t) = \sum_{i=1}^{L} a_i c_i(t) g(t - \tau_i) + n(t) \tag{4.35}$$

For example, for the 5−path channel model given in Figure 4.7, the corresponding channel impulse response, h(t), is observed in Figure 4.10 with the same average power levels for all the paths, (i.e., same $|a_i|^2$).

The channel impulse response, $h(t)$, is estimated periodically with a given fre-

quency of the pilot signal. Let the frequency of the pilot signal be $f_s = 1/T_s$. This means that the pilot signal is sent in every T_s second. Therefore, we would be able to estimate the channel impulse response in every T_s seconds, $h(kT_s)$. During each estimation process, we find M coefficients of the impulse response. The number of estimated channel impulse response coefficients, M, for each pilot interval depends on the filter sampling rate, pilot signal interval and the maximum observed in the multipath channel. With fractionally spaced sampling (e.g., $T/2$), the total number of M's are $4N + \lceil 2\tau_{max}/T \rceil + 1$ where τ_{max} is the maximum delay observed by any path in the multipath channel. For example for $N = 4$ and $\tau_{max} = 2T$, the number of estimated coefficients in the channel impulse response is 21 for any kT_s instant. Therefore, each coefficient is denoted by $h_{k,m} = h(kT_s + mT/2)$ and given as

$$h_{k,m} = \sum_{i=1}^{L} c_i(kT_s + mT/2)g(kT_s + mT/2 - \tau_i) + n(kT_s + mT/2) \tag{4.36}$$

Note that the symbol interval, T, is much smaller than sampling interval, T_s. Since each $c_i(kT_s + mT/2)$ coefficients shows very little variations in $mT/2$ interval, it is assumed that $c_i(kT_s + mT/2) = c_i(kTs)$ for all m values. Therefore, we define $ci, k = c_i(kTs)$. Furthermore, since the pilot symbol is sent in every T_s second and the channel coefficients are calculated every T_s seconds, the $g(kT_s + mT/2 - \tau_i)$ can be considered as periodic with T_s. Therefore, $g(kT_s + mT/2 - \tau_i) = g(mT/2 - \tau_i)$ for all kT_s channel sampling interval. Finally, $h_{k,m} = h(kT_s + mT/2)$ is given as

$$h_{k,m} = \sum_{i=1}^{L} c_{i,k}g(mT/2 - \tau_i) + n_{k,m} \tag{4.37}$$

These coefficients are illustrated in Figure 4.11 for the channel impulse response, $h(t)$, given in Figure 4.10.

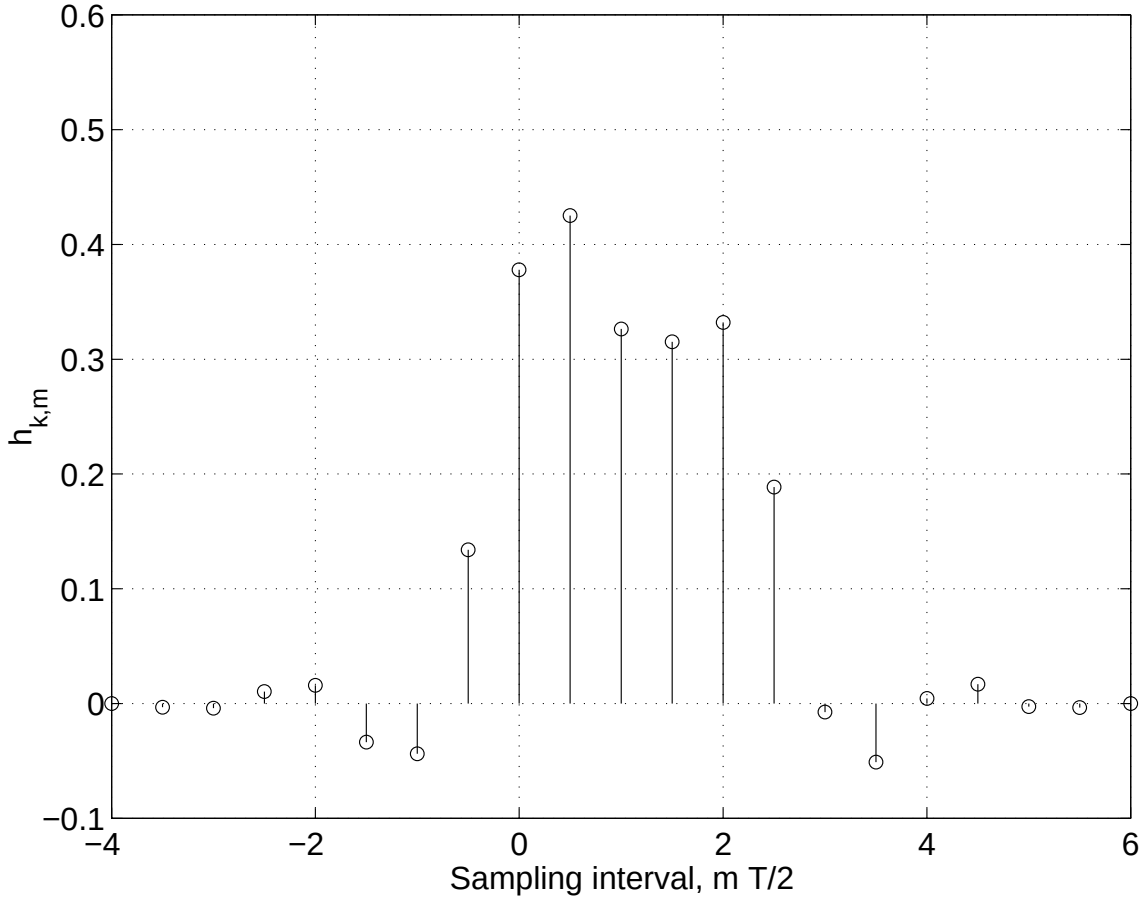

Figure 4.11: Impulse response sampled by $T/2$, $h_{k,m}$

These estimated channel impulse response coefficients are used in the design of various adaptive equalizers at the receiver to combat Inter-Symbol Interference (ISI) as we will discuss later. These coefficients could also be fed back to the transmitter and could be utilized to reduce the effect of ISI and to gain diversity from the frequency selectivity of the channel. Among its applications, these estimated channel coefficients are also used as a channel side information for transmitter antenna diversity [38, 72, 73, 74], adaptive modulation and adaptive coding

[63, 64, 75, 76, 77, 78, 79, 80, 81] (and the references therein). However, using the current estimates limits the performance of many adaptive techniques both at the receiver and at the transmitter. Especially, for the fast fading conditions, implementation of these techniques and equalizers both at the receiver and at the transmitter become unfeasible without performance degradation and the delay tolerance. In the next Section, we will show that it is possible to predict the future channel impulse response of the general frequency selective fast fading channels given present and past estimated samples. Then, we will illustrate how this novel long range prediction technique enables effective equalization techniques both at the receiver and at the transmitter. Before we go into details of these equalizers, lets first discuss the feasibility and the performance of the long range prediction technique for the frequency selective multipath channels.

4.3.2 Long Range Prediction of the Frequency Selective Multipath Channels

The long range prediction capability for the complex valued fading channel was demonstrated in the previous Chapter. In previous work, we concentrated on flat fading channels, i.e., prediction of $c(t)$ with single path, i.e., $L = 1$. Our linear prediction (LP) method is based on the AR channel modeling. We demonstrated that we were able to predict the flat fading channel far beyond its coherence time by using our novel long range prediction technique in the previous chapter. In order to enhance the transmitter antenna diversity techniques, we also applied our long range prediction technique to some specific frequency selective channels [38]. These frequency selective channels are modeled with L independently Rayleigh fading paths and each path is separated from the previous one by exactly a chip interval, T_c.

In [38], the objective was to predict total channel power at the transmitter. This has been achieved in several ways, by either predicting individual paths' powers and summing them up or first by summing them up and then predicting the total power. In this section, we did not limit the path delays to be exactly a chip interval, T_c. In our analysis, we developed our novel long range technique further and applied for any frequency selective channel with arbitrary delays.

In the previous Section, we explained the estimation of the channel impulse response using the pilot signaling. These estimated coefficients are given in Eq. (4.37). For our long range prediction purposes, the frequency of the pilot signaling should be at least twice the maximum Doppler shift, f_{dm} [16].

It is feasible to predict $h_{k,m}$ (see Eq. (4.37)) by utilizing the long range prediction technique. From Eq. (4.37)), we observe that the coefficient $h_{k,m}$ is the linear combination of $c_{i,k}$'s with corresponding constant weighting $g(mT/2 - \tau_i)$ for each m coefficients. Since each $c_{i,k}$ is Raleigh distributed, we previously showed that they are predictable by using our novel long range prediction technique. Therefore, it would be possible to predict $h_{k,m}$ coefficients for any frequency selective multipath channels with arbitrary path delays.

We developed two approaches below to perform the long range prediction of the channel impulse response of the frequency selective channels. The first approach is the optimal approach in the MMSE sense, and the second approach is the suboptimal approach but less complex than the first approach. These approaches along with their both theoretical and simulation performance results are discussed next.

Approach 1:

In this approach, the objective is to predict channel impulse response coefficients, $h_{k,m}$ (see Eq. (4.37)). As explained in the previous section, there is m number of

estimated channel coefficients for each estimation interval, kT_s. In our analysis, we used $T/2-$spaced sampling, therefore, the total number of estimated coefficients is $M = 4N + \lceil 2\tau_{max}/T \rceil + 1$ where τ_{max} is the maximum delay observed by any path in the multipath channel.

For the optimal prediction performance in the minimum mean squared error (MMSE) sense, each of m coefficients are predicted by using p previously observed channel samples $h_{k-1,m}$, $h_{k-2,m}$, ..., $h_{k-p,m}$, (Note that the noise is already included in Eq. (4.37))

$$\hat{h}_{k,m} = \sum_{j=1}^{p} d_{j,m} h_{k-j,m} \tag{4.38}$$

where d_j's are the coefficients of the LP filter.

The optimal $d_{j,m}$ coefficients are computed for each m coefficient of the channel impulse response as

$$\boldsymbol{d = R^{-1} r} \tag{4.39}$$

where $\boldsymbol{d}$= $(d_{1,m} \dots d_{p,m})$. $\boldsymbol{R}$ is the autocorrelation matrix $(p \times p)$ with coefficients $R_{ij,m} = \mathrm{E}[h_{n-i,m} h^*_{n-j,m}]$ and $\boldsymbol{r}$ is the autocorrelation vector $(p \times 1)$ with coefficients $r_{j,m} = \mathrm{E}[h_{n,m} h^*_{n+j,m}]$. By using the Eq. (4.37), the autocorrelation function, $r_{j,m}$, can be calculated as

$$r_{j,m} = \sum_{i=1}^{L} g^2(mT/2 - \tau_i) J_0(2\pi f_{dm} j T_s) + (N_0/2)\delta(j) \tag{4.40}$$

where $J_0(.)$ is the zero-order Bessel function of the first kind. Therefore, the resulting MMSE for each particular m coefficient is given by

$$\xi_{k,m} = E[|e_{k,m}|^2] = E[|h_{k,m} - \hat{h}_{k,m}|^2] \tag{4.41}$$

$$\xi_{k,m} = r_{0,m} - \sum_{j=1}^{p} d_{j,m} r_{j,m} \tag{4.42}$$

Approach 2:

In the first approach, in order to get the optimum performance for the long range prediction, we calculated LP coefficients, $d_{j,m}$, for each m coefficients separately. Then, we applied to the LP as given in Eq. (4.38). Therefore, in Approach 1, for optimal performance we are required to find $d_{j,m}$ coefficients for each channel impulse response coefficients (total m) separately.

However, when we study each channel coefficients in details, we observe that each coefficient, $h_{k,m}$ consists of all the independent paths, c_i's, in the channel response (see Eq. (4.37)). The only difference for each channel coefficients, $h_{k,m}$, is the weighting factors, $g(mT/2 - \tau_i)$. Due to the characteristics of the RC filter, $g(t)$, and its overall effects during the estimation interval. We would be able to sum all the $h_{k,m}$ coefficients and we would be still able to preserve all the independent paths, c_i's, in the channel. Therefore, let the sum of all estimated m coefficients be

$$h_{k,T} = \sum_{m=1}^{M} h_{k,m} \tag{4.43}$$

where $M = 4N + \lceil 2\tau_{max}/T \rceil + 1$ and $h_{k,m}$ as given in Eq. (4.37) (Note that the noise is already included in $h_{k,m}$.) In the sum above, we would still observe all the individual paths and their corresponding oscillator frequencies (for each scatterer), but this time, with different weighting constants. Substituting Eq. (4.37) into Eq. (4.43), the corresponding autocorrelation function, $r_{j,T}$ for $h_{k,T}$ can be found as

$$r_{j,T} = E[h_{n,T} h^*_{n+j,T}] \tag{4.44}$$

$$r_{j,T} = K(N)) J_0(2\pi f_{dm} j T_s) + (M N_0/2)\delta(j) \tag{4.45}$$

where $K(N) = \sum_{m=1}^{M} \sum_{i=1}^{L} g^2(mT/2 - \tau_i)$.

Then, the $d_{j,T}$ coefficients are calculated once in every estimation interval and found from:

$$\boldsymbol{d} = \boldsymbol{R^{-1}r} \tag{4.46}$$

where $\boldsymbol{d}$= $(d_{1,T} \ldots d_{p,T})$. $\boldsymbol{R}$ is the autocorrelation matrix $(p \times p)$ with coefficients $R_{ij,T} = \mathrm{E}[h_{n-i,T} h^*_{n-j,T}]$ and $\boldsymbol{r}$ is the autocorrelation vector $(p \times 1)$ with coefficients $r_{j,T} = \mathrm{E}[h_{n,T} h^*_{n+j,T}]$ given in Eq. (4.45).

Note that since $d_{j,T}$ coefficients are calculated once in every estimation interval, we will have lower computational complexity for this approach. Since $d_{j,T}$ reflects the characteristics of the all independent paths in the channel, we can use the same $d_{j,T}$ coefficients to predict each of m channel impulse response coefficients such that

$$\hat{h}_{k,m} = \sum_{j=1}^{p} d_{j,T} h_{k-j,m} \tag{4.47}$$

Since $d_{j,T}$ is calculated with different weighting constants, the performance of the Approach 2 will not be the same as performance of optimal Approach 1 with optimal $d_{j,m}$ coefficients. Therefore, Approach 2 is a suboptimal approach. The advantage of this approach is that it would have less computational complexity than approach 1, because $d_{j,T}$ is calculated only once as opposed to m times in approach 1. Therefore, the resulting average MSE (not optimum, therefore not Minimum MSE) for each m is given by

$$\xi'_{k,m} = E[|e_{k,m}|^2] = E[|h_{k,m} - \hat{h}_{k,m}|^2] \tag{4.48}$$

$$\xi'_{k,m} = E[(h_{k,m} - \sum_{j=1}^{p} d_{j,T} h_{k-j,m})(h_{k,m} - \sum_{j=1}^{p} d_{j,T} h_{k-j,m})^*] \tag{4.49}$$

$$\xi'_{k,m} = r_{0,m} - 2\sum_{j=1}^{p} d_{j,T} r_{j,m} + \sum_{j=1}^{p}\sum_{j'=1}^{p} d_{j,T} d_{j',T} r(j-j') \tag{4.50}$$

Note that the Eq. (4.42) can also be derived from Eq. (4.50). In Eq. (4.50), if d coefficients were calculated from original $r_{j,m}$ then, we would have $d_{j,m}$ instead of $d_{j,T}$. Therefore, from orthogonality, $\boldsymbol{d = R^{-1}r}$, we would have $\sum_{j=1}^{p}\sum_{j'=1}^{p} d_{j,T} d_{j',T} r(j-j') = \sum_{j=1}^{p} d_{j,m} r_{j,m}$. Then, as expected, $\xi'_{k,m}$ (see Eq. (4.50)) would be same as $\xi_{k,m}$ (see Eq. (4.42)).

Performance Comparisons of Approach 1 and 2:

In this section, we provide both theoretical and simulation performance results in terms of average MSE with respect to various system parameters for Approach 1 and Approach 2. The long range prediction technique can be generalized to predict any time τ ahead, where τ is the prediction range. In (4.38) and (4.47), the prediction is one step ahead, i.e. $\tau = T_s$. In practical implementation, we iterate this one-step prediction to forecast the channel further than one sampling interval ahead by utilizing previously predicted samples instead of the observations. It was shown in the previous chapter that the key to the long range prediction is the sufficiently long memory span achieved for moderate model order p by selecting low sampling rate, f_s (much lower than the data rate). Later, depending on the application, interpolation could be used to perform prediction at the data rate.

The MSE performance of the long range prediction is compared in Figure 4.12. A model order, $p = 20$, $SNR = 80$ dB, sampling frequency, $f_s = 500$ Hz, and maximum Doppler frequency, $f_{dm} = 100$ Hz, are chosen to illustrate the performance comparison. Both theoretical and simulation results for the average MSE of Approach 1 and Approach 2, i.e., $\xi_{k,m}$ and $\xi'_{k,m}$ are averaged over total number of m, are plotted in the figure. For example, for $f_{dm} = 100$ Hz, the range of 0.2 on the $x-$axis corresponds to

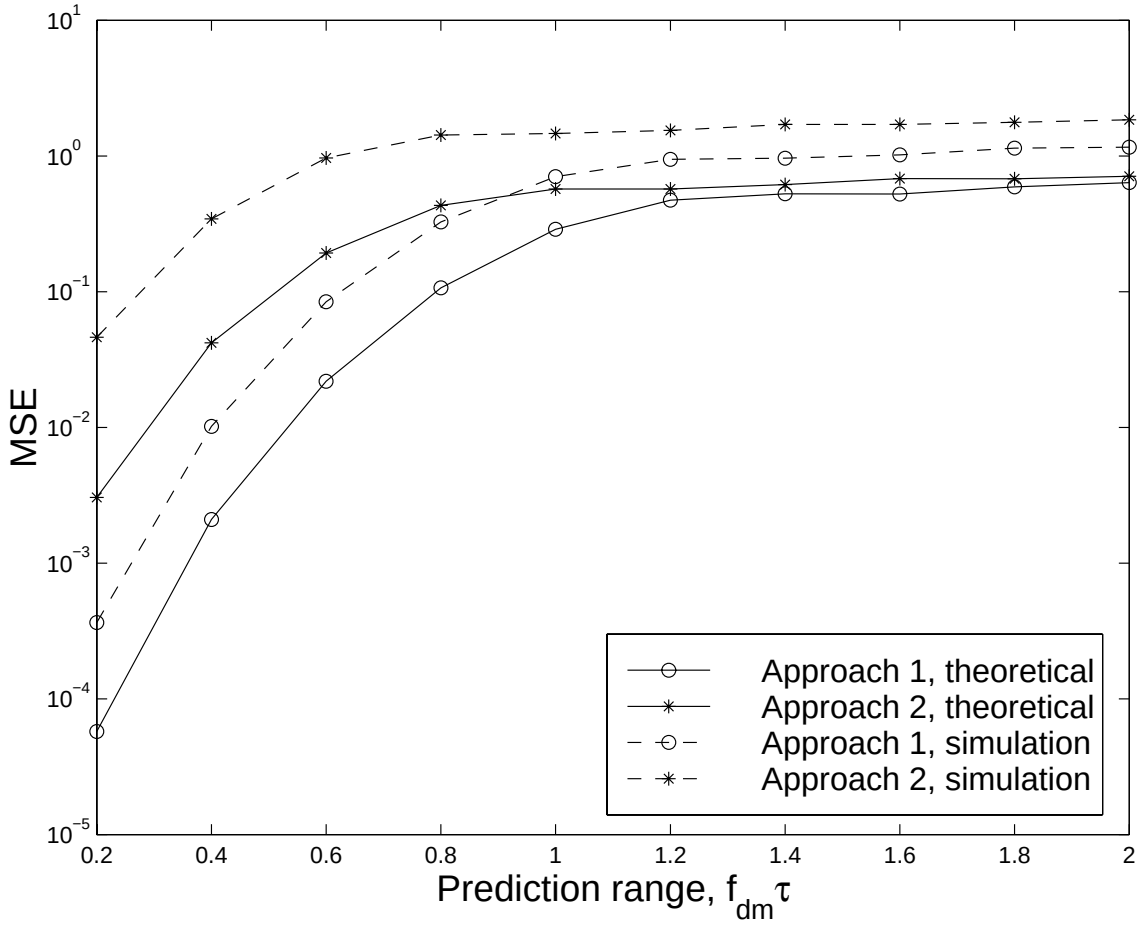

Figure 4.12: MSE vs prediction range for sampling frequency, $f_s = 500$ Hz , $SNR = 80$ dB, model order, $p = 20$ and $f_{dm} = 100$ Hz.

50 data points ahead with the data rate of 25 kHz and 1 sampling point ahead with a lower sampling rate of 500 Hz. As seen from the figure, future values can be predicted with by using the low sampling rate. Approach 1 provides the optimal performance while Approach 2 has performance degradation. Although Approach 2 has lower performance, but it has less computational complexity as we explained in the previous section. Although it is not an optimum performance, it also provides acceptable per-

formance results which might be a favorable approach when the computational power is limited. In Figure 4.12, we also show the simulation results. In our simulations, we used a model similar to the Jakes model. In Jakes model, the oscillators are placed around the mobile equally spaced on a circle, i.e., the spacing between the oscillators are deterministic and given by $2p/N$ where N is the total number of oscillators [16]. However, in our simulation, we remove the deterministic spacing between the oscillators. Instead, the oscillators are placed around the mobile randomly with uniform random parameter. This randomness ensures that each multipath, with the same number of oscillators, is generated with different uniformly distributed oscillator frequencies. Our analysis also shows that this uniformly random distributed oscillators still depict the characteristics of the Rayleigh fading channel. Therefore, this new modified model enables us to compare the two approaches described earlier more realistically. The simulation results for the new model with random oscillators are given in Figure 6 for both Approaches. Due to the channel mismatch as explained in chapter 3, simulations do not closely match theoretical results, but the performance trends are the same with the theoretical results.

The effect of the sampling rate is explored further in Figure 4.13. In this figure, the average MSE vs f_s is plotted for Approaches 1 and 2 at the prediction range, $f_{dm}\tau = 0.2$. As seen from the figure, for each model order there is an optimal low sampling rate that minimizes the MSE. This optimal rate is between 500Hz - 1KHz for model order $p = 20$. Similarly, Approach 2 has lower performance. But, since it has less computational complexity, it might be preferable for some applications. Again, the simulation results do not closely match theoretical results, but performance trends are the same due to the channel mismatch.

Finally, in Figure 4.14, the average MSE vs model order, p, is plotted for $f_{dm}\tau =$

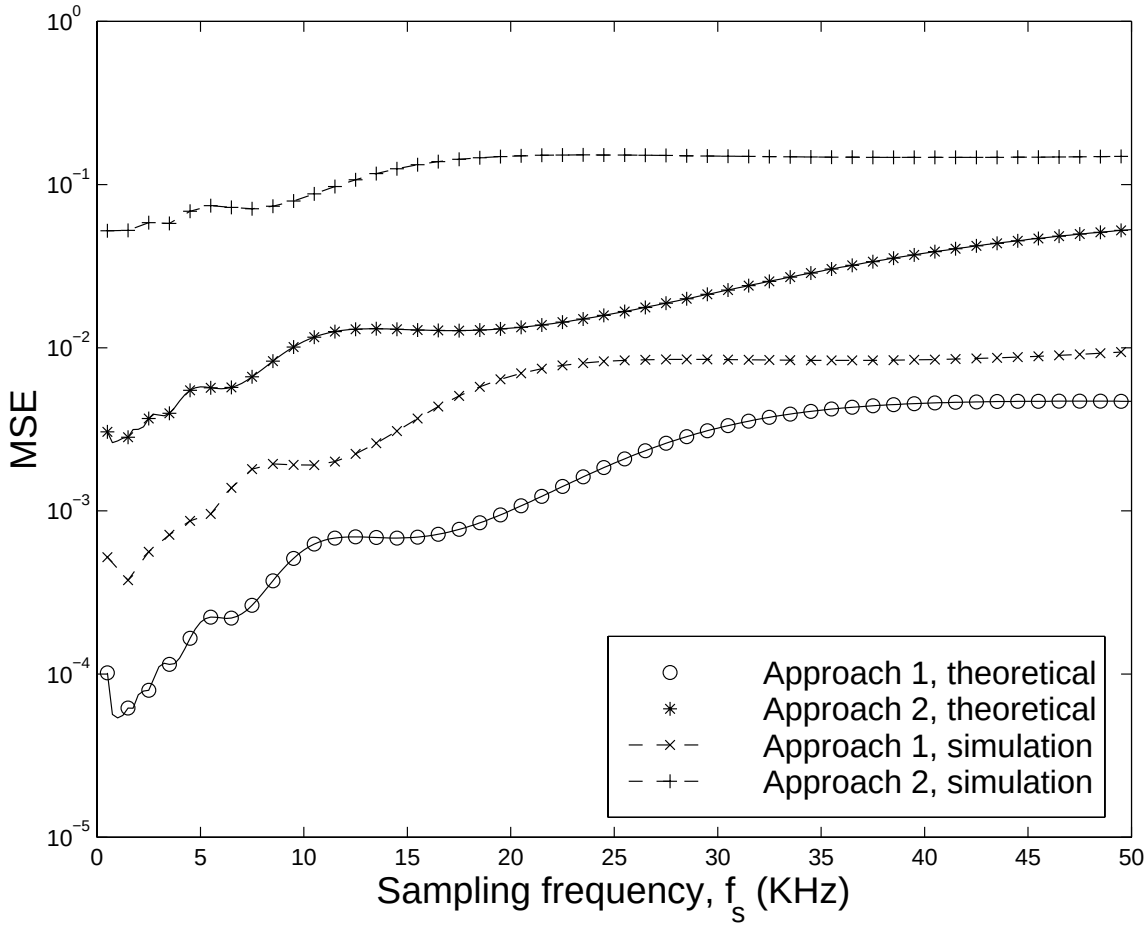

Figure 4.13: MSE vs sampling rate, f_s; prediction range $\tau = 2$ ms, $SNR = 80$ dB, model order, $p = 20$ and $f_{dm} = 100$ Hz.

0.2, $f_{dm} = 100$ Hz, $f_s = 500$ Hz, and SNR = 80 dB, for both approaches. As p increases the average MSE saturation level is approached. As expected, the optimal Approach 1 performs better than the suboptimal but less complex approach 2. For the theoretical curves, the average MSE floor corresponds to the prediction error given an infinite number of past observations for the fading process sampled at 500 Hz. Due to observation interval and the channel mismatch as explained in chapter 3,

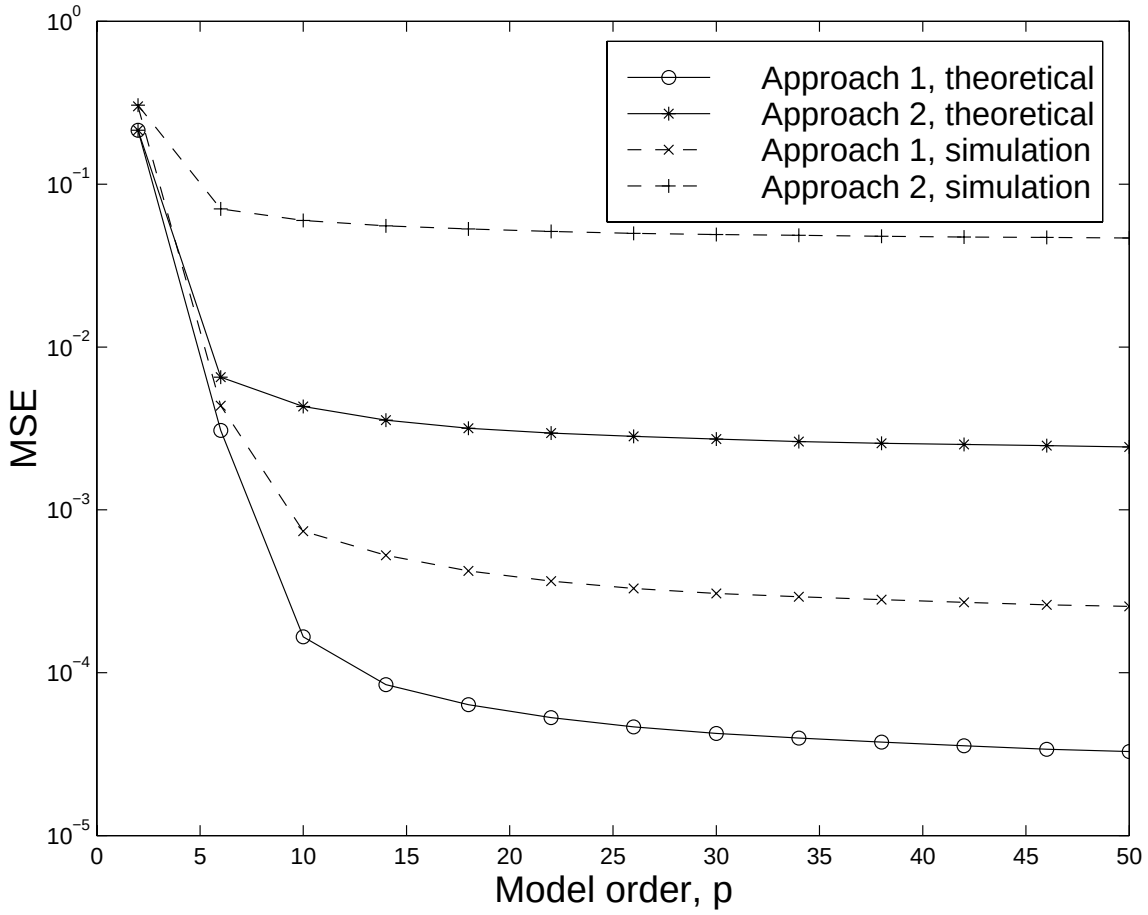

Figure 4.14: MSE vs model order, p, for sampling frequency, $f_s = 500$ Hz , $SNR = 80$ dB, prediction range $\tau = 2$ ms and $f_{dm} = 100$Hz

simulations do not closely match theoretical results, but performance trends are the same.

Based on the analysis done above, we showed that the frequency selective multipath channels with arbitrary path delays could also be predicted using our novel long range prediction technique. In the following two sections, we will illustrate how to utilize the prior knowledge of the predicted channel impulse responses both at the receiver and at the transmitter. Basically, this novel long range prediction technique

enables more efficient adaptive equalizers at the receiver and transmitter precoder (preequalizer) at the transmitter.

4.4 Performance Enhancements at the Receiver

The time-variant multipath propagation of the signal through the frequency selective channel results in intersymbol interference (ISI). Therefore, the digital transmission at a rate exceeding the coherence bandwidth of the frequency selective fading channel requires equalization to compensate and the reduce the ISI. For bandlimited signal transmission, the optimal equalizer should have infinite length to remove all ISI. However, in practice, finite length equalizers spanning most of the energy of the channel impulse response (CIR) are commonly used. Moreover, most practical equalizers are implemented as direct form finite-duration impulse response (FIR) filters in the form of a tapped-delay-line (TDL). They are also known transversal filters [5, 94]. There are two broad classes of equalizers, linear and non-linear. Lets first briefly review the Equalizers:

Linear Equalizer (LE):

The linear equalizer (LE) is implemented as a finite-duration impulse response (FIR) filter (also called a transversal filter) with adjustable coefficients as shown in Figure 4.15. These filter structures have a computational complexity that is a linear function of the channel dispersion length. LE tries to invert the folded spectrum of the overall CIR, H(z), to satisfy the Nyquist criterion. Therefore, the equalizer in frequency domain is found as [5]

$$U(z) = \frac{1}{H(z)}. \tag{4.51}$$

Note that the equalizer, with transfer function, $U(z)$, is simply the inverse of CIR.

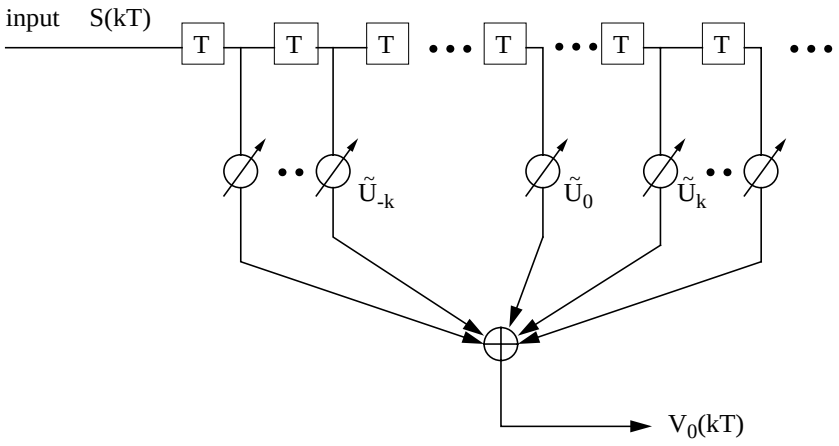

Figure 4.15: Linear Equalizer in the form of transversal filter

In other words, complete elimination of the ISI requires the use of an inverse filter of $H(z)$. These types of filters are called *Zero-Forcing (ZF)* filters. Furthermore, the cascade of the noise whitening filter having the transfer function, $1/H^*(z^{-1})$ and the zero-forcing equalizer having the transfer function, $1/H(z)$ results in an equivalent zero-forcing equalizer having the transfer function

$$U(z) = \frac{1}{H(z)H^*(z^{-1})} = \frac{1}{X(z)}. \tag{4.52}$$

However, if the channel contains a spectral null in its frequency response or takes on small values as we have in wireless channel, the linear zero-forcing equalizer attempts to compensate for this by introducing an infinite gain at that frequency. But this compensates for the channel distortion at the expense of enhancing the additive noise. Therefore, the performance of the equalizer is poor and it suffers from unacceptable noise enhancement whenever folded spectral characteristics possesses nulls [5, 68, 94]. In order to overcome the noise enhancement problem of ZF criterion, we also

investigate an alternative *Mean Square Error (MSE)* criterion. The MSE criterion reduces noise enhancement by allowing residual ISI at the output and attempt to minimize the sum of the ISI and noise. With the noise whitening filter incorporated into $U(z)$, The MSE equalizer has the corresponding transfer function [5]

$$U(z) = \frac{1}{H(z)H^*(z^{-1}) + N_0} = \frac{1}{X(z) + N_0} \tag{4.53}$$

where N_0 is the noise spectral density factor. Note that this expression for MSE criterion is similar to that of ZF criterion as N_0 goes to zero, and they both yield the same solution for tap weights. Consequently, when $N_0 = 0$, the minimization of the MSE results in complete elimination of the ISI. On the other hand, when $N_0 \neq 0$, there are both residual ISI and additive noise at the output of the equalizer.

Since the linear equalizer does not perform well on channels with spectral nulls in their frequency response characteristics, the nonlinear equalizers are used where channel distortion is too severe for the linear equalizer to handle [5, 68, 95].

Nonlinear Equalizers:

There are three types of non-linear equalization schemes. The first one is a symbol-by-symbol detection algorithm based on the *maximum a posteriori* (MAP) criterion proposed by Abend and Fritchman [96]. The second one is a sequence detection algorithm, based on the Maximum-likelihood Sequence Estimation (MLSE) criterion, which is efficiently implemented by the Viterbi algorithm (VA) [97]. Although the MLSE results in better performance results it has a computational complexity that grows exponentially with the length of the channel time dispersion [5]. In most channels of practical interest, such a large computational complexity is very expensive to implement. The third one is decision feedback equalization (DFE). When decision error propagation is not severe, DFE receiver suffers only small theoretical perfor-

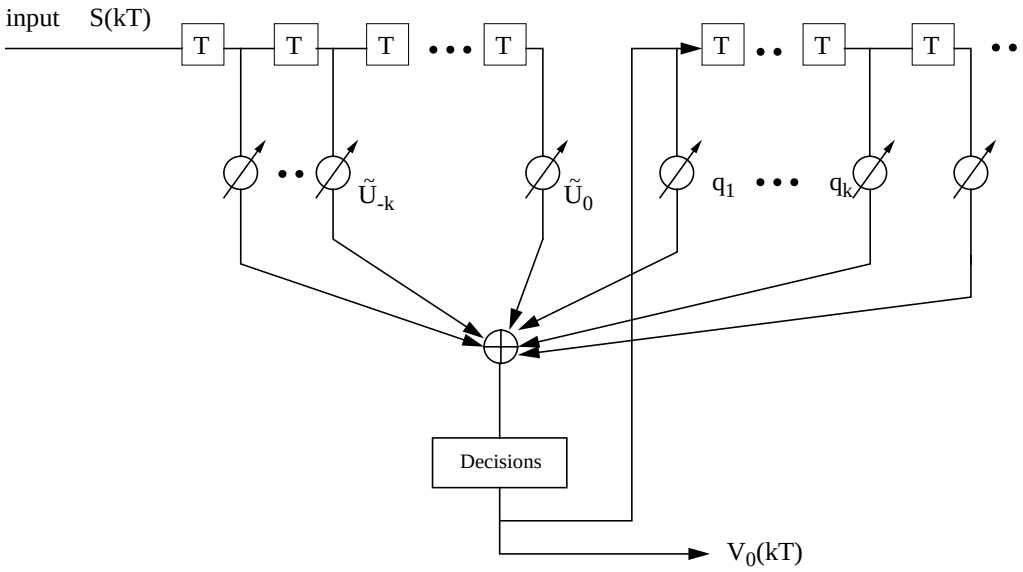

Figure 4.16: Structure of a Decision Feedback Equalizer

mance degradation relative to the more complex nonlinear equalization methods such as MLSE receiver. Another advantage of the DFE is that it has the same level of complexity as LE and lower complexity than MLSE.

The DFE consists of a feedforward filter (FFF) and a feedback filter (FBF) as illustrated in Figure 4.16. The FBF is driven by decisions at the output of the detector and the coefficients are adjusted to cancel the ISI on the current symbol that results from past detected symbols (postcursor). The FFF is identical to the linear transversal equalizer described in the previous section. The FFF compensates or removes the precursor ISI based on the criterions described in the previous section, i.e., ZF and MSE criterions. As long as FFF spans at least the CIR length, the causal FBF only needs to span at most the CIR length.

Adaptive Equalization:

In the development of equalization methods described above, we implicitly assumed that the channel characteristics, either the impulse response or the frequency response, were known at the receiver. However, in most communication systems that employ equalizers, the channel characteristics are unknown a priori. Furthermore, in many cases, the channel response is time-variant, such as wireless communication channels. In that case, the equalizers are designed to be adjustable to the channel response and, for time variant channels, to be adaptive to the time variations in the channel response. The adjustment of equalizer coefficients is usually performed adaptively during the transmission of information by using the decisions at the output of the detector in forming the error signal for the adaptation.

One of the adaptive equalizer technique is to calculate the equalizer coefficients adaptively in decision directed mode [5, 68]. The most common decision directed adaptive algorithms are Least Mean Square (LMS) algorithm and Recursive Least-Squares (RLS) (also known as Kalman) Algorithm (RLS) [5, 68]. These adaptive techniques are shown to work well in slowly fading channels. However, they fail to track to variations of the fast fading channels. Another Adaptive Equalization technique, known as block adaptation scheme, is initially introduced by [69, 59] and developed by [70, 71]. Originally, the start of each data frame contains a known training sequence or pilot symbols which are used to estimate the channel impulse response (CIR). Instead of explicitly tracking the time-varying CIR by using a continuous, decision-directed adaptive algorithm like LMS or RLS, block-adaptive strategy computes the time-varying CIR by interpolating a set of estimated CIR values. Then, it uses this interpolated CIR values to compute the receiver parameters to adapt it to the fast fading channel [70]. However, when the data in this system is differentially encoded, the successive CIR estimates have an inherent phase ambiguity. In order

to the remove the phase ambiguity between the successive CIR estimates, a phase alignment technique has been used as explained in Appendic C [98]. In this block adaptive scheme, since coefficient computation is shared over all the symbols of a block, per-symbol computational effort can be significantly less than that for decision directed adaptive systems.

Extensive study has been done on the design of optimal block adaptive equalization technique by Eyceoz et. al. [70, 71] and Lo et. al. [59]. This technique has been proven to work well under fast fading conditions for the frequency selective channels. However, this technique has an inherent processing delay since the interpolation has been performed using past and future channel estimates. Therefore, we need to wait for the future estimates to perform interpolation to find the channel impulse response which is used in the design of the block adaptive equalizer. Let the pilot signal be transmitted in every T_s interval to get the channel impulse response estimate and the data rate be 25 kbps. For example, if the rate of pilot signaling is $f_s = (1/T_s)$ is 500 Hz, that means the channel estimation is performed in every 50 data symbols. With the design proposed in [70, 71, 59] the processing delay is given as $2T_s$, or 100 data symbols. Some systems will not be able to tolerate this long delay.

The performance of the Block Adaptive Equalization scheme is illustrated in Figure 4.17 for the frequency selective channel given in Figure 4.7. When we tolerate $2T_s$ delay in the system at the receiver, the performance of the equalizer is very effective. If we only tolerate T_s delay in the system, the performance of the equalizer gets worse, and finally without any delay tolerance, we get the worst performance. Without delay tolerance means that receiver calculates equalizer coefficients at the beginning of data block and uses the same equalizer coefficients through the all block without any adaptation. For performance comparison, we also plotted the performance of decision

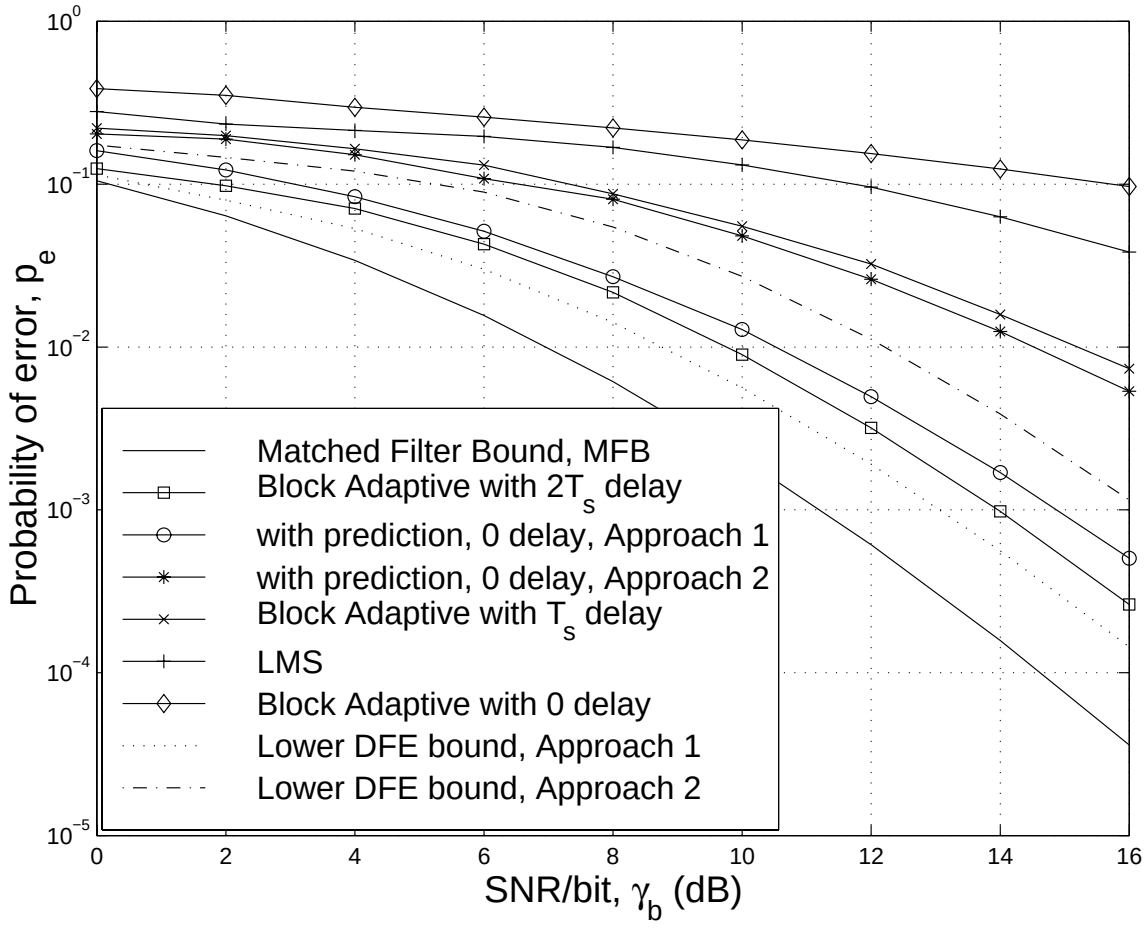

Figure 4.17: Performance of the block adaptive equalization technique with or without prediction.

directed equalizer employing LMS algorithm. But, it can be seen from the figure that it fails to track the variations of the fast fading channels and the performance is far from the matched filter bound (MFB).

In the previous section, we showed that we are able to predict the channel impulse response of the frequency selective channels up to few low sampling interval, T_s, ahead by using our novel long range prediction technique. The capability of predicting

the channel impulse response accurately eliminates the need for the delay which is a major drawback for block adaptive equalization schemes. We implemented our long range prediction scheme at the receiver for the same channel model given in Figure 4.7. In our analysis, we sample the channel and predict the channel impulse response at the rate of 500 Hz. We also assume that the transmission data rate is 25 kbps and maximum Doppler frequency, $f_{dm} = 100$ Hz. We predicted the future channel impulse response coefficients at $(k+1)T_s$ and at $(k+2)T_s$ ahead in time. Then, we used these predicted future values and the present estimate at kT_s and one past estimate at $(k-1)T_s$ to interpolate the future channel impulse response. Then, we constructed our equalizer similar to the block adaptive equalizer to combat the channel impairments. We predicted the future channel impulse responses by using both optimal approach 1 and suboptimal approach 2. The BER performance results with both approaches are plotted in Figure 4.17. It can be seen that the performance of the equalizer which employed prediction with Approach 1 is very close to the performance of the original Block Adaptive equalizer. The difference is due to the prediction error. Note that when we employ long range prediction, we are able to eliminate the delay which is a necessity and big drawback for original Block Adaptive equalizer. Similarly, we repeated the experiment with the prediction using Approach 2. As we studied earlier, Approach 2 is a subobtimal technique but it has less computational complexity. Although Approach 2 has subobtimal performance and, consequently, more prediction error, it still provides acceptable performance. As seen from the figure, its performance is still better than decision directed LMS equalizer and Block Adaptive Equalizer with T_s delay. Therefore, Approach 2 might also find applications when the computational complexity is an issue. However, if the computational complexity is not an issue, then Approach 1 should be preferred due

to its superior performance.

Furthermore, in [99], the impact of the channel estimation errors on the performance of the Decision Feedback Equalizer has been theoretically analyzed. Authors in [99] also define the estimation error as $e(m) = h(m) - \hat{h}(m)$ where $h(m)$ is the overall channel impulse response and $\hat{h}(m)$ is the estimate of the $h(m)$. They also represent the channel as a Gaussian process, as it is the case for Raleigh fading, as well as the estimation error. Defining

$$H(m') = E\{h(m)h^*(m - m')\} \tag{4.54}$$

$$E(m') = E\{e(m)e^*(m - m')\} \tag{4.55}$$

the autocorreletion function is given by [99]

$$R(m') = E(0) + \alpha \sum_{m'<0} H(m') + \alpha \sum_{m'>0} E(m') + N_0/2\delta(m') \tag{4.56}$$

where the scale factor $\alpha = 0.25$ was found in [99] to give excellent results with respect to theoretical results and measured data. The probability of error is also given in [99] as

$$P_e = \sum_{i:\lambda_i<0} A_i \tag{4.57}$$

where $A_i = \prod_{j\neq i} \frac{1}{1-\lambda_j/\lambda_i}$ where λ_i's are the eigenvalues of the matrix A whose elements are given as a function of $H(m')$, $E(m')$, and $R(m')$ as derived in [99]. In [99], authors obtained the expression for the average probability of error in terms of the channel estimation error autocorrelation function as given in Equation (4.57). In the previous Section, we were able to find the autocorrelation functions for both Approach 1 and Approach 2. In our analysis, these autocorrelation functions are utilized to find the long range prediction performance in the minimum mean squared error (MMSE)

sense. The resulting MMSE for Approach 1 and Approach 2 are given as $\xi_{k,m}$ (see Eq. (4.42)) and $\xi'_{k,m}$ (see Eq. (4.50)) respectively. Therefore, we used the autocorrelation functions calculated in Section 3.2 and the results of [99] to find the theoretical lower bound of the performance of the Decision Feedback Equalizer with a given prediction error performance. These theoretical lower DFE performance bounds with prediction error are also plotted in Figure 4.17 for both Approach 1 and Approach 2.

4.5 Performance Enhancements at the Transmitter

In the previous Section, we demonstrated how the long range prediction technique enables powerful adaptive equalizers at the receiver by removing their bottlenecks, such as inherent processing delays. In this section, we will explore how we can utilize our novel long range prediction technique at the transmitter. In our recent work, we showed that long range prediction enables transmitter diversity techniques [38]. This work could be also used to extend our results presented in [38] for any multipath channel with arbitrary delays (previously the delays were considered only a multiple of chip interval, T_c). The technique presented in this paper could also help in development of more powerful adaptive modulation and coding techniques [63, 64, 75, 76, 77, 78, 79, 80, 81] (and the references therein). In this research, we investigate the performance improvements and the availability of the transmitter precoder (preequalizer) for the rapidly varying fading channels. It has been shown that the transmitter precoder works well under slowly varying fading channel conditions [85, 86, 87, 88]. However, these implementations do not work under rapidly varying channel conditions. They rely only the current knowledge of the channel information. Therefore, our novel long range prediction capability enables powerful transmitter

precoders for the rapidly varying fading channels as well.

The transmitter precoding (preequalizer) is also called Tomlinson-Harashima (TH) Precoding, in honor of its coinventors [83, 84]. The idea of precoding is to move the cancellation of the postcursor ISI to the transmitter, where the past transmitted signals are known without the possibility of errors. Therefore, the transmitter precoder does not suffer from error propagation which is inherent to the DFE. Since no decision feedback is necessary at the receiver when using the transmitter precoding, powerful coding techniques with a Viterbi decoder or trellis precoding techniques [85, 86, 87, 88] can be used in the system to further improve the transmission performance without significantly increasing the complexity of the mobile unit.

In the previous section, we showed that the DFE can be implemented as shown in Figure 4.18. The channel impulse response, h_k, is referred to using the formal $D-$transform

$$H(D) = \sum_k h_k D^k. \tag{4.58}$$

Similarly, the feedforward and the feedback filters are indicated by $F(D)$ and $B(D)$ respectively. The input sequence, b_k, is filtered by the channel, $H(D)$, and the Additive White Gaussian Noise (AWGN), n_k, is added producing the sequence seen at the receiver.

TH precoding is originally proposed for Pulse Amplitude Modulation (PAM) systems [83, 84]. The postcursor ISI cancellation is done at the transmitter by implementing the feedback filter at the transmitter as shown in Figure 4.19. It is assumed that channel characteristics are known at the transmitter. In order to stabilize the precoder, TH procoding uses a non-linear modulo-arithmetic operation before being transmitted and being applied back to the feedback filter. Let the $\Gamma_M(.)$ operator

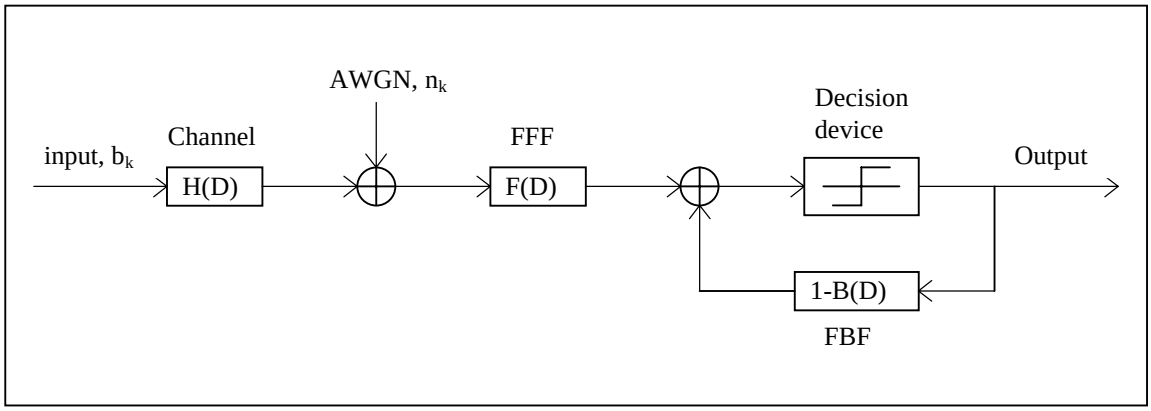

Figure 4.18: System with Decision Feedback Equalizer

represent modulo$-M$ operation. The $\Gamma_M(.)$ operator maps the real numbers onto the interval $(-M/2, M/2]$ according to $\Gamma_M(x) = x + mM$ where m is the integer for which $\Gamma_M(x) \in (-M/2, M/2]$. Typically for iid b_k, x_k will be approximately iid and approximately uniformly distributed on $(-M/2, M/2]$. If b_k is iid with uniform distribution on $(-M/2, M/2]$, then x_k will be exacly iid and uniform on $(-M/2, M/2]$. As studied by Mazo [100], when b_k is a PAM signal, x_k will have a slightly larger power than b_k. The desired signal b_k is recovered at the receiver by applying the same modulo$-M$ operation [83, 84, 101].

Using the $D-$transform notation, the channel impulse response can be represented by $H(D)$. Similarly, the feedforward and the feedback filters are indicated by $F(D)$ and $B(D)$ respectively. The input sequence, b_k, is filtered by the channel, $H(D)$, and the Additive White Gaussian Noise (AWGN), n_k, is added. In TH precoding, $B(D)$ must be causal and monic so that feedback filter $1 - B(D)$ in Figure 4.19 requires only the previous values of x_k. $F(D)$ may be any linear FIR filter. The feedforward filter (FFF), $F(D)$, and the feedback filter (FBF), $B(D)$, could be chosen to minimize

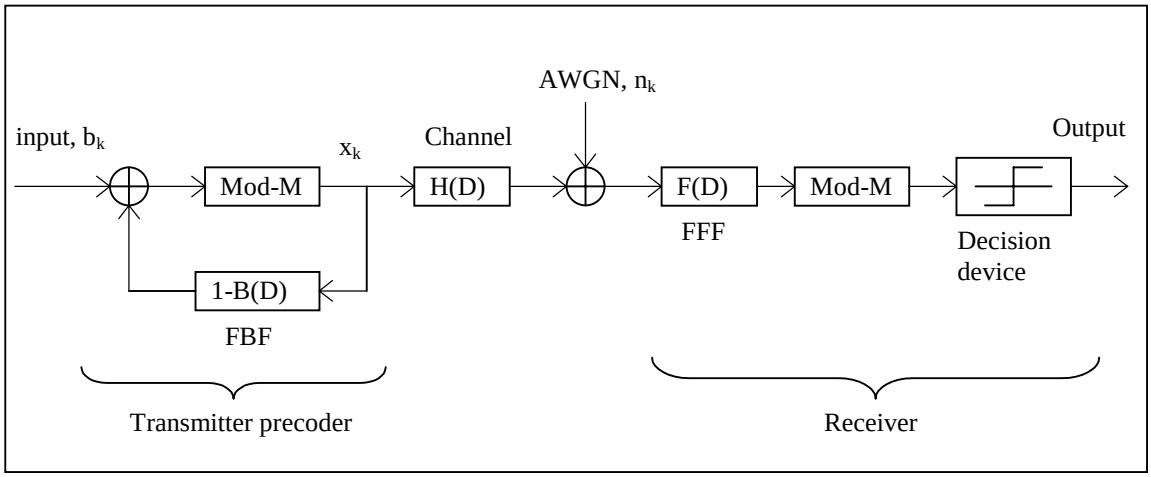

Figure 4.19: System with Transmitter Precoder

zero-forcing (ZF) or minimum mean-square error (MSE) optimality criteria [102].

TH precoding was originally proposed for a wired communication system which does not have the problem of channel fading. Therefore, TH precoding can not be directly applied to time varying fading channels where amplitude fading causes severe errors in retrieving the original amplitude information at the receiver, due to corresponding modulo-arithmetic reduction. Phase modulation such as phase-shift keying (PSK) is usually preferred to Pulse Amplitude Modulation (PAM) in wireless communication systems due to its frequency spectral efficiency. Using PSK, it is desired to have a constant precoded signal amplitude, even though in practice pulse shaping is commonly used to meet out-of-band spectral emission requirements. Pulse shaping after precoding results in fluctuations of the envelope of the transmitted signal. When the time varying envelope of the precoded and filtered signal is amplified by a nonlinear power-efficient output amplifier, signal distortions occur and transmission performance degrades. If the precoder keeps a constant signal amplitude, then the

envelope variations at the amplifier input are solely due to pulse shaping and therefore are smaller than those when TH precoding is used (since TH precoding introduces extra envelope variations). An adaptive channel precoding technique has been proposed for phase modulation over a slowly fading channel [103]. An automatic gain control (AGC) unit is used in the adaptive precoder to achieve a constant amplitude. However, the AGC unit also introduces nonlinear distortion to the precoded signal and results in channel equalization errors. In order to reduce the equalization error, another precoding method intended for $M-$ary PSK(MPSK) has been proposed in [104], which establishes a relationship between the phase and amplitude of the received signal by a spiral curve design, known as phase precoding. By adaptively choosing the spiral curve according to channel fading status, the precoding method can keep a constant transmitted signal amplitude, stabilize the precoder, and ensure ISI-free transmission. Different from the approach given in [104], in [101] a different channel precoding technique is proposed for a time-division multiple-access (TDMA) indoor radio system operating in a time-division duplex (TDD) mode using quaternary PSK (QPSK). The precoding technique is developed based on a new dimension partitioning technique. With this technique, only the carrier phase is pre- distorted so that the precoded signal amplitude can be kept constant. As a result, this precoding technique is claimed to overcome the drawbacks of TH precoding slowly time varying channels by keeping the stability of the precoder.

These techniques described above are efficient methods to implement TH precoding at the transmitter for slowly varying fading wireless channel only. They all fail to track the variations of the fast fading channels. Therefore, the real challenge is to develop a precoding system at the transmitter for the "rapidly varying" fading channels. Our novel approach to the long range prediction of the fast fading channels

also enables us to implement TH precoder with some modifications for fast fading frequency selective fading channels. Therefore, in this work, we propose a new modified TH precoder which is designed specifically for rapidly varying fading channels. The key point in this design comes from our long range prediction capability. As we discussed earlier, we are able to predict the impulse response of the frequency selective multipath channel far ahead before we transmit. We use this prior knowledge of the channel impulse response to ensure both the stability of the TH precoder and the design of the feedback filter at the transmitter.

In TH precoding, the feedback filter, $B(D)$, is made available to the transmitter. This can be accomplished in regular time interval, with the rate of our low sampling rate, f_s. Therefore, as explained earlier, pilot signal sent from transmitter to the receiver, receiver measures the channel impulse response, $h(t)$, then this information is fed back to the transmitter. Then, the transmitter applies long range prediction algorithm to predict the future values of the channel impulse response, and finally, these predicted values are used to construct feedback filter, $B(D)$. Since, in our long range algorithm, we are able to predict several ms ahead the feedback delay can be compensated by the long range prediction capability. This feedback filter is similar to the one we used at the receiver in the previous section. Since we can not tolerate any delay at the transmitter for the TH precoder, we were unable to implement Block Adaptive Scheme at the transmitter without predicting the future channel impulse response. Therefore, our novel long range prediction technique enables Block Adaptive feedback filter at the transmitter for the rapidly varying fading channels. Filter coefficients are updated similar to the original Block Adaptive Equalizer implementation [70, 71, 59].

The operation of the precoder is described as follows. Let $B(D) = 1 + B_1 D +$

$B_2D^2 + \ldots$, and denote the output of the precoder $x(D) = x_0 + x_1D + x_2D^2 + \ldots$ with the initial values $x_k = 0$ for $k < 0$. Then, we can write x_k as

$$x_k = b_k + \sum_{j \geq 1} x_{k-j} b_j + M z_k \tag{4.59}$$

where z_k is integer chosen to minimize the absolute value of x_k by Mod$-M$ operation. If the input sequence, b_k is iid with uniform distribution on $(-M/2, M/2]$, then the precoder output, x_k will be iid and uniform on $(-M/2, M/2]$. Furthermore, the total channel power, E_s (see Eq. (4.26)), is also predicted and the corresponding data bits are multiplied by the inverse of the square-root of the total channel power before the Mod$-M$ operation to ensure the proper use of modulo-arithmetic in TH precoder. We can also write Eq. (4.59) in $D-$transform domain as

$$x(D) = b(D) + x(D)[B(D) - 1] - M z(D) \tag{4.60}$$

and consequently,

$$x(D)B(D) = b(D) - M z(D) \tag{4.61}$$

In the receiver, after the feed forward filter, a sequence received samples $v(D) = v_0 + v_1D + v_2D^2 + \ldots$ is generated at the symbol rate. This sequence can be written in the form

$$v(D) = x(D)H(D)F(D) - n(D)F(D) \tag{4.62}$$

$$v(D) = y(D) - w'(D) \tag{4.63}$$

Note that the residual noise, $w'(D) = n(D)F(D)$, is the same as the one obtained in the conventional DFE. The error free received sequence, $y(D)$ is given as

$$y(D) = x(D)B(D) \tag{4.64}$$

by substituting $x(D)$ from Eq. (4.61) as $x(D) = [b(D) - Mz(D)]/B(D)$ into Eq. (4.64), we obtain

$$y(D) = b(D) - Mz(D) \tag{4.65}$$

which has elements $y_k = b_k - Mz_k$. Before making a decision. The samples y_k are reduced by Mod$-M$ operation to he interval $(-M/2, M/2]$ to obtain folded samples of y'_k as

$$y'_k = b_k - w'_k \tag{4.66}$$

where the signal component of b'_ks corresponds to the elements of the original information sequence $b(D)$.

The BER performance of the transmitter precoder with or without prediction is illustrated in Figure 4.20 for the channel model given in Figure 4.7. In Figure 4.20, MFB is plotted as a reference performance curve and it provides lower performance bound. When the transmitter precoder is implemented without any prediction of the future channel impulse response, it does not perform its complete functionality. Therefore, original transmitter precoder does not work for the rapidly varying fading frequency selective channel. However, when we employ long range prediction at the transmitter to predict future channel impulse response coefficients, and apply them to the transmitter precoder scheme, we observe significant performance improvement. In our analysis, we sample the channel and predict the channel impulse response at the rate of 500 Hz. We also assume that the transmission data rate is 25 kbps and maximum Doppler frequency, $f_{dm} = 100$ Hz. When the Approach 1 used in the prediction, it provides very close performance to the performance of optimum block adaptive equalizer implemented at the receiver with $2T_s$ delay. The slight lower performance for the prediction with approach 1 is mainly due to the prediction

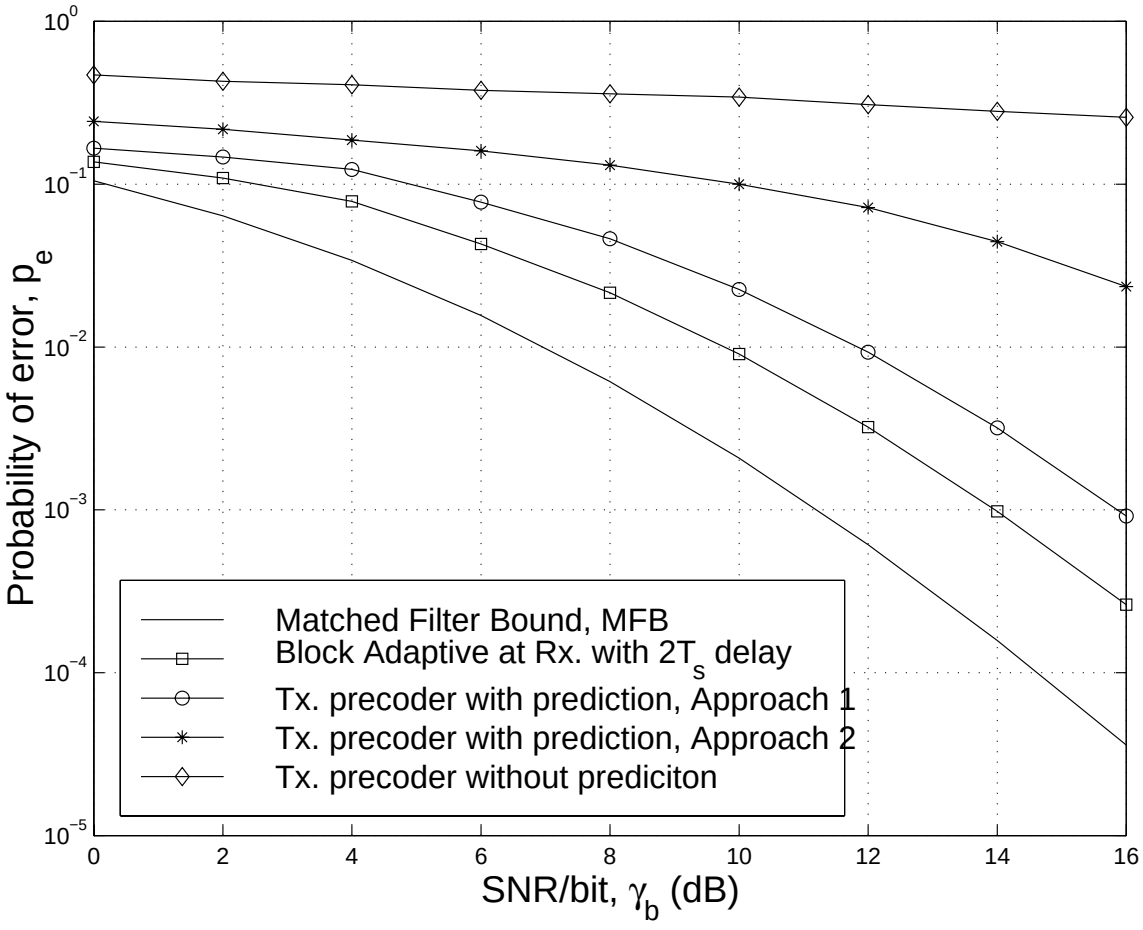

Figure 4.20: Performance of the Transmitter Precoder technique with and without prediction.

error and the nature the nature of the precoder [100] where the transmitted signal, x_k, has slightly larger power than the input signals, b_k. The transmitter precoder employing Approach 2 has lower performance than the Approach 1. This is expected because Approach 2 is a subobtimal approach and it has higher prediction MSE but lower computational complexity than Approach 1. Nonetheless, Approach 2 still provides acceptable performance and it can be used in the mobile unit which requires

lower computational complexity to extend its battery life. However, the Base Station transmitter has high capability to perform intense computations. Therefore, applying Approach 1 for prediction and getting higher performance could be preferred at the Base Station transmitters.

In conclusion, in this section, we demonstrated that we can modify the TH precoder by utilizing our novel long range prediction technique for the rapidly varying fading channels. Therefore, for the first time in the literature, we were able to apply this powerful precoding technique to the rapidly varying fading wireless communication systems. When the precoder is implemented at the Base Station transmitter, we are able to reduce the load at the receiver on the mobile unit since no equalizer is needed at the receiver once the preequalizer is implemented at the transmitter. This means less processing and hence longer battery life for the mobile unit. Moreover, this modified precoder can be combined with the powerful coding techniques [85, 86, 87, 88] to improve the system performance further. The strong coding techniques are made possible with the preequalizers implemented at the transmitter while it would not be possible with the conventional DFE implemented at the receiver.

Chapter 5

Modeling and Performance with Antenna Diversity

The diversity scheme is a very effective method that is used to utilize information from several signals transmitted over independently fading paths [5, 7]. In a system with diversity, several replicas of the same information signal transmitted over independently fading channel are supplied to the receiver. Therefore, since deep fades seldom occur simultaneously during the same time intervals on two or more paths, the probability that all the signal components will fade simultaneously is reduced considerably. For example, if p is the probability that any one signal will fade below some critical value, then p^L is the probability that all L independently fading replicas of the same signal will fade below the critical value.

Frequency, time and antenna diversity are the three techniques in which L independently fading replicas of the same information signal can be provided to the receiver.

In the frequency diversity technique, the same information signal is transmitted on L carriers, where the separation between successive carriers equals or exceeds to the coherence bandwidth, $(\Delta f)_c$, of the channel [3, 5]. The frequency diversity technique has the disadvantage of larger spectrum requirements.

In the time diversity technique, transmitted signals are separated at time intervals equal to or larger than the coherence time, $(\Delta t)_c$, of the channel [3, 5]. One disadvantage of time diversity technique is that it introduces time delay. When the Doppler spread is very small (i.e. mobile is moving slowly, consequently coherence time is very large), the separation in time is required to be very large which introduces larger time delays. Therefore, the time diversity technique is not suitable for mobile radio channels.

The antenna diversity can be achieved by space, angle, polarization and field diversity techniques [7, 105]. Among these techniques, we concentrate on space diversity where multiple antennas spaced sufficiently far apart so that their received signals fade independently. Therefore, from now on, when we refer to the antenna diversity, we mean space diversity only, and antenna diversity reflects the properties of space diversity technique. Antenna diversity plays an increasingly important role in high-speed wireless communications [13, 67, 106, 107, 108, 109]. It has been shown that deploying multiple antennas at both the transmitter and receiver can offer enormous gains in the capacity of wireless channels [110, 111, 112, 113]. In this chapter, we will explain how we incorporate our novel long range prediction technique into the antenna diversity systems. We will be addressing antenna diversity for both flat and frequency selective channels and both at the transmitter and at the receiver. Then, we will generalize the effect of the antenna diversity on both the transmitter and the receiver and their combinations. We will also extend our discussions to the transmitter antenna diversity schemes proposed for the 3rd generation (3G) Code Division Multiple Access (CDMA) systems [114, 115, 72, 73, 74]. We will demonstrate how we utilize the prediction to improve the performance of the selective transmitter diversity (STD) systems proposed for the 3G CDMA systems. Three different approaches

to the long range prediction of the total channel power, which is used for antenna selection in STD, will be analyzed and performance results will be compared.

5.1 Antenna Diversity at the Receiver

If the receiver has multiple antennas, spaced sufficiently far apart so that their received signals fade independently, then they can be used for diversity reception. In the space diversity technique, the necessary space separation required to obtain two or more uncorrelated signals (depending on number of antennas at the receiver) must be determined. The correlation coefficient $\rho_r(d)$ is defined as [7]

$$\rho_r(d) = J_0^2(\beta v \tau) = J_0^2(\beta d) \tag{5.1}$$

where $J_0(.)$ is the zero order Bessel function, τ is the time separation, v is the mobile speed, and $\beta = 2\pi/\lambda$ where λ is the wavelength.

For uniform angular distribution of wave arrivals, $\rho_r(d)$ has its first null at $d = 0.4\lambda$. Theoretically, when the separation between two receiver antennas is around $d = 10\lambda$, the signals arriving these receiver antennas are considered almost uncorrelated. However, in pactice due to the limited space at the receiver, a separation of $d = \lambda/2$ is used to obtain almost uncorrelated signals at the receiver using the fact that as long as the correlation coefficient is less than 0.2, the two signal are considered to be uncorrelated for most practical applications [7].

In order to maximize the output decision SNR, signals received from the L diversity channels are combined. In general, the signal received by each diversity branch is independently weighted. Then, their sum produces the output signal. There are four different combining techniques. They are *selective, switched, equal-gain* and *maximal-ratio* combining [5, 7, 16]. In selective diversity combining technique, the

received signal from the diversity branch with the largest signal power is chosen. Selective combining is very difficult to implement, because a floating threshold level is needed. Therefore, switched combining is a practical alternative since it is based on a fixed threshold level. In switched combining, the selected received signal branch remains until its signal strength drops below a fixed threshold level. Then the combiner switches to the branch signal with the highest signal strength when the current signal drops below a fixed threshold level. Hence, the switched-combined signal always performs worse than the selectively combined signal [7]. In equal-gain combining, all branch signals are summed with equal gain. In maximal-ratio combining, L signals are weighted for optimum performance before being combined. Therefore, it provides maximum SNR at the combiner output. The combiner weights are adaptively updated by using channel impulse response (CIR) estimates to track the random time variations in the channel.

When the maximal-ratio combining is used, the total channel envelope for $L = 2$ is given by

$$|c^T|^2 = |c^A|^2 + |c^B|^2. \tag{5.2}$$

where c^A and c^B are Rayleigh distributed frequency non-selective (flat) fading channel coefficients observed by each receiver antennas. Assuming an equal average power for each path A and B, i.e., $\sigma_A^2 = \sigma_B^2 = \sigma_P^2$, pdf of $|c^T|^2$ is given by the convolution of the pdfs of the each path, A and B, and is found as (Appendix B):

$$p(|c^T|^2) = \frac{1}{(2\sigma_P^2)^2}|c^T|^2 e^{-\frac{|c^T|^2}{2\sigma_P^2}}, \qquad 0 \leq |c^T|^2 < \infty \tag{5.3}$$

Then, we can utilize our long range prediction technique to predict the total power, $|c^T|^2$, at the transmitter. Once we predict accurately how the channel would fade the

signal during the transmission, we can compensate the expected power loss at the transmitter. For example, we can utilize the channel inversion technique here as well. That is, the transmitter interrupts the transmission if the power level, $|c^T|^2$ is below a previously chosen threshold value, ρ. Furthermore, if $|c^T|^2$ is above the threshold, the transmitter sends the data bits, b_k, by multiplying them with the inverse of the $|c^T|$ values. The similar performance results apply here as we investigated in Chapter 4 for two path model.

Receiver antenna diversity system is also utilized for frequency selective channels. Using multiple antennas at the receiver providess additional diversity gain the system along with the suitable combiner and equalizer [70, 116]. Note that, this additional performance improvement is directly related to the number of receiver antennas used at the receiver. Further performance improvement is possible by predicting the total channel power at the transmitter by using our novel long range prediction technique. This will enable accurate power control, more effective modulation and coding schemes to be implemented at the transmitter.

5.2 Antenna Diversity at the Transmitter

Implementing multiple antennas at the receiver is a way to gain diversity. However, it is desired to have simple receivers at the mobile units for several reasons. First of all, the space is limited to put additional antennas on the mobile unit. Moreover, adding more antennas causes more complex receivers and higher computational power that reduces the battery life. Therefore, one solution is to implement antenna diversity at the transmitter. Transmitter antenna diversity schemes are proposed for current and future wireless communication system. In this section, we will discuss two different

ways to get diversity effect at the transmitter. In the next section, we will explore more on diversity schemes that has been proposed for the 3rd generation wireless systems.

The simplest transmitter diversity technique could be adapted for flat fading channels is as follows. At the transmitter, two antennas spaced sufficiently apart to ensure independently fading paths are used. At the receiver, with single receiver antenna, each path is resolved by the aid of pilot signal or training sequence and send back to the transmitter. The transmitter predicts future fading coefficients for each path by using the Linear Prediction technique introduced in Chapter 3. Then, the transmitter selects the antenna which result in the larger gain at the receiver. This creates a similar effect as using two receiver antennas and combining the signal based on selective combining strategy as explained in the previous section. Furthermore, the channel inversion technique is also applied for further performance improvement. Although this techniques provides a performance improvement of selective diversity, it is not the optimum way to combine as opposed to maximal ratio combining.

The second transmitter diversity technique is to provide diversity benefit to a receiver in a flat fading environment [117]. In this transmitter diversity technique, multiple antennas transmit delayed version of a signal to create frequency selective fading at a single antenna at the receiver. Assuming the delay is equal the one symbol duration, T, the dual transmitter diversity is the same as what we studied for in Chapter 4 for the frequency selective case with 2-path channel model. Note that, since this system would be equivalent to the frequency selective case, there will be ISI in the system and a suitable equalizer would be implemented at the receiver to mitigate the effect of ISI. This technique could be implemented for frequency selective fading channels as well. However, for the frequency selective case, this delay should

be chosen more carefully. The delay should be at least twice the multipath delay spread in order to ensure further diversity. Moreover, as discussed previously, the total channel power could be predicted by using long range prediction technique and the prior knowledge of the channel characteristics could be utilized to improve the performance further.

We have presented that using multiple antennas at the receiver provides diversity effect in both flat and frequency selective channels. We also showed that the similar diversity can be obtained at the transmitter by implementing the antennas at the transmitter instead of at the receiver. We can also put multiple antennas both at the transmitter and at the receiver at the same time. In this case, the total number of independent fading diversity paths would be $L_T L_R$, where L_T and L_R are the number of transmitter and receiver antennas, respectively.

5.3 Application of Long Range Prediction to the Selective Transmitter Diversity (STD) for WCDMA

In this section, we will extend our results to the Direct Sequence Code Division Multiple Access (DS/CDMA) channels. DS/CDMA technology is attractive for wireless access because of its numerous advantages over other multiple access techniques such as Time Division Multiple Access and Frequency Division Multiple Access. Some of the advantages of CDMA over other techniques are its ability to provide soft handoff, graceful degradation, exploitation of multipath fading through Rake combining, and direct capacity increase by the use of cell sectorization. However the current DS/CDMA is optimized for basic services only. Therefore, Wideband DS/CDMA (WCDMA) has been developed as a predominant radio access technology for the next

generation global wireless standard [114, 115]. The proposed WCDMA offers significant improvements over current CDMA system. These include support of higher rate data services, improved coverage and capacity due to wider bandwidth and coherent detection, fast and efficient packet acces control, capability to support multimedia services. One of the novel features of WCDMA is support for transmitter antenna diversity for the downlink [72, 73, 74].

Some of the proposed transmitter antenna diversity schemes are Orthogonal Transmitter Diversity (OTD), Transmitter Adaptive Array (TxAA), Selective Transmitter Diversity (STD), and Space Time Transmitter Diversity (STTD). TxAA and STD can result in better performance than OTD and STTD, but require feedback of channel state information (CSI) from the mobile to the base station. In practice, the performance of these schemes can be degraded due to imperfect and delayed CSI. In particular, even small delay can result in significant degradation due to the time varying nature of the fading channel.

In this section, we will present how to utilize the long range prediction technique to improve the performance of transmitter diversity systems. In particular, we focus on Selective Transmitter Diversity. Using the long range prediction technique, we are able predict both flat and frequency selective fast fading channels accurately far beyond the coherence time. This prior knowledge of the channel for the entire duration of the next frame or slot provided by long range prediction would enable more efficient antenna switching at the transmitter.

5.3.1 STD with Prediction in WCDMA Systems

WCDMA utilizes bandwidths of 5 MHz to 20 MHz. Because of these large transmission bandwidths, the wireless radio channel is often frequency selective. There-

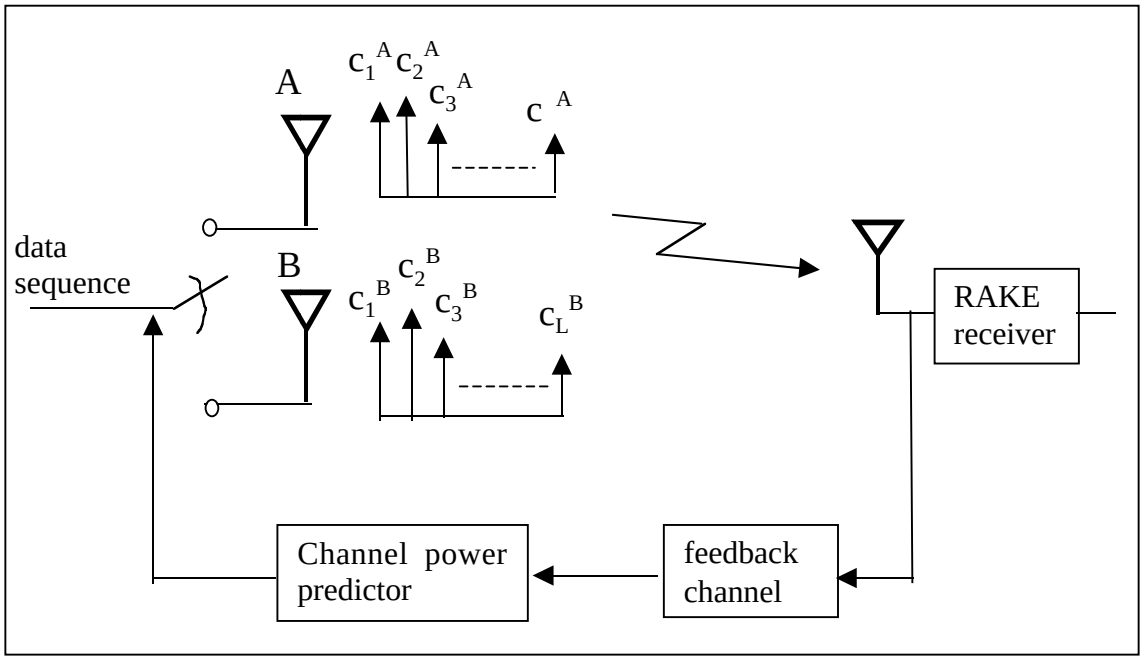

Figure 5.1: Selective Transmitter Diversity System

fore, large diversity gain can be realized using the RAKE receiver. This gain can be further enhanced by utilizing antenna (diversity) arrays. In practice, the mobile is often limited to a single antenna, whereas the base station can employ several antennas. Thus, transmitter antenna diversity techniques for downlink signaling have been recently investigated by many researchers [72, 73, 74]. We consider a Selective Transmitter Diversity (STD) system shown in Figure 5.1 for two antennas (it can be easily extended to a greater number of antennas). For each antenna, the channel is characterized as frequency selective Rayleigh fading with L paths. The signal of the desired user is transmitted either from antenna A or from antenna B. All paths are

i.i.d. and each channel has unit average power, i.e.,

$$E[|c_k^A|^2] = E[|c_k^B|^2] = \frac{1}{L} \qquad k = 1, \ldots, L \tag{5.4}$$

The total instantaneous powers associated with the channels of antennas A and B are: $\Omega^A = \sum_{k=1}^{L} |c_k^A|^2$ and $\Omega^B = \sum_{k=1}^{L} |c_k^B|^2$, respectively. Both Ω^A and Ω^B are Chi-Square distributed with $2L$ degrees of freedom. For an STD system, the transmission antenna is selected based on the power comparison between Ω^A and Ω^B. The antenna that results in a stronger signal at the receiver will be used as the transmission antenna. Therefore, in the STD systems for WCDMA, we need to determine the future total power for each antenna in order to decide which antenna will be selected for transmission. However, in contrast to the channels with phase ambiguity, in the proposed 3rd generation WCDMA systems, coherent channel estimates are available at the receiver since the pilot channel is used. Therefore, complex fading coefficients associated with different multipath components and transmitter antennas can serve as observations. In the next section, we will analyze three approaches to long range power prediction of the channel power for each transmitter antenna given a sequence of channel observations associated with that antenna.

One of the key features that makes WCDMA feasible globally is its high carrier frequency of 2 GHz. However, this high carrier frequency results in very large Doppler shifts at moderate vehicular speeds (e.g. 65 mi/h corresponds to $f_{dm} = 200$ Hz.) These high Doppler shifts result in significant variations of the fading channel coefficient over short time periods. Thus, outdated channel estimates fed back to the transmitter become less useful for adaptive signaling application, and long range fading prediction capability becomes more important. Using accurately predicted future channel power, the transmitter can appropriately select the signaling method for the

future frame even when channel varies rapidly due to fast fading.

We exploit three approaches to long range prediction of the channel power for each transmitter antenna given a sequence of channel observations associated with that antenna. This information about future channel power allows the mobile to make a suitable selection of the base station antenna for the next transmission interval. In this analysis, we assume that present and past samples of the i.i.d. Rayleigh fading coefficients c_k for L paths ($k = 1, \ldots, L$) are observed at the mobile for each transmitter antenna (i.e. samples of $c_k^A(t)$ and $c_k^B(t)$ are observed, but we suppress the antenna (A or B) and time indices in the sequel). This analysis can be extended to include noise present in the observations (e.g. noisy pilot symbols). In this work, we restrict the derivation to the noiseless case to show the potential of long range power prediction for the ideal Rayleigh fading channel. The noisy case can be examined through simulation and the performance can be further improved by adaptive tracking methods by reducing the effect of noise.

CASE 1:

In this approach, each future complex Gaussian fading coefficient $c_k(t)$ is predicted separately for each path and each antenna, and the total predicted power for each antenna is calculated using these estimates. These future predicted samples are denoted as $\hat{c}_1$, $\hat{c}_2$, $\ldots$ $\hat{c}_L$. The autocorrelation function of each component is [4]:

$$r_j = (1/L)(\Omega_0/2)J_0(2\pi f_{dm} j T_s) \tag{5.5}$$

where $E[|c_i|^2] = \Omega_0/L$. The prediction MMSE per component is $\xi_i = E[|e_i|^2]$, where $e_i = c_i - \hat{c}_i$. Our purpose is to find the total power prediction mean squared error, ξ_T

$$\xi_T = E\left[\left|\sum_{i=1}^{L}|c_i|^2 - \sum_{i=1}^{L}|\hat{c}_i|^2\right|^2\right] = E\left[\left|\sum_{i=1}^{L}(|c_i|^2 - |\hat{c}_i|^2)\right|^2\right] \tag{5.6}$$

let $e_i' = |c_i|^2 - |\hat{c}_i|^2$, therefore,

$$\xi_T = E\left[\left|\sum_{i=1}^{L} e_i'\right|^2\right] = \sum_{i=1}^{L} E[|e_i'|^2] + \sum_{k\neq j} E[e_k' e_j'] \tag{5.7}$$

In Appendix D, the right hand side of the equation has been analyzed carefully, and the following result is obtained for the total power prediction mean squared error, ξ_T

$$\xi_T = L\left(4\frac{\Omega_0}{L}\xi_i - 2\xi_i^2\right) + (L^2 - L)\xi_i^2 \tag{5.8}$$

$$\xi_T = 4\Omega_0\xi_i + (L^2 - 3L)\xi_i^2 \tag{5.9}$$

Since $\xi_i = \xi_{flat}/L$, where ξ_{flat} is the MMSE of the complex fading coefficient prediction for $L = 1$, the ξ_T is given as

$$\xi_T = \left(4\frac{\Omega_0}{L}\right)\xi_{flat} + \left(1 - \frac{3}{L}\right)\xi_{flat}^2 \tag{5.10}$$

CASE 2:

In this case, we apply linear MMSE prediction directly to the observations of powers $\Omega_1, \Omega_2, \ldots, \Omega_L$, where $\Omega_i = |c_i|^2$ represents the power of the fading channel associated with the $i-$th multipath component for a given antenna. The total predicted power will be computed using these individual estimates $\hat{\Omega}_i$. This Case (and Case 3) are particularly useful to investigate for channels with phase ambiguity since they do not require the knowledge of the phases of the fading coefficients. Each Ω_i has the autocorrelation function [4]:

$$r(\tau) = (\Omega_0/L)^2 J_0^2(2\pi f_{dm}\tau) + (\Omega_0/L)^2 \tag{5.11}$$

Our purpose is to find the total power prediction mean squared error, ξ_T given the

powers of the fading channel associated with each multipath component such that

$$\xi_T = E\left[\left|\sum_{i=1}^{L}\Omega_i - \sum_{i=1}^{L}\hat{\Omega}_i\right|^2\right] = E\left[\left|\sum_{i=1}^{L}(\Omega_i - \hat{\Omega}_i)\right|^2\right] \tag{5.12}$$

Let $e_i = \Omega_i - \hat{\Omega}_i$, therefore,

$$\xi_T = E\left[\left|\sum_{i=1}^{L} e_i\right|^2\right] = \sum_{i=1}^{L} E[|e_i|^2] + \sum_{k\neq j} E[e_k e_j] \tag{5.13}$$

Again, in Appendix D, the right hand side of the equation has been analyzed carefully, and the following result is obtained for the total power prediction mean squared error for this case, ξ_T

$$\xi_T = \frac{\Omega_0^2}{L}\left(1 - \sum_{j=1}^{p} d_j\right) + \frac{\Omega_0^2}{L}\left(1 - \sum_{j=1}^{p} d_j J_0^2(2\pi f_{dm} j T_s)\right) + (L^2 - L)\left(\frac{\Omega_0}{L}\right)^2\left(1 - \sum_{j=1}^{p} d_j\right)^2 \tag{5.14}$$

This can be simplified further and the total MMSE for Case 2 is given as:

$$\xi_T = \Omega_0^2\left(1 - \sum_{j=1}^{p} d_j\right)^2 + \frac{\Omega_0^2}{L}\left(1 - \sum_{j=1}^{p} d_j\right)\left(\sum_{j=1}^{p} d_j\right) + \frac{\Omega_0^2}{L}\left(1 - \sum_{j=1}^{p} d_j J_0^2(2\pi f_{dm} j T_s)\right) \tag{5.15}$$

CASE 3:

In this approach, we form the linear MMSE prediction of the total power of the fading channel for each antenna using previous total power samples observed at the receiver. The total power is given as $\Omega_T = \Omega_1 + \Omega_2 + \ldots + \Omega_L$. In Appendix D, we

showed that the autocorrelation function of Ω_T is

$$r(\tau) = \frac{\Omega_0^2}{L} J_0^2(2\pi f_{dm}\tau) + \Omega_0^2 \tag{5.16}$$

and the MMSE $E[|\Omega_T - \hat{\Omega}_T|^2]$, for Case 3 can be expressed as (see Appendix 3 for the derivation)

$$\xi_T = \Omega_0^2 \left(1 - \sum_{j=1}^{p} d_j\right) + \left(\frac{\Omega_0^2}{L}\right) \left(1 - \sum_{j=1}^{p} d_j J_0^2(2\pi f_{dm} j T_s)\right) \tag{5.17}$$

Performance Comparisons of 3 Cases:

In this section, MSEs of the three approaches derived above for the noiseless case are compared. In our analysis, the total channel power for each antenna is normalized to 1. To make system parameters consistent with the third-generation WCDMA system, we assume the carrier frequency is 2 GHz and $f_{dm} = 200$ Hz. In the theoretical calculation of the model coefficients, it is required to invert the autocorrelation matrices obtained from sampling (5.5), (5.11) and (5.16) for Cases 1, 2, and 3, respectively. We found that higher sampling rates f_s (e.g., 1.6KHz) cause matrix singularities when the model p is large. This is due to oversampling the channel relative to the Nyquist rate of 400 Hz. When we sample the channel by the rate higher than the Nyquist rate and at the same time use large model order, p, the matrix becomes over-determined and the solution for LP coefficients d_j's are not unique. If the sampling rate is chosen closer to 400 Hz, the matrix does not become singular for large p. In practice, additive noise and the finite observation interval result in a non-singular matrix. In this comparison of the ideal noiseless MSEs, we concentrate on cases when the matrix is not singular. This is assured by choosing sufficiently low f_s for a given value of p.

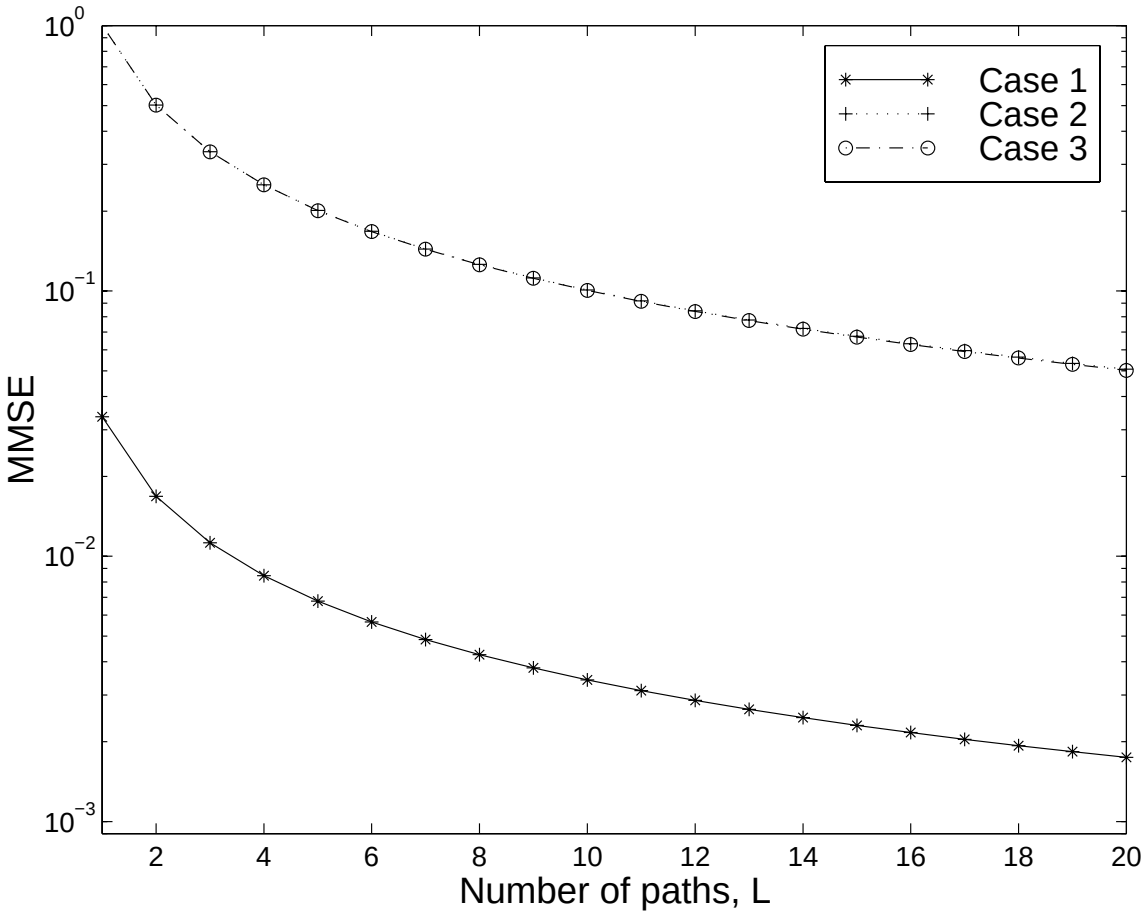

Figure 5.2: Theoretical prediction MMSE of the total multipath channel power for model order, $p = 50$, the channel sampling rate, $f_s = 500$ Hz, and the prediction range, $\tau = 2$ ms

In Figure 5.2 and Figure 5.3, we fix the prediction range $\tau = 2$ ms, and examine two choices of prediction parameters. The first selection ($p = 50, f_s = 500$ Hz in Figure 5.2) corresponds to much larger memory span p/f_s than the second set ($p = 15, f_s = 1$ KHz in Figure 5.3). However, the second selection results in much lower MSE for Case 1, suggesting that it is beneficial to sample recent observation at sufficiently high rate (of course 1 KHz is still much lower than the data rate). We

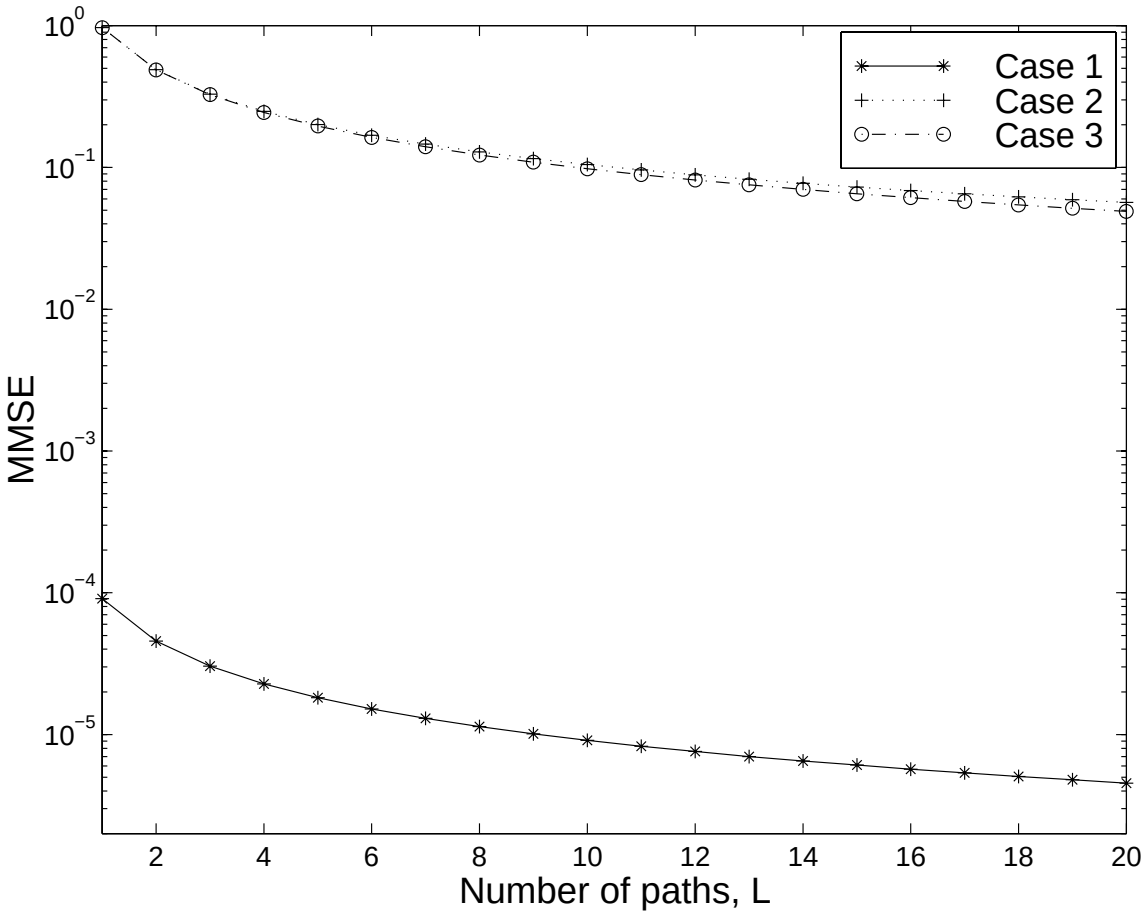

Figure 5.3: Theoretical prediction MMSE of the total multipath channel power for model order, $p = 15$, the channel sampling rate, $f_s = 1000$ Hz, and the prediction range, $\tau = 2$ ms

find that the total MSEs for all 3 cases decrease as L grows and approach the saturation values that can be determined from (5.10), (5.15), and (5.17). The theoretical MSEs of cases 2 and 3 for both choices are close enough to be considered as same. In general, these cases perform much poorer than Case 1 for realistic prediction ranges and number of paths. However, Case 3 requires only one predictor per antenna, so its complexity is lower than that of Cases 1 and 2, which require L predictors for each

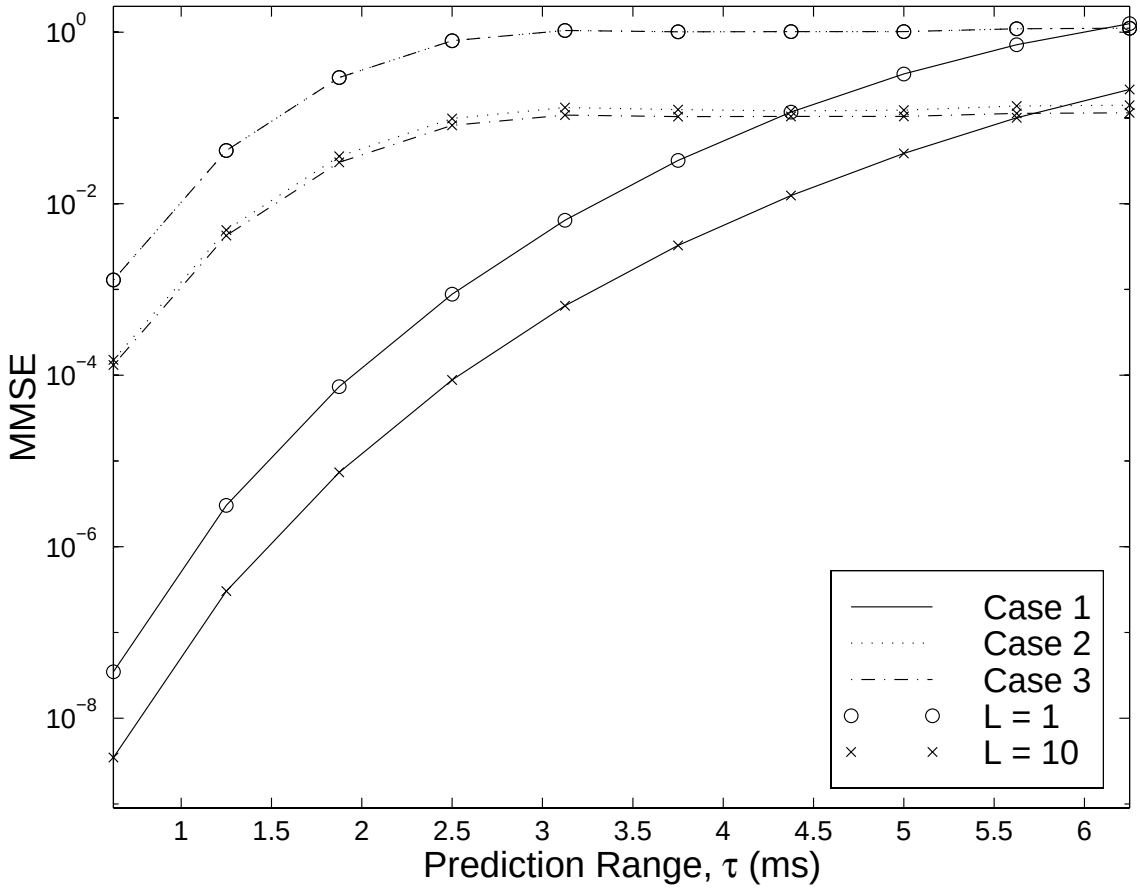

Figure 5.4: Theoretical prediction MMSE vs. the prediction range, τ

antenna. Of course, in the presence of phase ambiguity Case 1 is not feasible, and Case 3 is the better choice.

In Figure 5.4, we consider the MSE performance versus the prediction range for the sampling rate, $f_s = 1.6$ KHz, and $p = 10$. We observe that Cases 2 and 3 outperform Case 1 for sufficiently large prediction range. We also found that as L increases and f_s decreases, this cross-over occurs for a lower value of the prediction range. Thus, when prediction far ahead is desired, Case 1 is not always the best choice, considering

its high complexity. However, for most practical applications Case 1 would result in the best performance.

5.4 Practical Issues - Level Crossing Rates and Average Fade Durations

In the final section in this thesis, we would like to discuss some practical issues we would experience in real life. Changing the power level for every symbol interval might not be very practical from the implementation point of view because of the limitations on the nonlinear power amplifiers. Therefore, instead of inverting the channel for every bit, we could just "invert" the channel once every 50 to 100 bits depending on the average channel statistics. Two of the most important ones for the mobile communications are the Level Crossing Rate (LCR) and the Average Fade Duration (AFD) of the fading channel envelope [4, 7]. These second order statistics were first introduced by Lee [118] and they are defined as follows.

The envelope LCR, L_ρ, is a measure of how often the envelope crosses a specified level (threshold), ρ. It is defined as a rate at which the envelope crosses level ρ in the negative (or positive) direction. For the Rayleigh fading channel, the LCR is found as for a given level, ρ and the maximum Doppler frequency, f_{dm}

$$L_\rho = \sqrt{2\pi} f_{dm} \sqrt{\rho} e^{-\rho} \tag{5.18}$$

The AFD, t_ρ, is a measure of how long the envelope remains below a specified level, ρ. Similarly, for the Rayleigh fading channel, the AFD can be calculated as

$$t_\rho = \frac{e^\rho - 1}{\sqrt{2\pi} f_{dm} \sqrt{\rho}} \tag{5.19}$$

Note that $L_\rho t_\rho$ is the cumulative distribution function (cdf) of α^2-power (3.16)

calculated at a specified level, ρ, i.e.,

$$L_\rho t_\rho = F_\alpha(\rho) = 1 - e^{-\rho} \tag{5.20}$$

For example, for the maximum Doppler frequency, $f_{dm} = 100$ Hz and the threshold, $\rho = 0.1$, the corresponding LCR is, $L_\rho = 72$ fades/sec, and the AFD is , $t_\rho = 1.327$ msec. In North American Cellular System Standards the symbol interval is, $T = 40$ μsec. Therefore, the AFD would be, $t_\rho/T = 33$ symbols on the average. These statistics can be utilized as follows. If the AFD is 33 symbols for a given Doppler frequency and a threshold, that means once the signal level is under that threshold the following 33 symbols on the average would be below that threshold value as well. Therefore, we would rather not to send the whole frame of 50 symbols between the two channel samples at the low channel sampling rate of 500 Hz when it is predicted to be under that threshold. These statistics could also be useful from practical point of view when incorporated into power control schemes, adaptive modulation and coding algorithms along with the our proposed novel long range prediction technique.

Chapter 6

Conclusions

This research is an interdisciplinary effort in communication theory, physics, and signal processing that encompasses novel physical models for multipath fading, channel prediction and tracking methods, adaptive equalization and power-control algorithms, and the receiver and the transmitter diversity techniques for the current and evolved wireless communication systems.

In this work, we propose a novel *long range* fading prediction method by utilizing the physics of the fast fading channel. We explain the parameters that characterize the fading channel in Mobile Radio Systems. We give an insight to the fading channel in terms of important scatterers which allows us a new view to look at the fading channel deterministically. We describe the prediction algorithm which characterizes the channel as an autoregressive model (AR) with low sampling rate, and computes the MMSE estimate of the future fading coefficient sample based on a number of past observations. Then, we interpolate to get the predicted channel coefficients at data rate. This algorithm can reliably predict future fading coefficients far beyond the coherence time for a fading channel with an arbitrary number of scatterers. The superior performance of our long range prediction method comes from its lower channel sampling rate (on the order of twice the Doppler shift) unlike the conventional

methods which assume sampling at data rate for channel modeling and estimation. The lower rate utilizes the large sidelobes of the autocorrelation function of the fading process, permitting prediction further in to the future. By using conventional methods, even with a very accurate coefficient adjustment, it is impossible to specify future channel coefficients from past observations - the filter length is not long enough. The potential of long range prediction for fading channels and the performance of the algorithm are illustrated by considering the parameters involved in the MMSE prediction. We investigate the effect of the sampling rate, prediction range, number of scaterers, filter length and the SNR on the MMSE of the long range prediction.

The main factors that affect the prediction accuracy of this algorithm are error propagation (since the previously predicted values used to predict the future fading coefficients), additive noise and decision - directed tracking, limited number of observations used in initial acquisition of the LP coefficients (short observation interval), and limited order p of the AR model. Therefore, Least Mean Squares (LMS) adaptive tracking method is employed in conjunction with the channel inversion algorithm to eliminate the error propagation and to mitigate the effect of noisy observations and other limitations. When the transmitter uses the updated estimates of the adaptive tracking to predict future fading values, rather than relying on previous estimates, a considerable improvement is observed in the performance. This adaptive algorithm enables us to approximate the performance of the theoretical curves.

As well as investigating the long range prediction of the fading channel based on the observation of the complex valued channel coefficients, we examine the long range prediction of the fading channel power using the observed power samples. This prediction approach is very useful especially when there is a phase ambiguity in the received signal and absolute phases are not available. For example, in decision directed chan-

nel estimation, phase ambiguity requires differential encoding, and absolute phases are not available. The potential of long range power prediction for fading channels and the performance of the algorithm are illustrated by considering the parameters involved in the MMSE prediction. We investigate the effect of the sampling rate, prediction range, number of scaterers, filter length and the SNR on the MMSE of the long range power prediction.

This technique is initially developed for flat fading channels. We demonstrated that how he novel long range prediction provides enabling technology for powerful techniques both at the transmitter and at the receiver to combat fast fading channels. Then, we extend the proposed long range prediction technique to the frequency selective fast fading channels which introduces ISI and large multipath delay spread to the system. We discuss how to utilize the frequency selectivity of the channel into our advantage by using a matched filter (MF) followed by an equalizer. Basically, an equalizer is used to compensate and reduce the ISI introduced by the frequency selective channels. The combination of MF and an equalizer is a way to gain diversity. The Matched Filter Bounds (MFB) are derived for the general frequency selective fading channels with arbitrary number of distinct paths, delays and path strengths. Then, we use this MFB as a reference performance bound in our analysis.

We investigated the estimation of the channel impulse response by using pilot signaling. Then, we demonstrated the feasibility of the long range prediction of the channel impulse response of the frequency selective fading channels by using these estimated channel impulse response coefficients. Two different approaches used for the long range prediction are introduced and performance comparisons are provided.

The time-variant multipath propagation of the signal through the frequency selective channel results in intersymbol interference (ISI). Therefore, the digital trans-

mission at a rate exceeding the coherence bandwidth of the frequency selective fading channel requires equalization at the receiver to compensate and to reduce the ISI. In most communication systems that employ equalizers, the channel characteristics are unknown a priori. Furthermore, in many cases, the channel response is time-variant, as we experience in wireless communication channels. In that case, the equalizers are designed to be adjustable to the channel response and, for time variant channels, to be adaptive to the time variations in the channel response. The adjustment of equalizer coefficients is usually performed adaptively during the transmission of information by using the decisions at the output of the detector in forming the error signal for the adaptation. However, these decision directed adaptive techniques fail to track the variations of the fast fading channels. In this thesis, we investigated how the novel long range prediction technique enabled more efficient equalizer techniques at the receiver.

We expanded our research on how we utilize the prior knowledge of the predicted channel impulse response at the transmitter. It has been shown that there is a big potential for this technique to be used in more efficient transmitter antenna diversity, adaptive modulation and adaptive coding. Our work on the long range prediction of the generalized frequency selective channels provides more insights and flexibility for these transmitter adaptive techniques. We investigated the transmitter precoder (preequalizer) to combat the ISI at the transmitter. TH precoding was originally proposed for a wired communication that does not have a problem of time varying channel fading observed in wireless communication systems. It also requires the perfect knowledge of impulse response of the channel at the transmitter. TH precoder at the transmitter has the same ISI compensation and the noise suppression advantages as using a decision feedback equalizer in the receiver, but without its disadvantages

of error propagation. Since the feedback part is implemented at the transmitter, the complexity of receiver at the mobile unit is reduced. TH precoders have a further advantage of interworking easily with power-efficient and bandwith-efficient coded modulation techniques. Our novel long range prediction capability enabled powerful transmitter precoders for the fast fading channels as well. New design of the transmitter precoder with the help of long range prediction for the fast fading channels is discussed in the thesis.

We also studied the effect of our long term prediction and channel inversion techniques on the antenna diversity systems. We address antenna diversity for both flat and frequency selective channels both at the transmitter and at the receiver. We show that the further performance improvement is possible when the long rang prediction is implemented. We also extend our results to the Direct Sequence Code Division Multiple Access (DS/CDMA) channels. DS/CDMA technology is attractive for wireless access because of its numerous advantages over other multiple access techniques such as Time Division Multiple Access and Frequency Division Multiple Access. The proposed WCDMA offers significant improvements over current CDMA system. These include support of higher rate data services, improved coverage and capacity due to wider bandwidth and coherent detection, fast and efficient packet access control, capability to support multimedia services. One of the novel features of WCDMA is support for transmitter antenna diversity for the downlink. We present how to utilize the long range prediction technique to improve the performance of transmitter diversity systems. In particular, we focus on Selective Transmitter Diversity (STD). Using the long range prediction technique, we are able predict both flat and frequency selective fast fading channels accurately far beyond the coherence time. This prior knowledge of the channel for the entire duration of the next frame or

slot provided by long range prediction enable more efficient antenna switching at the transmitter. In the STD systems for WCDMA, we determine the future total power for each antenna in order to decide which antenna will be selected for transmission. However, in contrast to the channels with phase ambiguity, in the proposed 3rd generation WCDMA systems, coherent channel estimates are available at the receiver since the pilot channel is used. Therefore, complex fading coefficients associated with different multipath components and transmitter antennas can serve as observations. We study the performance of the three approaches to long range power prediction of the channel power for each transmitter antenna given a sequence of channel observations associated with that antenna. This information of the future channel power allows the mobile to make a suitable selection of the base station antenna for the next transmission interval.

6.1 Impact of the Proposed Research and Future Directions

This research contribute to the theory and practice of wireless communications in several important ways. The ability to accurately forecast signal fading far beyond the coherence time opens up a host of new ways to cope with multipath fading. The new physical models for fading will serve to identify the important scatterers in various environments and provide insight on how they evolve with time. These insights can be used to better predict future channel conditions. The novel long range prediction capability provides enabling technology for more efficient techniques both at the receiver and at the transmitter to combat both flat and frequency selective fading channel impairments. The development of mobile communication systems that can accurately predict and adapt to changing fading conditions would have a substantial impact on communication technology. This method could provide the

basis for communication systems that more fully exploit the potential capacity of the mobile radio channel, and in the process achieve higher spectral efficiency and lower power requirements. In cellular telephony, a substantial increase in spectral efficiency would permit more mobile units to access the same base station in a given bandwidth. Lower power requirements would translate into longer talk time and reduced battery size.

Appendix A

Probability Densities for Flat Fading

When there are large number of closely time-spaced propagation paths in the medium the time-variant impulse response $c(t)$ can be modeled as a complex-valued gaussian random process in the t variable. Then, by the central limit theorem, the real and imaginary parts of c, c_I and c_Q[1], are independent, zero-mean Gaussian random processes each having a variance σ^2 [5, 7, 9, 16].

$$c = c_I + jc_Q = \alpha e^{j\theta}. \tag{A.1}$$

The components c_I and c_Q are described by the bivariate Gaussian distribution with probability density function (pdf) of

$$p(c_I, c_Q) = \frac{1}{2\pi\sigma^2} e^{-\frac{c_I^2 + c_Q^2}{2\sigma^2}}. \tag{A.2}$$

Then, using the bivariate transformation of random variables, i.e.,

$$c_I = \alpha \cos\theta$$
$$c_Q = \alpha \sin\theta$$

It follows that

[1]the time dependence of channel impulse response is implicit.

$$\alpha = \sqrt{c_I^2 + c_Q^2}$$
$$\theta = \tan^{-1}(\tfrac{c_Q}{c_I})$$

and the corresponding bivariate transformation of (A.2) in terms of random variables α and θ is

$$p(\alpha, \theta) = \frac{\alpha}{2\pi\sigma^2} e^{-\frac{\alpha^2}{2\sigma^2}}. \tag{A.3}$$

Therefore, the marginal pdf of α, $p(\alpha)$, which is found by calculating the integral $\int_0^{2\pi} p(\alpha, \theta) d\theta$, is given as

$$p(\alpha) = \frac{\alpha}{\sigma^2} e^{-\frac{\alpha^2}{2\sigma^2}}, \qquad 0 \leq \alpha < \infty \tag{A.4}$$

with the corresponding cumulative density function (cdf)

$$F(\alpha) = 1 - e^{-\frac{\alpha^2}{2\sigma^2}}, \qquad 0 \leq \alpha < \infty. \tag{A.5}$$

and the first and second moments

$$E(\alpha) = \int_{-\infty}^{\infty} \alpha p(\alpha) d\alpha = \sqrt{\tfrac{\pi}{2}}\sigma$$
$$E(\alpha^2) = \int_{-\infty}^{\infty} \alpha^2 p(\alpha) d\alpha = 2\sigma^2.$$

The pdf of the power of fading channel, $p(\alpha^2)$, can be found by defining $g(x) = y = \alpha^2$, and applying appropriate transformation [92]

$$p(y) = \frac{1}{2\sigma^2} e^{-\frac{y}{2\sigma^2}}, \qquad 0 \leq y < \infty \tag{A.6}$$

Therefore, pdf of the power of fading channel, α^2, is given by an exponential distribution

$$p(\alpha^2) = \frac{1}{2\sigma^2} e^{-\frac{\alpha^2}{2\sigma^2}}, \qquad 0 \leq \alpha^2 < \infty \tag{A.7}$$

with $E(\alpha^2) = 2\sigma^2$.

Furthermore, when the channel inversion technique is applied as explained in chapter 3, we need to know the pdf of the inverted power to investigate the effect of power inversion process. Let $z = 1/y$ where $p(y)$ is given in (A.6). Therefore, the pdf of z is found as

$$p(z) = \frac{1}{z^2}\frac{1}{2\sigma^2}e^{-\frac{1}{z2\sigma^2}}, \qquad 0 \leq z < \infty \tag{A.8}$$

Or equivalently, the pdf of inverted power, $p(\frac{1}{\alpha^2})$ is given as

$$p\left(\frac{1}{\alpha^2}\right) = \frac{\alpha^4}{2\sigma^2}e^{-\frac{\alpha^2}{2\sigma^2}}, \qquad 0 \leq \frac{1}{\alpha^2} < \infty \tag{A.9}$$

However, $E(\frac{1}{\alpha^2}) = \int_{-\infty}^{\infty} zp(z)dz = \infty$ which makes channel inversion impossible to apply. In order to overcome this limitation we introduce the concept of the threshold, ρ, in our encoding algorithm described in chapter 3. From now on we will assume average channel power, $E(\alpha^2) = 2\sigma^2 = 1$. With the given ρ, the conditional pdf of z is found as

$$p(z \mid z > \rho) = \frac{1}{e^{-\rho}}\frac{1}{z^2}e^{-\frac{1}{z}}, \qquad \rho \leq z < \infty \tag{A.10}$$

In other words, the new conditional pdf of the inverted power is found as

$$p\left(\frac{1}{\alpha^2} \mid \frac{1}{\alpha^2} < \frac{1}{\rho}\right) = \frac{\alpha^4}{e^{-\rho}}e^{-\alpha^2}, \qquad 0 \leq \frac{1}{\alpha^2} < \frac{1}{\rho}. \tag{A.11}$$

Then, the corresponding the finite average power calculated as

$$E\left(\frac{1}{\alpha^2} \mid \frac{1}{\alpha^2} < \frac{1}{\rho}\right) = \frac{1}{e^{-\rho}}\Gamma_{inc}(0, \rho) \tag{A.12}$$

where Γ_{inc} is the incomplete gamma function defined as $\Gamma_{inc}(0,\rho) = \int_0^{1/\rho} \frac{e^{-1/x}}{x} dx$ [119]. For any given ρ, $\Gamma_{inc}(0,\rho)$ can be calculated numerically or using the standard tables for Γ_{inc}. (Note that, $\lim_{\rho \to 0} \Gamma_{inc}(0,\rho) \to \infty$.)

Appendix B

Probability Densities for Frequency Selective Fading

We will derive the probability densities for frequency selective channel used in this report. The results are given for 2-path model (path A) and (path B) with relative delay $\tau = T$(Figure 4.1). As derived in Appendix A. each path (A and B) has envelope, α, phase, θ, and instantaneous power, $|c|^2 = \alpha^2$, have Rayleigh, uniform and exponential distributions, respectively

$$p(\alpha_A) = \frac{\alpha_A}{\sigma_A^2} e^{-\frac{\alpha_A^2}{2\sigma_A^2}}, \qquad 0 \leq \alpha_A < \infty \tag{B.1}$$

$$p(\theta_A) = \frac{1}{2\pi}, \qquad 0 \leq \theta_A \leq 2\pi \tag{B.2}$$

$$p(\alpha_A^2) = p(|c^A|^2) = \frac{1}{2\sigma_A^2} e^{-\frac{|c^A|^2}{2\sigma_A^2}}, \qquad 0 \leq |c^A|^2 < \infty \tag{B.3}$$

Similarly, the distributions for Path B can be obtained simply changing the index A to B.

At the receiver, the output of the MF is given by

$$|c^T|^2 = |c^A|^2 + |c^B|^2. \tag{B.4}$$

Assuming an equal power for each path A and B, i.e., $\sigma_A^2 = \sigma_B^2 = \sigma_P^2$, pdf of $|c^T|^2$ is given by the convolution of the pdfs of the each path (B.3), A and B,

$$\begin{aligned} p(|c^T|^2) &= p(|c^A|^2) * p(|c^B|^2) \\ &= \int_0^{|c^T|^2} \frac{1}{2\sigma_P^2} e^{-\frac{x}{2\sigma_P^2}} \frac{1}{2\sigma_P^2} e^{-\frac{|c^T|^2 - x}{2\sigma_P^2}} dx \end{aligned}$$

Calculating the integral above, it can be found that

$$p(|c^T|^2) = \frac{1}{(2\sigma_P^2)^2} |c^T|^2 e^{-\frac{|c^T|^2}{2\sigma_P^2}}, \qquad 0 \leq |c^T|^2 < \infty. \tag{B.5}$$

The expected value of $|c^T|^2$ is also calculated as letting $y = |c^T|^2$

$$E(|c^T|^2) = \int_{-\infty}^{\infty} y p(y) dy = 2(2\sigma_P^2) \tag{B.6}$$

Moreover, when the channel inversion technique is applied as explained in chapter 4, we need to know the pdf of the inverted power to investigate the effect of power inversion process. Let $z = \frac{1}{|c^T|^2}$ where $p(|c^T|^2)$ is given in (B.5). By applying the appropriate transformation [92], the pdf of z is found as

$$p(z) = \frac{1}{(2\sigma_P^2)^2} \frac{1}{z^3} e^{-\frac{1}{z 2\sigma_P^2}}, \qquad 0 \leq z < \infty \tag{B.7}$$

or

$$p\left(\frac{1}{|c^T|^2}\right) = \frac{1}{(2\sigma_P^2)^2} (|c^T|^2)^3 e^{-\frac{|c^T|^2}{2\sigma_P^2}}, \qquad 0 \leq \frac{1}{|c^T|^2} < \infty \tag{B.8}$$

with $E(\frac{1}{|c^T|^2}) = \frac{1}{2\sigma_P^2}$.

Furthermore, when we introduce threshold, ρ, the new pdf of the inverted power

for a given ρ is found as

$$p\left(\frac{1}{|c^T|^2} \mid \frac{1}{|c^T|^2} < \frac{1}{\rho}\right) = \frac{1}{(2\sigma_P^2)^2}(|c^T|^2)^3 e^{-\frac{|c^T|^2}{2\sigma_P^2}} \frac{1}{e^{\frac{\rho}{2\sigma_P^2}}(1+\frac{\rho}{2\sigma_P^2})}, \qquad 0 \leq \frac{1}{|c^T|^2} < \frac{1}{\rho} \tag{B.9}$$

with the average power given as

$$E\left(\frac{1}{|c^T|^2} \mid \frac{1}{|c^T|^2} < \frac{1}{\rho}\right) = \frac{1}{\rho + 2\sigma_P^2}. \tag{B.10}$$

Appendix C

Phase Alignment Technique

In block adaptation scheme, the start of each data frame contains a known training sequence or pilot symbols which are used to estimate the channel impulse response (CIR). An interpolation technique is used to obtain the CIR variations between successive CIR estimates. When the data in this system is differentially encoded, the successive CIR estimates have an inherent phase ambiguity. In order to the remove the phase ambiguity between the successive CIR estimates, a phase alignment technique has been developed as follows:

The method we used is to do phase interpolation. Suppose there are three channel estimates c_1, c_2, and c_3. On account of the differential encoding, there is a phase ambiguity with each of the estimates having one of the following four values, $\{\pi/4, 3\pi/4, -\pi/4, -3\pi/4\}$. The goal is to eliminate phase ambiguity between the three channel estimates (and not to find the true phase). This can be done in the following manner:

- Assume c_1 as the reference.

- Using c_1 and $c_3 e^{jk\pi/4}$, where $k = \{1, -1, 3, -3\}$, use interpolation to estimate c_2' and compare with the four possible orientations $c_2 e^{jm\pi/4}$, where $m = \{1, -1, 3, -3\}$. The value of k, m that produce the best fit is the most likely values to produce the

desired phase alignment.

- Alternatively, one can use c_1 and c_2 and extrapolate to obtain c_3, thereby achieving the same desired effect.

Appendix D

Analysis of Three Different Approaches to the Prediction of the Total Channel Power

In this Appendix, three approaches to the long range prediction of the total channel power for each transmitter antenna are exploited given a sequence of past channel observations associated with that antenna. We start with some background information for the MMSE of the Linear Prediction. Given a sequence of past channel observations, $c(n-k), k = 1, \ldots, p$, we predict the future channel coefficient, $\hat{c}(n)$ as

$$\hat{c}(n) = \sum_{k=1}^{p} d(k)c(n-k) \tag{D.1}$$

We are required to find Linear Prediction (LP) Filter coefficients, $d(k)$, that minimizes the mean squared error (MSE), ξ, such that

$$\xi = E[|e(n)|^2] = E[|c(n) - \hat{c}(n)|^2] \tag{D.2}$$

In order to find a set of filter coefficients to minimize ξ, it is necessary and sufficient that the derivative of ξ with respect to $d^*(k)$ be equal to zero for $k = 1, \ldots, p$, i.e.,

$$\frac{\delta\xi}{\delta d^*(k)} = \frac{\delta}{\delta d^*(k)} E[e(n)e^*(n)] = E\left[e(n)\frac{\delta e^*(n)}{\delta d^*(k)}\right] = 0 \tag{D.3}$$

Substituting $e(n) = c(n) - \sum_{k=1}^{p} d(k)c(n-k)$, it follows that

$$\frac{\delta e^*(n)}{\delta d^*(k)} = -c^*(n-k) \tag{D.4}$$

and Eqn. (D.3) becomes

$$E[e(n)c^*(n-k)] = 0, \qquad k = 1, \ldots, p \tag{D.5}$$

This equation is also known as orthogonality principle. Therefore, minimum MSE (MMSE)of the prediction of $c(n)$ is evaluated as follows: First, we write the Eqn. (D.2) more explicitely such that

$$\begin{aligned} \xi &= E[|e(n)|^2] = E\left[e(n)\left(c(n) - \sum_{k=1}^{p} d(k)c(n-k)\right)^*\right] \\ &= E[e(n)c^*(n)] - \sum_{k=1}^{p} d(k)E[e(n)c^*(n-k)] \end{aligned}$$

Recall that if $d(k)$ is the solution of the Weiner-Hoph equations, then from the orthogonality principle (see Eqn. (D.5)), the MMSE is given as

$$\xi_{min} = E[e(n)c^*(n)] \tag{D.6}$$

Futhermore, writing Eqn (D.6) more explicitely, we obtain

$$\begin{aligned} \xi_{min} &= E\left[\left(c(n) - \sum_{k=1}^{p} d(k)c(n-k)\right)c^*(n)\right] \\ &= E[c(n)c^*(n)] - \sum_{k=1}^{p} d(k)E[c(n-k)c^*(n)] \\ &= r(0) - \sum_{k=1}^{p} d(k)r(k) \end{aligned}$$

where $r(k) = E[c(n-k)c^*(n)]$ is the autocorrelation function. Now, after reviewing the fundementals of the MMSE, we analyze three approaches to the long range prediction of the total channel power:

CASE 1:

In this approach, each future complex Gaussian fading coefficient $c_k(t)$ is predicted separately for each path and each antenna, and the total predicted power for each antenna is calculated using these estimates. These future predicted samples are denoted as $\hat{c}_1$, $\hat{c}_2$, ... $\hat{c}_L$. The autocorrelation function of each component is [4]:

$$r_j = (1/L)(\Omega_0/2)J_0(2\pi f_{dm} j T_s) \tag{D.7}$$

where $E[|c_i|^2] = \Omega_0/L$. The prediction MMSE per component is $\xi_i = E[|e_i|^2]$, where $e_i = c_i - \hat{c}_i$. Now, we will explain the steps to find the total power prediction mean squared error, ξ_T. The total power prediction mean squared error is defined as

$$\xi_T = E\left[\left|\sum_{i=1}^{L}|c_i|^2 - \sum_{i=1}^{L}|\hat{c}_i|^2\right|^2\right] = E\left[\left|\sum_{i=1}^{L}(|c_i|^2 - |\hat{c}_i|^2)\right|^2\right] \tag{D.8}$$

let $e_i' = |c_i|^2 - |\hat{c}_i|^2$, therefore,

$$\xi_T = E\left[\left|\sum_{i=1}^{L} e_i'\right|^2\right] = \sum_{i=1}^{L} E[|e_i'|^2] + \sum_{k\neq j} E[e_k' e_j'] \tag{D.9}$$

Now, we will calculate each component individually to find final ξ_T. We will examine the first term in Step 1 and the second term in Step 2.

Step 1: Express

$$\xi_i' = E[|e_i'|^2] = E[|c_i|^4] + E[|\hat{c}_i|^4] - 2E[|c_i|^2|\hat{c}_i|^2] \tag{D.10}$$

Again, the first, the second and the third terms will be calculated individually in Step 1.1, Step 1.2, and Step 1.3 respectively.

Step 1.1: For the Rayleigh fading channel, c_i has complex Gaussian distribution with $E[|c_i|^2] = \Omega_0/L$. Therefore, the forth order statistics for the Gaussian distribution is given as

$$E[|c_i|^4] = 2\left(\frac{\Omega_0}{L}\right)^2 \tag{D.11}$$

Step 1.2: From Eqn. (D.1), it is observed that $\hat{c}_i$ is a linear combination of c_i. Since c_i has complex Gaussian distribution, $\hat{c}_i$ also has complex Gaussian distribution. By definition

$$\begin{aligned} \xi_i &= E[|e_i|^2] = E[|c_i - \hat{c}_i|^2] \\ &= E[|c_i|^2] + E[|\hat{c}_i|^2] - E[c_i\hat{c}_i^*] - E[c_i^*\hat{c}_i] \end{aligned}$$

Moreover, using Eqn. (D.6), i.e., $\xi_i = E[e_i c_i^*]$, we can calculate

$$E[c_i\hat{c}^*] = E[c_i^*\hat{c}] = E[|c_i|^2] - E[e_i c_i^*] = E[|c_i|^2] - \xi_i \tag{D.12}$$

Therefore,

$$\xi_i = E[|c_i|^2] + E[|\hat{c}_i|^2] - 2(E[|c_i|^2] - \xi_i) \tag{D.13}$$

$$\xi_i = E[|c_i|^2] - E[|\hat{c}_i|^2] \tag{D.14}$$

Consequently, $E[|\hat{c}_i|^2] = E[|c_i|^2] - \xi_i = \Omega_0/L - \xi_i$. Since $\hat{c}_i$ has complex Gaussian distribution with $E[|\hat{c}_i|^2] = \Omega_0/L - \xi_i$, the forth order statistics for the Gaussian distribution is given as

$$E[|\hat{c}_i|^4] = 2\left(\frac{\Omega_0}{L} - \xi_i\right)^2 \tag{D.15}$$

Step 1.3: Given $e_i' = |c_i|^2 - |\hat{c}_i|^2$ and $\xi_i' = E[|e_i'|^2]$, ξ_i' can also be represented by using Eqn. (D.6) as $\xi_i' = E[|c_i|^2 e_i']$. Therefore,

$$E[|c_i|^2|\hat{c}_i|^2] = E[|c_i|^2(|c_i|^2 - e_i')] = E[|c_i|^4] - E[|c_i|^2 e_i'] \tag{D.16}$$

$$E[|c_i|^2|\hat{c}_i|^2] = E[|c_i|^4] - \xi_i' \tag{D.17}$$

Therefore, combining steps 1.1, 1.2, and 1.3, we obtain the result the result of step 1 for Eqn. (D.10) such that

$$\xi_i' = E[|c_i|^4] + E[|\hat{c}_i|^4] - 2(E[|c_i|^4] - \xi_i') \tag{D.18}$$

$$\xi_i' = E[|c_i|^4] - E[|\hat{c}_i|^4] \tag{D.19}$$

$$\xi_i' = 2\left(\frac{\Omega_0}{L}\right)^2 - 2\left(\frac{\Omega_0}{L} - \xi_i\right)^2 \tag{D.20}$$

$$\xi_i' = 4\frac{\Omega_0}{L}\xi_i - 2\xi_i^2 \tag{D.21}$$

Step 2: Sice c_i are iid, $\hat{c}_i$ are also iid. Similarly, $|c_i|^2$ and $|\hat{c}_i|^2$ are also iid. Therefore, $e_i' = |c_i|^2 - |\hat{c}_i|^2$ are iid. Consequently, $E[e_k'e_j'] = E[e_k']E[e_j']$. Moreover,

$$E[e_i'] = E[|c_i|^2 - |\hat{c}_i|^2] = E[|c_i|^2] - E[|\hat{c}_i|^2] = \xi_i \tag{D.22}$$

Then, we obtain

$$E[e_k'e_j'] = \xi_i^2 \tag{D.23}$$

Then, we will combine the results of step 1 (Eqn. (D.21)) and step 2 (Eqn. (D.23))to obtain ξ_T. Therefore, Eqn. (D.9) is found as

$$\xi_T = L\left(4\frac{\Omega_0}{L}\xi_i - 2\xi_i^2\right) + (L^2 - L)\xi_i^2 \tag{D.24}$$

$$\xi_T = 4\Omega_0\xi_i + (L^2 - 3L)\xi_i^2 \tag{D.25}$$

Finally, since $\xi_i = \xi_{flat}/L$, where ξ_{flat} is the MMSE of the complex fading coefficient prediction for $L = 1$, the ξ_T is given as

$$\xi_T = \left(4\frac{\Omega_0}{L}\right)\xi_{flat} + \left(1 - \frac{3}{L}\right)\xi_{flat}^2 \tag{D.26}$$

CASE 2:

In this case, we apply linear MMSE prediction directly to the observations of powers $\Omega_1, \Omega_2, \ldots, \Omega_L$, where $\Omega_i = |c_i|^2$ represents the power of the fading channel associated with the $i-$th multipath component for a given antenna. The total predicted power will be computed using these individual estimates $\hat{\Omega}_i$. Each Ω_i has the autocorrelation function [4]:

$$r(\tau) = (\Omega_0/L)^2 J_0^2(2\pi f_{dm}\tau) + (\Omega_0/L)^2 \tag{D.27}$$

The total prediction MMSE is

$$\xi_T = E\left[\left|\sum_{i=1}^{L}\Omega_i - \sum_{i=1}^{L}\hat{\Omega}_i\right|^2\right] = E\left[\left|\sum_{i=1}^{L}(\Omega_i - \hat{\Omega}_i)\right|^2\right] \tag{D.28}$$

Let $e_i = \Omega_i - \hat{\Omega}_i$, therefore,

$$\xi_T = E\left[\left|\sum_{i=1}^{L} e_i\right|^2\right] = \sum_{i=1}^{L} E[|e_i|^2] + \sum_{k\neq j} E[e_k e_j] \tag{D.29}$$

Since e_i are iid,

$$\xi_T = (L)E[|e_i|^2] + (L^2 - L)E[e_k]E[e_j] \tag{D.30}$$

Furthermore,

$$E[|e_i|^2] = r_0 - \sum_{j=1}^{p} d_j r_j \tag{D.31}$$

$$E[|e_i|^2] = \left(\frac{\Omega_0}{L}\right)^2 - \sum_{j=1}^{p} d_j \left[\left(\frac{\Omega_0}{L}\right)^2 J_0^2(2\pi f_{dm} j T_s) + \left(\frac{\Omega_0}{L}\right)^2\right] \tag{D.32}$$

$$E[|e_i|^2] = \left(\frac{\Omega_0}{L}\right)^2 \left(1 - \sum_{j=1}^{p} d_j\right) + \left(\frac{\Omega_0}{L}\right)^2 \left(1 - \sum_{j=1}^{p} d_j J_0^2(2\pi f_{dm} j T_s)\right) \tag{D.33}$$

Moreover, $E[e_i]$ can be found as

$$E[e_i] = E[\Omega_i] - E[\hat{\Omega}_i] \tag{D.34}$$

$$E[e_i] = E[\Omega_i] - \sum_{k=j}^{p} d_j E[\Omega_i] \tag{D.35}$$

$$E[e_i] = \left(\frac{\Omega_0}{L}\right)\left(1 - \sum_{j=1}^{p} d_j\right) \tag{D.36}$$

Then incorporating Eqn. (D.33) and Eqn. (D.36) into Eqn. (D.30), we obtain

$$\xi_T = \frac{\Omega_0^2}{L}\left(1 - \sum_{j=1}^{p} d_j\right) + \frac{\Omega_0^2}{L}\left(1 - \sum_{j=1}^{p} d_j J_0^2(2\pi f_{dm} j T_s)\right) + (L^2 - L)\left(\frac{\Omega_0}{L}\right)^2 \left(1 - \sum_{j=1}^{p} d_j\right)^2 \tag{D.37}$$

Finally, Eqn. (D.37) can be simplified further and the total MMSE for Case 2 is given as:

$$\xi_T = \Omega_0^2\left(1 - \sum_{j=1}^{p} d_j\right)^2 + \frac{\Omega_0^2}{L}\left(1 - \sum_{j=1}^{p} d_j\right)\left(\sum_{j=1}^{p} d_j\right) + \frac{\Omega_0^2}{L}\left(1 - \sum_{j=1}^{p} d_j J_0^2(2\pi f_{dm} j T_s)\right) \tag{D.38}$$

CASE 3:

In this approach, we form the linear MMSE prediction of the total power of the fading channel for each antenna using previous total power samples observed at the receiver. The total power is given as $\Omega_T = \Omega_1 + \Omega_2 + \ldots + \Omega_L$. First, we find the autocorrelation function of Ω_T which is defined as

$$r(\tau) = E[\Omega_T(t)\Omega_T(t+\tau)] \tag{D.39}$$

$$r(\tau) = E[(\Omega_1(t) + \Omega_2(t) + \ldots + \Omega_L(t))((\Omega_1(t+\tau) + \Omega_2(t+\tau) + \ldots + \Omega_L(t+\tau))] \tag{D.40}$$

$$r(\tau) = \sum_{i=1}^{L} E[\Omega_i(t)\Omega_i(t+\tau)] + \sum_{k \neq j} E[\Omega_k(t)\Omega_j(t+\tau)] \tag{D.41}$$

Furthermore, since Ω_k and Ω_j are iid, for $k \neq j$

$$E[\Omega_k(t)\Omega_j(t+\tau)] = E[\Omega_k(t)]E[\Omega_j(t+\tau)] = \left(\frac{\Omega_0}{L}\right)^2 \tag{D.42}$$

And, $E[\Omega_i(t)\Omega_i(t+\tau)]$ is given as

$$E[\Omega_i(t)\Omega_i(t+\tau)] = \left(\frac{\Omega_0}{L}\right)^2 J_0^2(2\pi f_{dm}\tau) + \left(\frac{\Omega_0}{L}\right)^2 \tag{D.43}$$

Therefore, the autocorrelation function of Ω_T is found as

$$r(\tau) = L\left(\frac{\Omega_0}{L}\right)^2 J_0^2(2\pi f_{dm}\tau) + L\left(\frac{\Omega_0}{L}\right)^2 + (L^2 - L)\left(\frac{\Omega_0}{L}\right)^2 \tag{D.44}$$

$$r(\tau) = \frac{\Omega_0^2}{L} J_0^2(2\pi f_{dm}\tau) + \Omega_0^2 \tag{D.45}$$

Finally, the MMSE, $E[|\Omega_T - \hat{\Omega}_T|^2]$, for Case 3 can be found as

$$\xi_T = r_0 - \sum_{j=1}^{p} d_j r_j \tag{D.46}$$

$$\xi_T = \left(\frac{\Omega_0^2}{L} + \Omega_0^2\right) - \sum_{j=1}^{p} d_j \left(\frac{\Omega_0^2}{L} J_0^2(2\pi f_{dm} j T_s) + \Omega_0^2\right) \tag{D.47}$$

$$\xi_T = \Omega_0^2 \left(1 - \sum_{j=1}^{p} d_j\right) + \left(\frac{\Omega_0^2}{L}\right) \left(1 - \sum_{j=1}^{p} d_j J_0^2(2\pi f_{dm} j T_s)\right) \tag{D.48}$$

Bibliography

[1] J. E. Padgett, C. G. Gunther, and T. Hattori. "Overview of Wireless Personal Communications". *IEEE Communications Magazine*, pages 28–40, January 1995.

[2] D. C. Cox. "Wireless Personal Communications: What is it?". *IEEE Personal Communications*, pages 20–35, April 1995.

[3] T. S. Rappaport. *Wireless Communications*. Prentice Hall, NJ, 1996.

[4] G. L. Stuber. *Principles of Mobile Communication*. Kluwer, MA, 1996.

[5] J.G. Proakis. *Digital Communications*. McGraw-Hill, New York, 1995.

[6] W. C. Y. Lee. *Mobile Communications Design Fundamentals*. Wiley, NY, 1993.

[7] W. C. Y. Lee. *Mobile Communications Engineering*. McGraw-Hill, NY, 1998.

[8] V. K. Garg and J. E. Wilkes. *Wireless and Personal Communications Systems*. Prentice Hall, NJ, 1996.

[9] S. Stein. "Fading Channel Issues in System Engineering". *IEEE Journal on Selected Areas in Communications*, 5(2):68–89, February 1987.

[10] B. H. Fleury and P. E. Leuthold. "Radiowave Propagationin Mobile Communications: An Overview of Europian Research". *IEEE Communications Magazine*, pages 70–81, February 1996.

[11] B. Skalar. "Rayleigh Fading Channels in Mobile Digital Communication Systems Part I: Characterization". *IEEE Communications Magazine*, pages 90–100, July 1997.

[12] B. Skalar. "Rayleigh Fading Channels in Mobile Digital Communication Systems Part II: Mitigation". *IEEE Communications Magazine*, pages 102–109, July 1997.

[13] A. J. Paulraj and C. B. Papadias. "Space-Time Processing for Wireless Communications". *IEEE Signal Processing Magazine*, pages 49–83, November 1997.

[14] T. Eyceöz, A. Duel-Hallen, and H. Hallen. "Prediction of Fast Fading Parameters by Resolving the Interference Pattern". *Proceedings of the* 31^{st} *ASILOMAR Conference on Signals, Systems, and Computers*, pages 167–171, November 1997.

[15] T. Eyceöz, A. Duel-Hallen, and H. Hallen. "Using the Physics of the Fast Fading to Improve Performance for Mobile Radio Channels". *Proceedings of the IEEE International Symposium on Information Theory*, page 159, 1998.

[16] W. C. Jakes. *Microwave Mobile Communications*. John Wiley and Sons, New York, 1993.

[17] P. Dent, G. E. Bottomley, and T. Croft. "Jakes Fading Model Revisited". *Electronics Letters*, 29(13):1162–1163, June 1993.

[18] E. F. Casas and C. Leung. "A Simple Digital Fading Simulator for Mobile Radio". In *Proceedings of VTC*, pages 212–217, Sept. 1988.

[19] J. Lin, J. G. Proakis, F. Ling, and H. Lev-Ari. "Optimal Tracking of Time-Varying Channels: A Frequency Domain Approach for Known and New Algorithms". *IEEE Transactions on Selected Areas in Communications*, 13(1):141–154, January 1995.

[20] R. Haeb and H. Mayr. "A Systematic Approach to Carrier Recovery and Detection of Digitally Phase Modulated Signals on Fading Channels". *IEEE Transactions on Communications*, 37(7):748–754, July 1989.

[21] L. Lindbom. "Simplified Kalman Estimation of Fading Mobile Radio Channels: High Performance at LMS Computational Load". *Proceedings of IEEE ICASSP*, 3:352–355, April 1993.

[22] Z. Zvonar and M. Stanjovic. "Performance of Antenna Diversity Multiuser Receivers in CDMA Channels with Imperfect Channel Estimation". *Wireless Personal Communications Journal*, pages 91–110, July 1996.

[23] H. Y. Wu and A. Duel-Hallen. "Performance Comparison of Multiuser Detectors with Channel Estimation for Flat Raleigh Fading CDMA Channels". *Special Issue on Interference in Mobile Wireless Systems, Wireless Personal Communications Journal*, 6(12):137–160, January 1998.

[24] H. Y. Wu. *"Multiuser Detection and Channel Estimation for Flat Raleigh Fading CDMA Channels"*. PhD thesis, North Carolina State Univ., December 1996.

[25] R. A. Iltis. "Joint estimation of PN code delay and multipath using extended Kalman filter". *IEEE Trans. Commun.*, 38(10):1677–1685, October 1990.

[26] S. Vasudevan and M. Varanasi. "Receivers for CDMA communication over time-varying Rayleigh fading channel". *Proc. CTMC'93, Globecom'93, Houston, TX,*, pages 60–64, Nov. 29-Dec. 2 1993.

[27] M. K. Tsatsanis, G. B. Giannakis, and G. Zhou. "Estimation and equalization of fading channels with random coefficients". *Signal Processing*, 53(2-3):211–229, September 1996.

[28] Y. Liu and S. D. Blostein. "Identification of frequency non-selective fading channels using decision feedback and adaptive linear prediction". *IEEE Trans. Commun.*, 43(2-3-4):1484–1491, Feb/March/April 1994.

[29] A. N. A'Andrea, A. Diglio, and U. Mengali. "Symbol-aided channel estimation with nonselective Rayleigh fading channels". *IEEE Trans. Veh. Technol.*, 44(1):41–49, Feb. 1995.

[30] G. Colman, S. Blostein, and N. Beaulieu. ""An ARMA multipath fading simulator". *Wireless Personal Communications*, pages 37–48, 1997.

[31] B. D. O. Anderson and J. R. Moore. *Optimal Filtering.* Prentice-Hall, 1979.

[32] M. K. Tsatsanis and G. B. Giannakis. "Modeling and equalization of rapidly fading channels". *Int. J. Adaptive Control and Signal Processing*, 10(2-3):159–176, March 1996.

[33] M. K. Tsatsanis and G. B. Giannakis. "Equalization of rapidly fading channels: Self-recovering methods". *IEEE Trans. Commun.*, 44(5):619–630, May 1996.

[34] L. Lindbom. ""Adaptive equalization for fading mobile radio channels". Master's thesis, Uppsala University, Sweden,, 1992.

[35] T. Eyceöz, A. Duel-Hallen, and H. Hallen. "Deterministic Channel Modeling and Long Range Prediction of Fast Fading Mobile Radio Channels". *IEEE Communications Letters*, 2(9):254–256, September 1998.

[36] T. Eyceöz, S. Hu, A. Duel-Hallen, and H. Hallen. "Adaptive Prediction, Tracking and Power Adjustment for Frequency Non-Selective Fast Fading Channels". *Proceedings of the Eighth Communication Theory Mini-Conference (CTMC"99).*

[37] T. Eyceöz, S. Hu, and A. Duel-Hallen. "Performance Analysis of Long Range Prediction for fast Fading Channels". *Invited Paper - Proceedings of the 33rd Annual Conf. on Information Sciences and Systems (CISS'99).*

[38] S. Hu, T. Eyceöz, A. Duel-Hallen, and H. Hallen. "Transmitter Antenna Diversity and Adapive Signaling Using Long Range Prediction for Fast Fading DS/CDMA Mobile Radio Channels". *Proceedings of the WCNC'99*.

[39] T. Eyceöz, A. Duel-Hallen, and H. Hallen. "Deterministic Modeling and Long Range Prediction of Fast Fading Channels with Applications to Mobile Radio Systems". to be submitted to the IEEE Transactions on Communications.

[40] N. Ahmed and K.R. Rao. *Orthogonal Transforms for Digital Signal Processing*. Springer-Verlag, New York, 1975.

[41] A. Seville, U. Yilmaz, P. G. V. Charriere, N. Powel, and K. H. Crai. "Building Scatter and Vegetation Attenuation Measurements at 38 GHz". *Proceedings of the 9th International Conference on Antennas and Propagation*, Eindhoven, the Netherlands:46–50, 1995.

[42] T. J. Schmugge and T. J. Jackson. "a dielectric model of the vegetative effects on the microwave emission from soils". *IEEE Transactions on Geoscience and Remote Sensing*, 30(4):757–760, 1992.

[43] I. J. Dilworth and B . L'Ebraly. "Propagation Effects due to Foliage and Building Scatter at Millimeter Wavelengths". *Proceedings of the 9th International Conference on Antennas and Propagation*, Eindhoven, the Netherlands:51–53, 1995.

[44] M. S. Ding and M. O. Al-Nuaimi. "Prediction of Scatter Coefficient of Buildings at Microwave Frequencies in Site Shielding". *Proceedings of the 9th International Conference on Antennas and Propagation*, Eindhoven, the Netherlands:42–45, 1995.

[45] P. A. Mathews and B. Mohebbi. "Direction of Arrival and Building Scatter at UHF". In *Proceedings of 7th International Conference on Antennas and Propagation*, pages 147–150, 1991.

[46] J. Talvitie, V. Hovinen, H. Hamalainen, and I. Oppermann. ""Wideband channel measurement and characterization for wireless local loops". *Proc. 7th IEEE Int. Symp. on Personal, Indoor and Mobile Radio Commun.*, pages 5–9, Oct. 1996.

[47] T. S. Rappaport, S. Y. Seidel, and K. Takamizawa. "Statistical channel model for factory and open plan building radio communication system design". *IEEE Transactions on Communications*, 39(5):794–807, May 1991.

[48] A. Duel-Hallen, S. Hu, and H. Hallen. "Long-range Prediction of Fading Signals: Enabling Adaptive Transmission for Mobile Radio Channels". *IEEE Signal Processing Magazine*, pages 62–75, May 2000.

[49] O. S. Heavens and R. W. Ditchburn. *Insight into Optics*. Wiley, Chichester, UK, 1991.

[50] T. A. Russell, C. W. Bostian, and T. S. Rappaport. "A deterministic approach to predicting microwave diffraction by buildings for microcellular systems". *IEEE Trans. on Ant. and Prop.*, 41(12):1640–1649, Dec 1993.

[51] M. F. Hadi and M. Piket-May. ""A modified FDTD (2,4) scheme for modeling electrically large structures with high-phase accuracy". *IEEE Trans. on Ant. and Prop.*, 45(2):254–264, Feb. 1997.

[52] H. Hallen and A. Duel-Hallen. "Physical Insights into the Nature of the Fast Fading in Wireless Communication". *to be submitted to JSAC*, 1998.

[53] D. G. Manolakis J. G. Proakis. *Digital Signal Processing*. Prentice Hall, NJ, 1996.

[54] M. H. Hayes. *Statistical DSP and Modeling*. John Wiley and Sons, 1996.

[55] S. M. Kay and S. L. Marple. "Spectrum Analysis–A Modern Perspective". *Proceedings of the IEEE*, 69(11):1380–1419, November 1981.

[56] R. E Crocheire and L. R. Rabiner. *Multirate Signal Processing*. Prentice Hall, Englewood Cliffs, NJ, 1983.

[57] R. W. Schafer and L. R. Rabiner. "A Digital Signal Processing Approach to Interpolation". *Proceedings of the IEEE*, 61(6):692–702, June 1973.

[58] T. Eyceöz and A. Duel-Hallen. "Reduced Complexity Diversity Combining and Adaptive Equalization Using Interpolated Channel Estimates with Applications to Cellular Mobile Radio Channels". In *Proceedings of ICUPC*, pages 51–55, Sep. 30-Oct. 2 1996.

[59] N. W. K. Lo, D. D. Falconer, and A. U. H. Sheikh. "Adaptive Equalization and Diversity Combining for a Mobile Radio Channel using Interpolated Channel Estimates". *IEEE Transactions on Vehicular Technology*, 40(3):636–645, August 1991.

[60] J. Hayes. "Adaptive feedback communications". *IEEE Transactions on Communications*, 16:29–34, February 1968.

[61] J. Cavers. "Variable-rate transmission for Rayleigh fading channels". *IEEE Transactions on Communications*, 20:15–22, February 1972.

[62] A. Goldsmith. "Variable-rate coded MQAM for fading channels". *Proc. IEEE Global Commun. Conf.*, pages 186–190, 1994.

[63] A. Goldsmith and S. Chua. "Variable-Rate Variable-Power MQAM for Fading Channels". *IEEE Transactions on Communications*, 45(10):1218–1230, October 1997.

[64] A. Goldsmith and P. P. Variaya. "Capacity of fading channels with channel side information". *IEEE Trans. Inform. Theory*, 43(6):1986–1992, Nov. 1997.

[65] M. C. Vanderveen, A. J Van der Veen, and A. Poulraj. "Estimation of Multipath Parameters in Wireless Communications". *IEEE Transactions on Signal Processing*, 46(3):682–690, March 1998.

[66] P. A. Bello and B. D. Nelin. "The Effect of Frequency Selective Fading on the Binary Error Probabilities of Incoherent and Differentially Coherent Matched Filter Receivers,". *IEEE Trans. Commun. Sys.*, CS-II:170–186, June 1963.

[67] J. H. Winters. "Smart Antennas for Wireless Systems". *IEEE Personal Communications*, pages 23–27, February 1998.

[68] S. U. H. Qureshi. "Adaptive Equalization". *Proceedings of the IEEE*, 73(9):1349–1387, Sept. 1985.

[69] G. W. Davidson, D .D Falconer, and A. U. H. Sheikh. "An investigation of block-adaptive decision feedback equalization for frequency selective fading channels". *Can. J. Elect. Comp. Eng.*, 13(3-4):106–111, March 1988.

[70] T. Eyceöz. "Reduced Complexity Optimal Diversity Combining and Adaptive Equalization Using Interpolated Channel Estimates with Applications to Cellular Mobile Radio Channels.". Master's thesis, North Carolina State Univ., November 1995.

[71] T. Eyceöz and A. Duel-Hallen. "Simplified Block Adaptive Diversity Equalizer for Cellular Mobile Radio". *IEEE Communications Letters*, 1(1):1–5, January 1997.

[72] W. M. DeSevilla and E. Sousa. "Fading Resistant Transmission from Several Antennas ". *Proc. IEEE PIMRC'95*, pages 1218–1222, 1995.

[73] T. Heikkinen and A. Hottinen. "On Downlink Power Control and Capacity with Multi-Antenna Transmission ". *Proc. Conf. Inf. Sci. and Syst. (CISS'98), Princeton*, pages 475–479, March 1998.

[74] A. Hottinen and R. Wichman. "Transmit Diversity by Antenna Selection in CDMA Downlink ". *Proc. of IEEE 5th Int. Symp. on Spread Spec. Tech. and Appl.*, pages 767–770, September 1998.

[75] A. Goldsmith and S. Chua. "Adaptive Coded Modulation for Fading Channels". *IEEE Transactions on Communications*, 46(5):595–602, May 1998.

[76] M. Alouini, x. Tang, and A. Goldsmith. "An Adaptive Modulation Scheme for Simultaneous Voice and Data Transmission over Fading Channels". *IEEE Journal on Selected Areas in Communications*, 17(5):837–850, May 1999.

[77] D. L. Goeckel. "Adaptive Coding for Time-Varying Channels Using outdated Fading Estimates". *IEEE Transactions on Communications*, 47(6):844–855, June 1999.

[78] T. Ue, S. Sampei, and N. Morinaga. "Symbol Rate and Modulation Level Controlled Adaptive Modulation TDMA TDD System for High Bit Rate Wireless Data Transmission ". *IEEE Transactions on Vehicular Technology*, 47(4):1134–1147, Nov. 1998.

[79] J.M. Torrance and L. Hanzo. "Optimization of Switching Levels for Adaptive Modulation in Slow Rayleigh Fading". *Electronics Letters*, 32(13):1167–1169, June 1996.

[80] J.M. Torrance and L. Hanzo. "Upper Bound Performance of Adaptive Modulation in a Slow Rayleigh Fading Channel". *Electronics Letters*, 32(8):718–719, April 1996.

[81] W.T. Webb and R. Steele. "Variable Rate QAM for Mobile Radio ". *IEEE Transactions on Communications*, 43(7):2223–2230, July 1995.

[82] V.K.N. Lau and M.D. Macleod. "Variable Rate Adaptive Trellis Coded QAM for High Bandwidth Efficiency Applications in Rayleigh Fading Channels". In *Proceedings of the VTC*, pages 352–348, 1998.

[83] M. Tomlinson. "New Automatic Equalizer Employing Modulo-Arithmetic ". *Electron. Lett.*, 7:138–139, March 1971.

[84] H. Harashima and H. Miyakawa. "Matched-transmission Technique for Channels with Intersymbol Interference ". *IEEE Transactions on Communications*, 20:774–780, August 1972.

[85] G. D. Forney and A. R. Calderbank. "Coset Codes for Partial Response Channels; or, Coset Codes with Spectral Nulls ". *IEEE Transactions on Information Theory*, 35:825–933, Sept. 1989.

[86] A. R. Calderbank and J. E. Mazo. "Baseband Line Codes Via Spectral Factorization ". *IEEE Journal on Selected Areas in Communications*, 7:914–928, August 1989.

[87] M. V. Eyuboglu and G. D. Forney. "Trellis Precoding: Combined Coding, Precoding, and Shaping for Intersymbol Interference Channels ". *IEEE Transactions on Information Theory*, 38:301–314, March 1992.

[88] N. A. Zervos A. K. Aman, R. L. Cupo. "Combined Trellis Coding and DFE through Tomlinson Precoding". *IEEE Journal on Selected Areas in Communications*, 9:876–884, August 1991.

[89] J. E. Mazo. "Exact Matched Filter Bound for Two-Beam Rayleigh Fading". *IEEE Transactions on Communications*, 39(7):1027–1030, July 1991.

[90] Telecommunications Indus. Assoc. "EIA/TIA Interim Standard: Cellular System Dual-Mode Station-Base Station Compatibility Standard (IS−54)". 1992.

[91] F. Ling. "Matched Filter-Bound for Time-Discrete Multipath Rayleigh Fading Channels". *IEEE Transactions on Communications*, 43(2/3/4):710–713, Feb./March/April 1995.

[92] A. Papoulis. *Probability, Random Variables, and Stochastic Process*. McGraw-Hill, 1991.

[93] J. Ventura Travest et. al. "Impact of Diversity Reception on Fading Channel with Coded Modulation-Part I: Coherent Detection ". *IEEE Transactions on Communications*, 45(5):563–572, May 1997.

[94] E.A. Lee and D.G. Messerschmitt. *Digital Communications*. Kluwer Academic Publisher, Boston, 1994.

[95] J. Salz. "Optimum Mean-Square Decision Feedback Equalization". *Bell Systems Technical Journal*, 52(8):1341–1373, Oct. 1973.

[96] K. Abend and B. D. Fritchman. "Statistical Detection for Communication Channels with Intersymbol Interference ". *Proceedings of the IEEE*, pages 779–785, May 1970.

[97] G. D. Forney. "Maximum-likelihood Sequence Estimation of Digital Sequences in the Presence of Intersymbol Interferences". *IEEE Transactions on Information Theory*, 18:363–378, May 1972.

[98] R. L. Troy D. Koilpillai, S. Channakeshu. "Low Complexity Equalizers for U.S. Digital Cellular System". In *Proceedings of the IEEE 42nd VTC, Denver, CO*, pages 744–747, 1992.

[99] M. Stojanovic and J.G. Proakis. "Analysis of the Impact of Channel Estimation Errors on the Performance of a Decision-Feedback Equalizers in Fading Multipath Channels". *IEEE Transactions on Communications*, 43(2/3/4):877–886, April 1995.

[100] J. E. Mazo and J. Salz. "On the Transmitted Power in generalized Partial Response ". *IEEE Transactions on Communications*, 24(3):348–352, March 1976.

[101] Y-L Chan and W. Zhuang. "Channel Procoding for Indoor Radio Communications Using Dimention Partitioning ". *IEEE Transactions on Vehicular Technology*, 48(1):98–114, January 1999.

[102] R. D. Wesel and J. M. Cioffi. "Achiavable Rates for Tomlinson-Harashima Precoding ". *IEEE Transactions on Information Theory*, 44(2):824–831, March 1998.

[103] andP.A.Goud W.Zhuang, W.A.Krzymien. "Adaptive channel Precoding for Personal Communications ". *Electron.Lett.*, 30:1570–1571, Sept. 1994.

[104] W.Zhuang and V.W.Huang. "Phase Precoding for Frequency-selective Rayleigh and Rician Slowly Fading channels ". *IEEE Transactions on Vehicular Technology*, 46:129–142, Feb. 1997.

[105] R. G. Vaughan and J. B. Andersen. "Antenna Diversity in Mobile Communications". *IEEE Transactions on Vehicular Technology*, 36(4):149–172, Nov. 1987.

[106] L. C. Godora. "Applications of Antenna Arrays to Mobile Communications, Part I: Performance Improvement, Feasibility, and System Considerations". *Proceedings of the IEEE*, 85(7):1031–1060, July 1997.

[107] L. C. Godora. "Applications of Antenna Arrays to Mobile Communications, Part II: Beam-Forming and Direction-of-Arrival Considerations". *Proceedings of the IEEE*, 85(8):1195–1245, August 1997.

[108] R. B. Ertel et. al. "Overview of Spatial Channel Models for Antenna Array Communication Systems". *IEEE Personal Communications*, pages 10–22, February 1998.

[109] R. Kohno. "Spatial and Temporal Communication Theory Using Adaptive Antenna Array". *IEEE Personal Communications*, pages 28–35, February 1998.

[110] G. J. Foschini. ""Layered space-time architecture for wireless communication in a fading environment when using multi-element antennas". *Bell Labs Technical Journal*, 1, Autumn 1996.

[111] G. J. Foschini and M. J. Gans. "On limits of wireless communications in a fading environment when using multiple antennas". *Wireless Personal Communications*, 1997.

[112] T. Marzetta and B. Hochwald. "Capacity of a mobile multiple-antenna communication link in a Rayleigh flat-fading environment". *Proc. 35th Allerton Conf. on Commun., Control and Computing*, Sept. 1997.

[113] J. H. Winters. "The Impact of Antenna Diversity on the Capacity of Wireless Communication Systems". *IEEE Transactions on Communications*, 42(2/3/4):1740–1751, Feb./March/April 1994.

[114] E. Dahlman et al. "WCDMA - The Radio interface for Future Mobile Multimedia Communications ". *IEEE Transactions on Vehicular Technology*, 47:1105–1117, November 1998.

[115] F. Adachi, M. Sawahashi, and H. Suda. "Wideband DS-CDMA for Next Generation Mobile Communications Systems ". *IEEE Comm. Mag.*, pages 56–69, September 1998.

[116] P. Balaban and J. Salz. "Optimum Diversity Combining and Equalization in digital Data Transmission with Applications to Cellular Mobile Radio-Part I: Theoretical Considerations". *IEEE Transactions on Communications*, 40(5):885–894, May 1992.

[117] J. H. Winters. "The Diversity Gain of Transmit Diversity in Wireless Systems with Rayleigh Fading". *IEEE Transactions on Vehicular Technology*, 47(1):119–123, February 1998.

[118] W. C. Y. Lee. "Statistical Analysis of the Level Crossings and Duration of fades of the Signal from an Energy Density Mobile Radio Antenna". *Bell Sys. Tech. Journal*, 46:417–448, Feb. 1967.

[119] M. Abramowitz and I. Stegun. *Handbook of Mathematical Functions*. Dover Publ. Inc., NY, 1965.